EVALUATION OF DIFFUSER MODIFICATIONS FOR THE BOEING/AFOSR MACH-6 QUIET TUNNEL

A Thesis

Submitted to the Faculty

of

Purdue University

by

Michael J. Hannon, Jr.

In Partial Fulfillment of the

Requirements for the Degree

of

Master of Science in Aeronautics and Astronautics

August 2008

Purdue University

West Lafayette, Indiana

To my mother, Marcela, and my fiancée, Lindsay,

whose love and support made this accomplishment possible.

ACKNOWLEDGEMENTS

I would like to thank Professor Steven P. Schneider for providing me the opportunity to work on the Boeing/AFOSR Mach-6 Quiet Tunnel. I would also like to thank him for his patience and guidance throughout this whole process. I also appreciate the suggestions from my committee members, Professors Gregory Blaisdell and Charles Merkle.

Thanks to the technicians at the Aerospace Sciences Laboratory: Madeleine Chadwell, Jerry Hahn, Robin Snodgrass and Jim Younts as well as Scott Meyer from the High Propulsion Laboratory and Jeff Lynch from the Central Machine Shop. Their assistance with the hardware installation made this research possible. I am also grateful for the help of the technicians and engineers from Lagrange Products and Anderson Tool & Engineering for the fabrication of the new hardware.

I am indebted to the members of Dr. Schneider's research team: Shann Rufer, Erick Swanson, Matt Borg, Thomas Juliano, Rodrigo Segura, Katya Casper and Brad Wheaton. Their advice, assistance and leadership have proved invaluable during my time at Purdue.

Lastly, I am grateful to all friends and family who have supported me through such a difficult and transformative time in my life. I am especially thankful for the encouragement and advice given to me by Amy Brock, Gabriel Ford, Daniel and Darlene Griffin, Eric Kauffman, Terry Lu, Daniel McCormick and Nancy Mockros.

TABLE OF CONTENTS

Page

LIST OF TABLES vii

LIST OF FIGURES viii

SYMBOLS xiii

ABSTRACT xv

1 INTRODUCTION 1

1.1 Objective 1

1.2 Analytical Approach to the Starting Problem 1

1.3 Boundary-Layer Separation 4

1.4 Shock-Boundary Layer Interaction on the Tunnel Walls 6

1.5 Suggestions for Improved Starting Performance 7

2 APPARATUS 9

2.1 The Mach-6 Quiet Tunnel 9

2.2 Original Sting-Support/Diffuser Section 11

2.3 Modified Sting-Support/Diffuser Section 13

2.4 Sphere-Cone Model 15

3 MEASUREMENT AND CALCULATION TECHNIQUES 16

3.1 Kulite Pressure Transducers 16

3.2 Hot Films 17

3.3 Tektronix Oscilloscopes 18

3.4 Noise-Level-Calculation Technique 19

3.5 Mach-Number-Calculation Technique 20

Page

3.6 Calculating Technique for Fast Fourier Transform 21

4 EXPERIMENTAL ANALYSIS 22

4.1 Original Tunnel Configuration 22

4.1.1 2-Inch Model under Quiet Conditions 23

4.1.2 2.25-Inch Model under Quiet Conditions 30

4.1.3 2.5-Inch Model under Quiet Conditions 38

4.1.4 2-Inch Model under Noisy Conditions 42

4.1.5 Summary of Performance of Original Tunnel Configuration 45

4.2 Modified Tunnel Configuration 50

4.2.1 Streamwise Variation of Starting Performance 51

4.2.2 Starting Performance at Farthest Upstream Location 53

4.3 Summary of Performance of Modified Tunnel Configuration 55

5 CONCLUSIONS AND FUTURE WORK 58

LIST OF REFERENCES 61

APPENDICES

A. Detailed Analysis of Experiments 63

A.1 Periodic Oscillations at Lower Reynolds Number in Original Tunnel Configuration under Quiet Conditions 63

A.2 Periodic Oscillations with Larger Models under Quiet Conditions in Original Tunnel Configuration 65

A.3 Periodic Oscillations with Unstarted Runs in Original Tunnel Configuration 67

A.4 Periodic Oscillations with Modified Tunnel Configuration 69

B. Run-Data Tables 71

C. Schematics of Sphere-Cone Model 81

D. Additional Tunnel Hardware 82

Page

D.1 Fast-Acting Valve 82
D.2 Support System for Modified Configuration 91
D.3 Modified Trolleys 93
D.4 Traverse Bar 95
E. Matlab Source Codes 97
E.1 Noise-Level Calculator 97
E.2 Mach-Number Calculator 98
E.3 Fast-Fourier-Transform Calculator 100

LIST OF TABLES

Table — Page

B.1 2-inch model under quiet conditions in the original tunnel configuration (in decreasing order of p_d, model located at x = 11 inches) 71

B.2 2.25-inch model under quiet conditions in the original tunnel configuration (in decreasing order of p_d, model located at x = 11 inches) 73

B.3 2.5-inch model under quiet conditions in the original tunnel configuration (in decreasing order of p_d, model located at x = 11 inches) 75

B.4 2-inch model under noisy conditions in the original tunnel configuration (in decreasing order of p_d, model located at x = 11 inches) 76

B.5 2.25-inch model under noisy conditions in the original tunnel configuration (in decreasing order of p_d, model located at x = 11 inches) 77

B.6 2-inch model under quiet conditions in the modified tunnel configuration (in increasing order of x_{nose} then decreasing order of p_d) 78

B.7 2.25-inch model under quiet conditions in the modified tunnel configuration (in increasing order of x_{nose} then decreasing order of p_d) 79

B.8 2.5-inch model under quiet conditions in the modified tunnel configuration (in increasing order of x_{nose} then decreasing order of p_d) 79

B.9 2-inch model under noisy conditions in the modified tunnel configuration (in increasing order of x_{nose} then decreasing order of p_d) 80

LIST OF FIGURES

Figure		Page
1.1	Progress of a normal shock through a test section with a model (Figure 1:26 from Ref. [1])	2
1.2	Largest possible model diameter versus upstream Mach number to allow starting the flow in a supersonic tunnel (Figure 1:27 from Ref. [1])	4
1.3	Progression of boundary-layer separation (Fig. 4-5 from Ref. [5])	5
1.4	Conceptual drawing of velocity profiles for a laminar or turbulent boundary layer (Fig. 15.6 from Ref. [6])	6
1.5	Conceptual drawing of boundary layer separating due to impingement of strong incident shock (Fig. 7.13 from Ref. [7])	7
2.1	Schematic of the original BAM6QT setup	10
2.2	Schematic of the modified BAM6QT setup	11
2.3	Original sting-support and diffuser sections	12
2.4	Schematic of original sting-support and diffuser sections with test section. Dimensions in inches.	12
2.5	Junction of modified sting-support and diffuser sections with tunnel test section	14
2.6	Schematic of modified sting-support and diffuser sections with test section. Dimensions in inches.	14
2.7	Sphere-cone model used on blockage tests (top row left to right: 2.25-inch disk, 2.5-inch disk, 2.75-inch disk, and retaining nut; middle row: 2-inch sphere-cone model)	15
3.1	Close-up of model nose showing Kulite Pressure transducer	17
3.2	Hot-film array at downstream end of nozzle (Fig. 2.14 from Ref. [10])	18
3.3	Schematic of hot-film array (Fig. 2.13 from Ref. [10])	18
3.4	Tektronix oscilloscopes and Bruhn 6 constant-temperature anemometer (left to right: Tektronix TDS 7104, Tektronix DPO 7054, Bruhn 6 CTA)	19
3.5	Close-up schematic of bow shock created from a blunt sphere-cone model	21

Figure Page

4.1 Schematic of original tunnel configuration with sphere-cone model showing concept for oscillating flow. Dimensions in inches. 23

4.2 Contraction and nose pressure for 2-inch model under quiet conditions (p_d = 181.8 psia, p_v = 3.2 torr, Date: 29 March 2007, $p_{max,quiet}$ = 150 psia) 24

4.3 Uncalibrated hot-films located 7.5 inches apart on nozzle wall for 2-inch model under quiet conditions (p_d = 181.7 psia, p_v = 3.2 torr, Date: 29 March 2007, $p_{max,quiet}$ = 150 psia)..... 24

4.4 Noise level and Mach number for 2-inch model under quiet conditions (p_d = 181.8 psia, p_v = 3.2 torr, Date: 29 March 2007, $p_{max,quiet}$ = 150 psia) 25

4.5 Contraction and nose pressure for 2-inch model under quiet conditions (p_d = 85.6 psia, p_v = 3 torr, Date: 23 August, $p_{max,quiet}$ = 80 psia) 26

4.6 Noise level and Mach number for 2-inch model under quiet conditions (p_d = 85.6 psia, p_v = 3 torr, Date: 23 August 2007, $p_{max,quiet}$ = 80 psia) 28

4.7 Contraction and nose pressure for 2-inch model under quiet conditions (p_d = 40.6 psia, p_v = 6.5 torr, Date: 30 March 2007, $p_{max,quiet}$ = 150 psia) 29

4.8 Noise level and Mach number for 2-inch model under quiet conditions (p_d = 40.4 psia, p_v = 6.5 torr, Date: 29 March 2007, $p_{max,quiet}$ = 150 psia) 30

4.9 Contraction and nose pressure for 2.25-inch model under quiet conditions (p_d = 181.3 psia, p_v = 3.8 torr, Date: 16 October 2007, $p_{max,quiet}$ = 140 psia) 31

4.10 Noise level and Mach number for 2.25-inch model under quiet conditions (p_d = 181.3 psia, p_v = 3.8 torr, Date: 16 October 2007, $p_{max,quiet}$ = 140 psia) 32

4.11 Contraction and nose pressure for 2.25-inch model under quiet conditions (p_d = 142.1 psia, p_v = 2.5 torr, Date: 16 October 2007, $p_{max,quiet}$ = 140 psia) 33

4.12 Noise level and Mach number for 2.25-inch model under quiet conditions (p_d = 142.1 psia, p_v = 2.5 torr, Date: 16 October 2007, $p_{max,quiet}$ = 140 psia) 35

4.13 Contraction and nose pressure for 2.25-inch model under quiet conditions (p_d = 41.9 psia, p_v = 2.8 torr, Date: 17 October 2007, $p_{max,quiet}$ = 140 psia) 36

4.14 Noise level and Mach number for 2.25-inch model with open bleed (p_d = 41.9 psia, p_v = 2.8 torr, Date: 17 October 2007, $p_{max,quiet}$ = 140 psia) 37

4.15 Contraction and nose pressure for 2.5-inch model under quiet conditions (p_d = 140.8 psia, p_v = 1.15 torr, Date: 19 October 2007, $p_{max,quiet}$ = 140 psia) 39

4.16 Noise level and Mach number for 2.5-inch model under quiet conditions (p_d = 140.8 psia, p_v = 1.15 torr, Date: 19 October 2007, $p_{max,quiet}$ = 140 psia) 40

4.17 Contraction and nose pressure for 2.5-inch model under quiet conditions (p_d = 141.9 psia, p_v = 1.5 torr, Date: 16 October 2007, $p_{max,quiet}$ = 140 psia) 41

4.18 Contraction and nose pressure for 2-inch model under noisy conditions (p_d = 90.8 psia, p_v = 4.5 torr, Date: 21 July 2007, $p_{max,quiet}$ = 75 psia)..... 42

Figure Page

4.19 Noise level and Mach number for 2.25-inch model under noisy conditions (p_d = 90.8 psia, p_v = 4.5 torr, Date: 21 July 2007, $p_{max,quiet}$ = 75 psia) 43

4.20 Contraction and nose pressure for 2-inch model under noisy conditions (p_d = 89.2 psia, p_v = 16 torr, Date: 21 July 2007, $p_{max,quiet}$ = 75 psia) 44

4.21 Contraction and nose pressure for 2-inch model under noisy conditions (p_d = 89.5 psia, p_v = 4.5 torr, Date: 13 September 2007, $p_{max,quiet}$ = 60 psia) 45

4.22 Starting performance of the original tunnel configuration 46

4.23 Summary of the starting performance of the 2-inch and 2.25-inch models under quiet conditions in the original tunnel configuration 47

4.24 Summary of the starting performance of the 2.5-inch and 2.75-inch models under quiet conditions in the original tunnel configuration 48

4.25 Summary of the starting performance of the 2-inch model under noisy conditions in the original tunnel configuration 49

4.26 Schematic of modified tunnel configuration with sphere-cone model 50

4.27 Contraction and nose pressure for 2-inch model under quiet conditions and model nose located at the downstream end of the expansion ramp (p_d = 142.6 psia, p_v = 0.58 torr, Date: 1 February 2008, $p_{max,quiet}$ = 140 psia) 51

4.28 Contraction and nose pressure for 2-inch model under quiet conditions and model nose located 8.375 inches upstream of nozzle exit (p_d = 141.7 psia, p_v = 0.85 torr, Date: 31 January 2008, $p_{max,quiet}$ = 140 psia) 52

4.29 Noise level and Mach number for 2-inch model located 8.375 inches upstream of nozzle exit under quiet conditions (p_d = 141.7 psia, p_v = 0.85 torr, Date: 31 January 2008, $p_{max,quiet}$ = 140 psia) 53

4.30 Contraction and nose pressure for 2-inch model under quiet conditions and model nose located 10.125 inches upstream of nozzle exit (p_d = 139.7 psia, p_v = 3.35 torr, Date: 31 January 2008, $p_{max,quiet}$ = 140 psia) 54

4.31 Noise level and Mach number for model located 10.125 inches upstream of nozzle exit under quiet conditions (p_d = 139.7 psia, p_v = 3.35 torr, Date: 31 January 2008, $p_{max,quiet}$ = 140 psia) 55

4.32 Starting performance of the modified tunnel configuration with the model placed 10.25 inches upstream of nozzle exit 57

5.1 Schematic of 9-degree nylon insert in modified tunnel section 59

5.2 Schematic of steel straight-pipe insert in modified tunnel section. Dimensions in inches. 60

A.1 Close-up view of contraction and nose pressure traces for 2-inch model under quiet conditions (p_d = 40.6 psia, p_v = 6.5 torr, Date: 30 March 2007, $p_{max,quiet}$ = 150 psia) 64

Figure Page

A.2 Fast Fourier transform of nose pressure trace for 2-inch model under quiet conditions (p_d = 40.6 psia, p_v = 6.5 torr, Date: 30 March 2007, $p_{max,quiet}$ = 150 psia) 64

A.3 Close-up view of contraction and nose pressure traces for 2.25-inch model under quiet conditions (p_d = 142.1 psia, p_v = 2.5 torr, Date: 16 October 2007, $p_{max,quiet}$ = 140 psia) 66

A.4 Fast Fourier transform of nose pressure trace for 2.25-inch model under quiet conditions (p_d = 142.1 psia, p_v = 2.5 torr, Date: 16 October 2007, $p_{max,quiet}$ = 140 psia) 66

A.5 Close-up view of contraction and nose pressure traces for 2-inch model under noisy conditions (p_d = 123.6 psia, p_v = 4.1 torr, Date: 13 September 2007, $p_{max,quiet}$ = 60 psia) 68

A.6 Fast Fourier transform of nose pressure trace for 2-inch model under noisy conditions (p_d = 123.6 psia, p_v = 4.1 torr, Date: 13 September 2007, $p_{max,quiet}$ = 60 psia) 68

A.7 Close-up view of contraction and nose pressure traces for 2-inch model under quiet conditions at nozzle exit (p_d = 142.6 psia, p_v = 0.58 torr, Date: 1 February 2008, $p_{max,quiet}$ = 140 psia) 69

A.8 Close-up of uncalibrated hot-film traces for 2-inch model under quiet conditions at nozzle exit (p_d = 142.6 psia, p_v = 0.58 torr, Date: 1 February 2008, $p_{max,quiet}$ = 140 psia) 70

A.9 Fast Fourier transform of nose pressure trace for 2-inch model under quiet conditions at nozzle exit (p_d = 142.6 psia, p_v = 0.58 torr, Date: 1 February 2008, $p_{max,quiet}$ = 140 psia) 70

C.1 Schematic of 2-inch-diameter model. Dimensions in inches. 81

C.2 Schematic of sphere cone base diameter additions (left to right: 2.25 inch, 2.5 inch, 2.75 inch outer diameter). Dimensions in inches. 81

D.1 Fast valve installed in BAM6QT bleed line 82

D.2 Close-up view of augmented El-O-Matic actuator 83

D.3 Schematic of El-O-Matic actuator [15] 84

D.4 Schematic of Versa valve (left to right: valve-closed position, valve-open position) [16] 85

D.5 Exterior of fast valve electronics box 86

D.6 Schematic of fast-valve circuit 88

D.7 Summary of fast-valve response at different driver-tube pressures 89

D.8 Measured response of fast valve at low Reynolds number (p_d = 41.9 psia, p_v = 2.8 torr, Date: 17 October 2007, $p_{max,quiet}$ = 140 psia) 90

Figure Page

D.9 Crossbar support system connected to larger flanges on modified tunnel configuration 92

D.10 Schematic of support structure for the 25-½" outer diameter flanges of the new sections. Dimensions in inches. 92

D.11 Modified trolleys at the junction between the adapter flange and sting-support section 94

D.12 Modified-trolley ball bearings on bottom face of support I-beam 94

D.13 Slot machined at top center of adapter flange and upstream flange of new sting-support section. Dimensions in inches. [18] 95

D.14 Schematic of 1.5 inch wide modified traverse bar. Dimensions in inches. 96

SYMBOLS

A	cross-sectional area
d	diameter
F	frequency
M	Mach number
p	pressure
$R(x)$	root-mean-square (rms)
T	period
t	time
u	streamwise velocity
x	streamwise location (measured in inches upstream of the nozzle exit)
y	radial location
δ	boundary layer thickness
γ	ratio of specific heats (1.4 for air)
λ	stagnation-to-back pressure ratio (p_0/p_b) of the freestream flow
#	run number from the typically one-week tunnel entry

Superscripts

*	sonic value
rms	root-mean-square value
mean	mean value
nose	model nose

Subscripts

0	stagnation value (as a function of time)
1	pre-shock wave value
2	post-shock wave value
b	back or vacuum conditions (as a function of time)
d	initial driver tube conditions
fv	conditions near the fast-valve location
max	maximum value
pl	bleed-slot-plenum conditions
quiet	quiet conditions
sep	separated portion (of tunnel run)
unstart	unstarted portion (of tunnel run)
v	initial vacuum conditions
∞	freestream conditions

Acronyms

AAE	Aeronautics and Astronautics Engineering
ASL	Aerospace Sciences Laboratory
BAM6QT	Boeing/AFOSR Mach-6 Quiet Tunnel
FFT	Fast Fourier Transform
RMS	Root Mean Square

ABSTRACT

Hannon, Jr., Michael J. M.S.A.A., Purdue University, August, 2008. Evaluation of Diffuser Modifications for the Boeing/AFOSR Mach-6 Quiet Tunnel. Major Professor: Steven P. Schneider.

Experiments performed in the BAM6QT have used mostly slender, streamlined models. However, it is more difficult to start blunt models in this and other tunnels. This is due to blockage of the flow from the model and to complications created by the interaction of the bow shock from the model and the nozzle-wall boundary layers. Nonetheless, testing the largest possible blunt models is important to re-entry vehicles such as the Apollo and Orion capsules. Thus, tests were performed from March 2007 to October 2007 to determine the starting capabilities of the tunnel using a sphere cone with a 70-degree half angle and variable base diameter. These tests resulted in a maximum starting diameter of 2.5 inches in quiet flow and nearly 2 inches in noisy flow. In an attempt to improve this performance, larger sting-support and diffuser sections were installed in December 2007. These sections would allow the bow shock from the model to impinge on the flow downstream of an expansion at the end of the test section. This adjustment would hopefully prevent any disturbances from separating the boundary layer upstream and unstarting the flow when placing the model downstream of the test section. Unfortunately, the initial modification with a 45-degree expansion only worsened the starting performance. The maximum starting model size in quiet and noisy flow remained the same when moving the model far forward in the test section. However, the flow unstarted a 2-inch model when running with the model downstream of the test section in quiet and noisy flow.

1 INTRODUCTION

1.1 Objective

Experimental measurements on blunt models are helpful for vehicles such as the Apollo, Orion or other re-entry capsules. During re-entry, these vehicles see hypersonic speeds and low freestream noise. Changes in freestream noise have been known to influence hypersonic boundary-layer transition on vehicle models tested in wind tunnels. These changes in transition have large implications in properties such as heating and skin-friction drag. Historically, experimental data with low freestream noise levels have been recorded using very expensive flight tests. Thus, a hypersonic quiet-tunnel facility could give insightful and inexpensive data that may influence the construction of future blunt vehicles. Currently, the BAM6QT is the only operational hypersonic quiet tunnel in the world, but its abilities to run blunt models is limited. In an attempt to improve the tunnel performance, larger sting-support and diffuser sections were built and tested. The purpose of this current thesis is to evaluate the starting performance before and after the installation of the new sections.

1.2 Analytical Approach to the Starting Problem

When running blunt models in a supersonic wind tunnel, the blockage created by the model as well as the interaction of the bow shock from the model and the boundary layers along the tunnel walls may prevent the flow from becoming supersonic. When this occurs, the flow is said to have “unstarted”. Unfortunately, there is very little literature on this subject, since, more often than not, the interest from each wind-tunnel research group is merely to start the flow in their respective facilities. Nonetheless, Pope and Goin [1] briefly discuss the matter and give a

broad description of the starting problem. Figure 1.1 gives a qualitative inviscid analysis of a normal shock traveling through the test section of a supersonic tunnel with a model placed inside. Under these conditions, the main constraint on the starting performance of the tunnel is the blockage in the flow created by the model. In a constant-area test section, the effective flow area is smallest at the streamwise location where the cross-sectional area of the model is largest. If at this location the effective flow area is sufficiently small, the flow chokes, and the normal shock is no longer able to travel downstream of the model. As a result, the flow will not reach supersonic speeds. This is the conventional definition of an unstarted run in a supersonic tunnel. During typical started runs, the flow remains supersonic until the falling ratio of stagnation-to-back-pressure, λ, causes a normal shock to travel upstream of the model. This process is seen by reversing the order of the tunnel run segments shown on Figure 1.1 (from d. to a.).

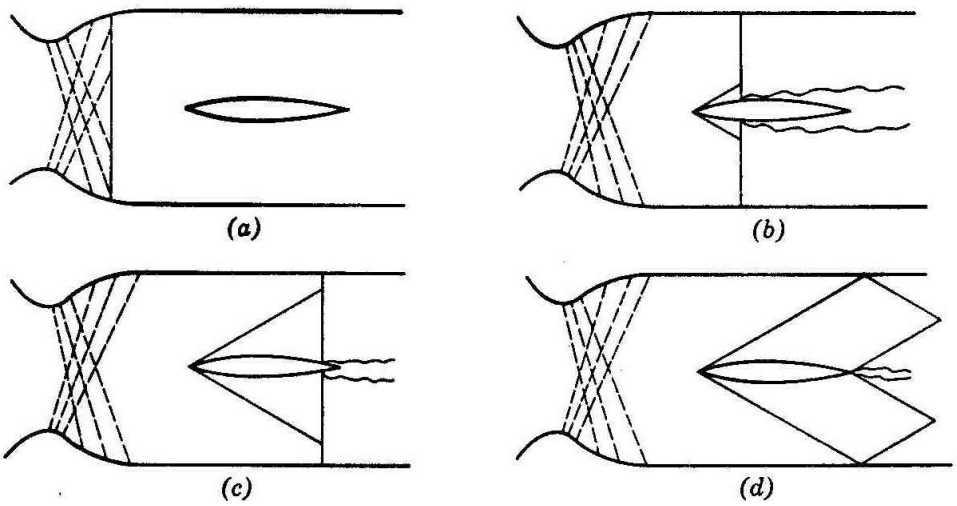

Figure 1.1. Progress of a normal shock through a test section with a model (Figure 1:26 from Ref. [1])

This analysis of conventional unstarting of tunnel flows can be performed analytically by equating the mass flow of the air upstream of the normal shock to that of the air downstream of the shock. When simplifying, equation 1.1 is obtained.

$$\frac{A_2^*}{A_1^*} = \frac{p_{0,1}}{p_{0,2}} \tag{1.1}$$

Since the total pressure loss across a normal shock is dependent on the upstream Mach number, an expression can be made relating the largest possible diameter of a model in a supersonic wind tunnel to the freestream Mach number. Figure 1.2 shows a plot of the largest model size to start in a supersonic tunnel based on its design Mach number. Note that the line labeled “theory” is based on this analytical analysis, while the other line labeled “actual” was determined based on empirical results using blunt models in various wind tunnels [3]. This analysis would say that sharp and blunt cones of same base area start with the same maximum size, but, due to viscous effects, they do not. Note also that the test-section area of the wind tunnel, *A*, in Figure 1.2 refers to the area of the inviscid core, meaning the inner area of the test section after subtracting the area of the nozzle-wall boundary layer. Since laminar boundary layers are thinner than turbulent boundary layers [4], the inviscid core area is smaller in conventional noisy tunnels, which have turbulent boundary layers on the walls of the test section. Taking this increased blockage into account, one would expect larger models to start in a quiet tunnel, with laminar boundary layers on the tunnel walls [2]. However, as will be shown in sections 1.3 and 1.4, more effects need be taken into account before making such an assessment.

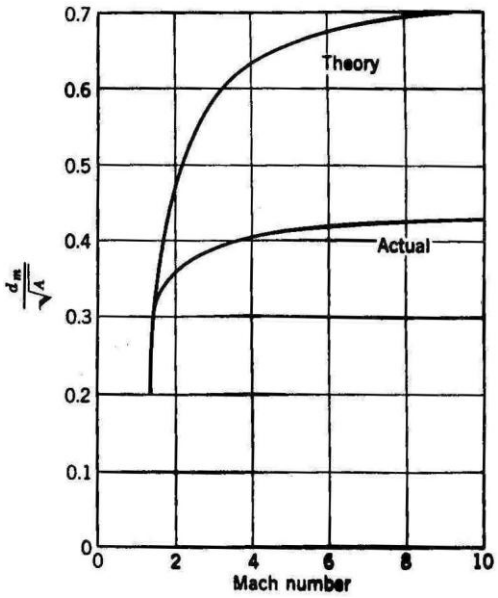

Figure 1.2. Largest possible model diameter versus upstream Mach number to allow starting the flow in a supersonic tunnel (Figure 1:27 from Ref. [1])

1.3 Boundary-Layer Separation

It is also possible for the flow to become only partially supersonic due to large separated regions near the wall. Another form of blockage in the flow comes from separation of the nozzle-wall boundary layers caused by adverse pressure gradients. Figure 1.3 gives a conceptual drawing of the velocity profile of a boundary layer on a flat plate [5]. Figure 1.3 (a) shows that when the pressure gradient is favorable, the boundary layer remains thinnest and attached to the surface. However, as the pressure gradient becomes adverse the velocity profile of the boundary layer weakens near the surface. As the pressure gradient becomes more adverse, the profile contains a point of inflection and is on the brink of separation. Figure 1.3 (b) shows the effect of an increasingly adverse pressure gradient on the boundary layer. This increase in pressure causes the velocity to continue to drop until the velocity gradient decreases to zero at the surface, which is the inception of separation. After this point, the velocity near the surface points in the opposite direction of the freestream, and an area of re-circulating flow is created. Note that the thickness of the boundary layer increases as the adverse pressure gradient rises.

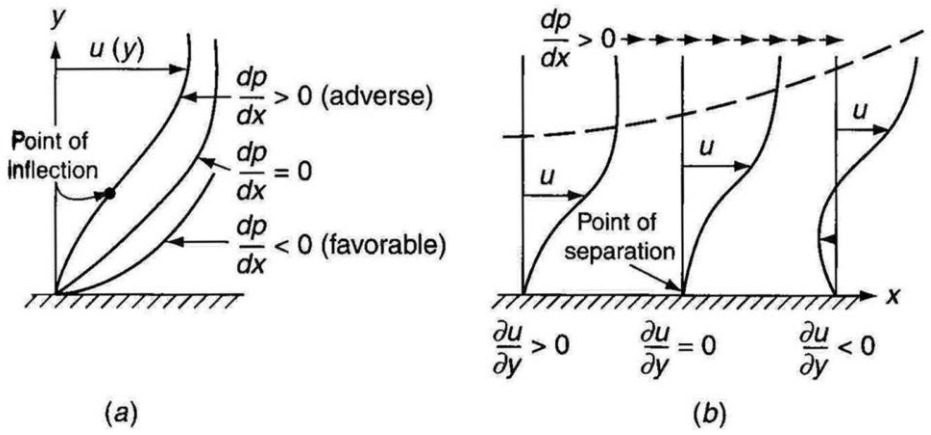

Figure 1.3. Progression of boundary-layer separation (Fig. 4-5 from Ref. [5])

Lastly, one must consider the tendency of a laminar or turbulent boundary layer to separate. Figure 1.4 shows the difference in velocity profiles between the two types of boundary layers. Due to the momentum mixing effect [6] the turbulent velocity profile is fuller closer to the surface. Thus, turbulent boundary layers are less prone to separate since they require stronger adverse pressure gradients to counteract the higher velocities near the surface. Conversely, laminar boundary-layer velocity profiles are less full near the surface, meaning they are much more prone to separate due to adverse pressure gradients. Due to this effect, one would expect that a conventional tunnel with turbulent boundary layers on the walls of the test section would be more difficult to unstart than a quiet tunnel with laminar boundary layers.

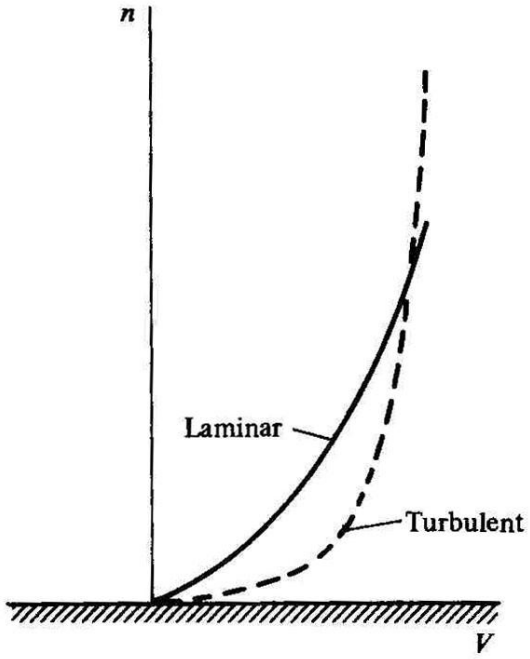

Figure 1.4. Conceptual drawing of velocity profiles for a laminar or turbulent boundary layer (Fig. 15.6 from Ref. [6])

1.4 Shock-Boundary Layer Interaction on the Tunnel Walls

Differences in the theoretical and empirical values for the maximum model diameter in Figure 1.2 can be attributed to the interaction of the bow shock from the blunt model and the tunnel-wall boundary layer. A strong shock impinging on the boundary layer creates a highly adverse pressure gradient, which may cause the boundary layer to separate from the surface. If this separation creates enough blockage in the flow of the tunnel, it could cause the flow around the model to choke. This separated flow could also feed upstream and cause separation throughout the entire tunnel-wall boundary layer. Figure 1.5 shows a conceptual drawing of the effects of a shock-boundary layer interaction. This interaction is complex. However, it is safe to say that flow blockage from such a disturbance could have a strong effect on the starting performance of blunt models in any supersonic tunnel. And although this might not necessarily cause the flow in the tunnel to unstart in the conventional sense mentioned above, it still results in disturbed flow from which meaningful data cannot be obtained.

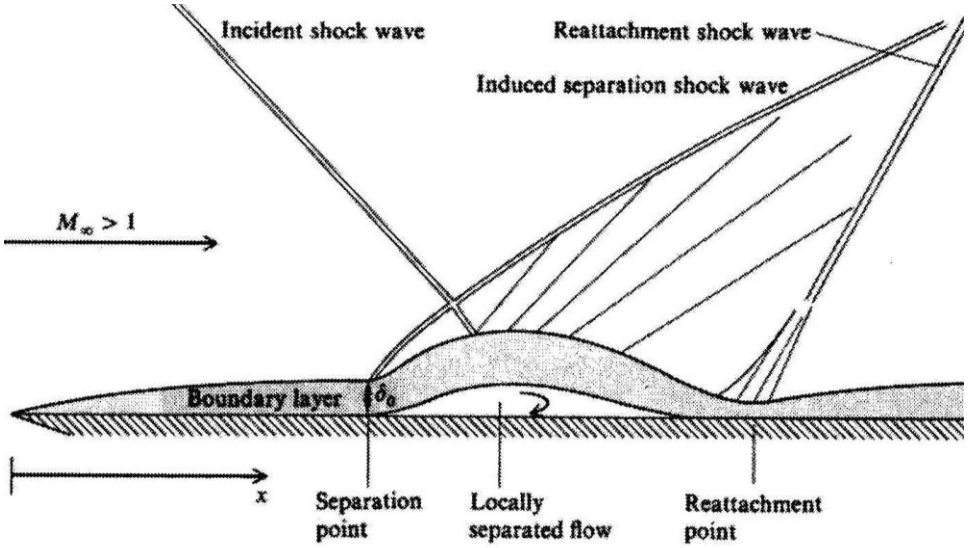

Figure 1.5. Conceptual drawing of boundary layer separating due to impingement of strong incident shock (Fig. 7.13 from Ref. [7])

1.5 Suggestions for Improved Starting Performance

In addition to the analytical analysis given on Figure 1.2, Ref. [1] also provides a list of suggestions for improving starting performance of a high-speed wind tunnel. These suggestions are listed below.

1. Moving the model forward in the test section.
2. Squirting a spray of water into the stagnation chamber.
3. Adding an afterbody to the model.
4. Blowing air out of holes near the nozzle throat.
5. Increasing the diffuser area.
6. Increasing the tunnel pressure ratio, λ.
7. Adding a removable sharp nose to the model.

Note that this reference also mentions the importance of visual experimental techniques such as a Schlieren or shadowgraph to determine any likely causes for unstarting the tunnel. While this would be most helpful, such capabilities are not yet available in the BAM6QT.

2 APPARATUS

2.1 The Mach-6 Quiet Tunnel

All experiments were performed in the Boeing/AFOSR Mach-6 Quiet Tunnel, located at the Aerospace Sciences Laboratory on the campus of Purdue University. The BAM6QT is a Ludwieg Tube facility with clean, dry air pressurized in all sections upstream of the double diaphragm section shown on Figure 2.1. Piping downstream of this section leads to a 4000 cubic foot vacuum tank where the air can be evacuated to about 0.5 torr. The nozzle expands to a 9.5 inch inner diameter at its downstream end, which is used as the test section. In the original configuration, this leads to a straight sting-support section and a diffuser section that expands to a 12-inch inner diameter. In order to better control the initial stagnation pressure in the tunnel, air in the gap between two diaphragms is held to half the upstream driver-tube pressure. When suitable initial conditions are met, a tunnel run is performed by evacuating the air in the gap until the pressure difference across the upstream diaphragm bursts it, causing the downstream diaphragm to burst as well.

In order to run with quiet flow, a number of additional tasks had to be performed [2]. The bleed-slot plumbing evacuates the boundary layers on the upstream end of the throat, allowing a new boundary layer to develop on the nozzle walls. These walls are polished to a mirror finish to reduce any roughness on the walls that may trip the boundary layer. The diverging nozzle is 102 inches long with a 4-degree-maximum divergence angle. This long and slender nozzle diminishes Görtler instabilities by reducing the curvature of the wall. The air pressurized in the tunnel is highly filtered to eliminate any contaminants which may damage the throat. Also, since this is a Ludwieg-tube facility, there are fewer disturbances in the freestream flow that could help cause boundary-layer transition on the nozzle walls.

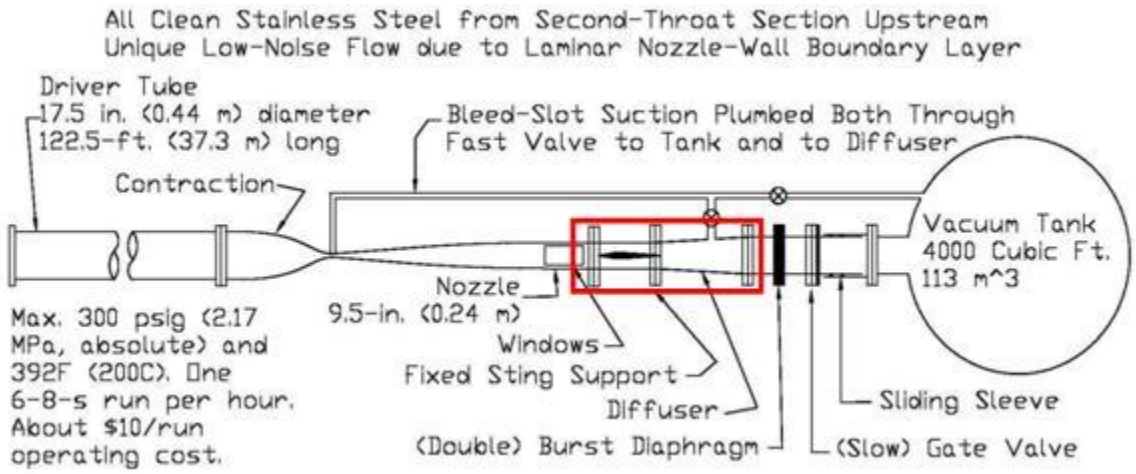

Figure 2.1. Schematic of the original BAM6QT setup

Midway through these experiments the setup of the tunnel was amended to allow an expanded sting-support and diffuser section, in an attempt to improve starting performance. The reasoning for this will be explained in section 4.2. Figure 2.2 shows a schematic of the modified tunnel setup. Note also the removal of the additional bleed line to the diffuser section. When running with bleeds open in previous experiments air bled from the throat was ducted to the diffuser instead of directly to the vacuum tank due to poor performance of the fast valve in the bleed line. This fast valve was replaced to have a quicker response, and all experiments performed with the modified tunnel configuration ran bleed air directly to the vacuum tank through the new fast-acting valve. Appendix D.1 gives a description of the operation and performance of the new valve.

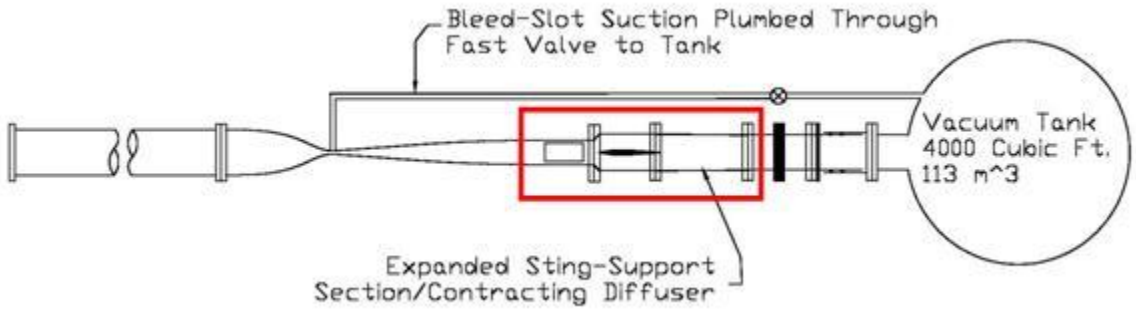

Figure 2.2. Schematic of the modified BAM6QT setup

2.2 Original Sting-Support/Diffuser Section

The original tunnel configuration contained a straight sting-support section immediately downstream of the nozzle exit. Since the inner diameter of the nozzle is approximately 9.5 inches at the test section, the sting-support section has a 9.5 inch inner diameter as well. This diameter is held constant throughout the entire length of the sting-support section until reaching the diffuser section. The diffuser section then has a gradual expansion to a 12-inch inner diameter at the downstream end [8]. The remaining piping for the tunnel—consisting of the diaphragm section, gate valve, sliding sleeve and pipes leading to the vacuum tank—is held at a constant inner diameter of 12 inches. Figure 2.3 shows a picture of the original sting-support and diffuser sections. This figure also shows the flexible hose from the bleed system connected to the diffuser, which is shown on Figure 2.1. The system running bleed-air straight to the diffuser, called the “passive bleed system,” was used until a suitable system running the bleed air straight to the vacuum tank was devised. Figure 2.4 gives a schematic of the original tunnel configuration.

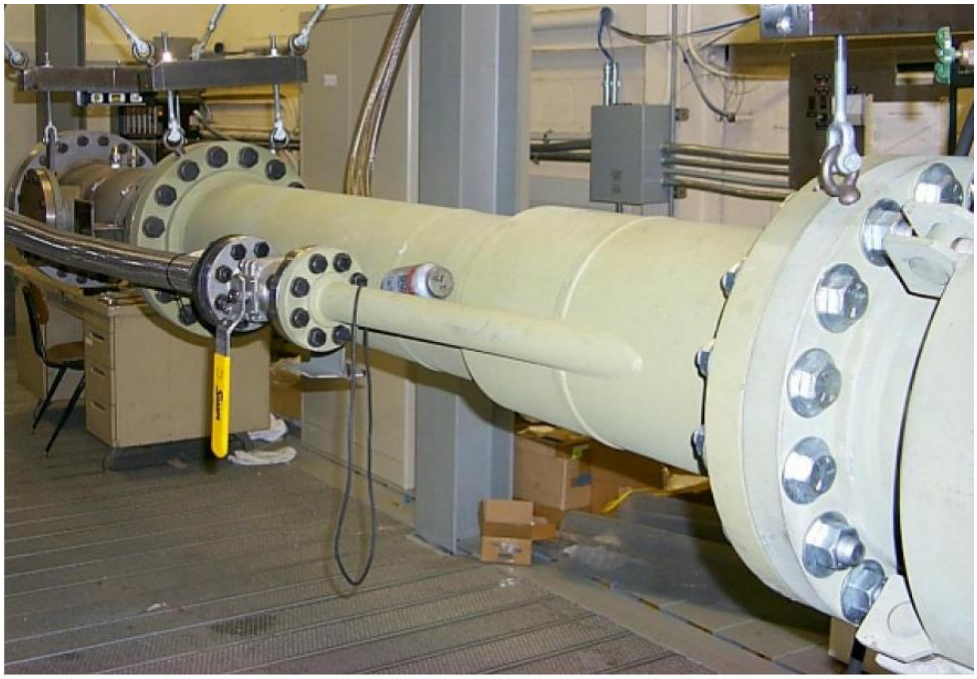

Figure 2.3. Original sting-support and diffuser sections

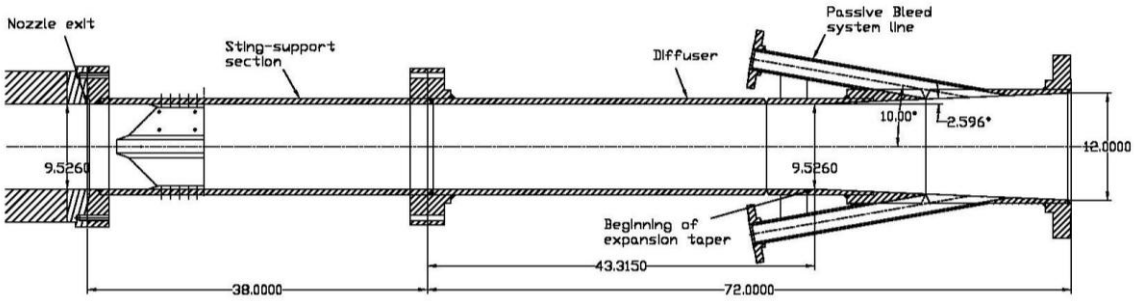

Figure 2.4. Schematic of original sting-support and diffuser sections with test section. Dimensions in inches.

2.3 Modified Sting-Support/Diffuser Section

The modified tunnel configuration contains a larger sting-support section immediately downstream of the nozzle exit. Instead of holding a constant inner diameter of 9.5 inches, there is an adapter flange attached at the end of the nozzle with a 45° expansion to an inner diameter of 14.125 inches. This inner diameter is held constant throughout the entire length of the sting-support section until reaching the new diffuser section. The diffuser section then has a contraction taper of approximately 0.9° throughout the entire length, reaching an inner diameter of 12 inches at the downstream end. This section connects to the remaining downstream sections of the original tunnel configuration. Figure 2.5 is a close-up image of the nozzle, adapter flange, new sting-support section and the upstream end of the new diffuser. The original intent of the new sections was to add inserts downstream of the nozzle exit to control the flow. However, delays in building the new sections caused the present thesis to be completed before results from these inserts could be included. Note that the new diffuser section has no flexible hose connecting it to the bleed system. This change in the bleed system is shown on Figure 2.2. The system running bleed-air straight to the vacuum tank, called the “active bleed system,” is now used all the time. Figure 2.6 gives a schematic of the modified tunnel setup.

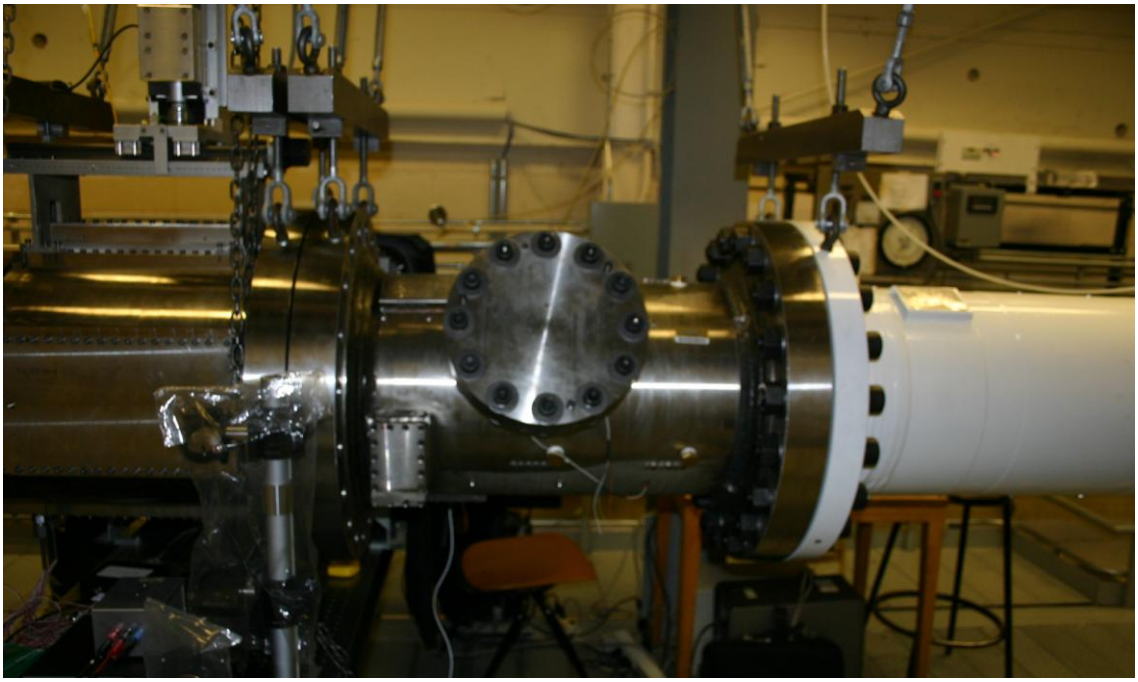

Figure 2.5. Junction of modified sting-support and diffuser sections with tunnel test section

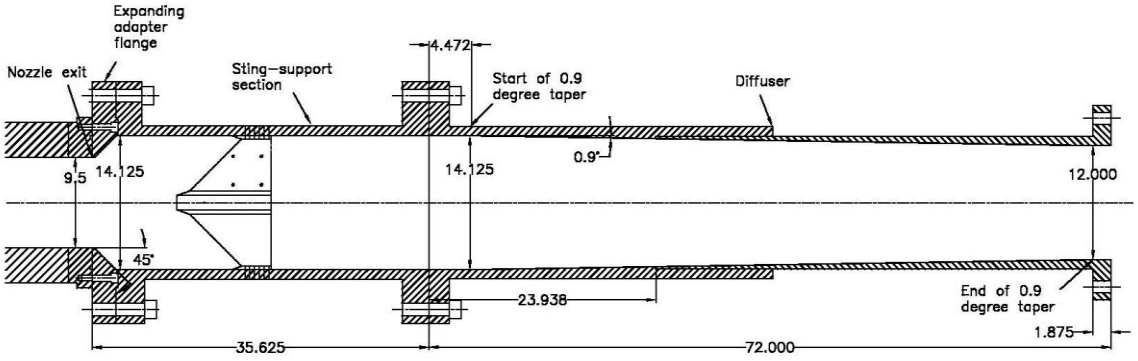

Figure 2.6. Schematic of modified sting-support and diffuser sections with test section. Dimensions in inches.

2.4 Sphere-Cone Model

To measure the blunt-model starting performance of the tunnel, a 70º half-angle sphere cone with variable base diameter was used. The spherical nose of this model has a 2.9-inch radius of curvature. This shape roughly approximates any blunt capsule shape that may be of interest for testing in the tunnel. Starting with a 2-inch base diameter, discs enable increasing the base diameter in increments of 0.25 inches to 2.75 inches. Figure 2.7 shows the blunt model as well as the various additions. It fits the 1.5-inch sting currently used in the tunnel. This model was placed on the centerline of the tunnel for all experiments. For a more detailed description of the dimensions of the model, see Appendix C.

Figure 2.7. Sphere-cone model used on blockage tests (top row left to right: 2.25-inch disk, 2.5-inch disk, 2.75-inch disk, and retaining nut; middle row: 2-inch sphere-cone model)

3 MEASUREMENT AND CALCULATION TECHNIQUES

3.1 Kulite Pressure Transducers

A Kulite pressure transducer was placed at the nose of the model to determine the stagnation-point pressure, which is the indicator of the starting performance of the tunnel. Figure 3.1 shows a close-up view of the front face of the 2-inch-base-diameter model with the pressure transducer installed at the nose. Kulite model XCQ-062-15A transducers were used throughout these tests. At first, serial number model 6217-2A-276 was used. It had a range of 0 – 21 psia. However, this transducer malfunctioned in the middle of the experiments on 3 October 2007, and was replaced with serial number model 5867-8A-39, which has a range of 0 – 31 psia. Both of these pressure transducers contain a mechanical stop to shield the transducer hardware from higher pressures. This allows both the durability to handle higher pressures before startup along with providing more precise measurements at lower pressures during the run. Also, a Kulite model XTEL-190-200A transducer is located on the wall of the tunnel at the entrance of the contraction. Since the Mach number there is very low, measurements taken from this sensor provide an accurate measurement of the stagnation pressure of the flow throughout the run.

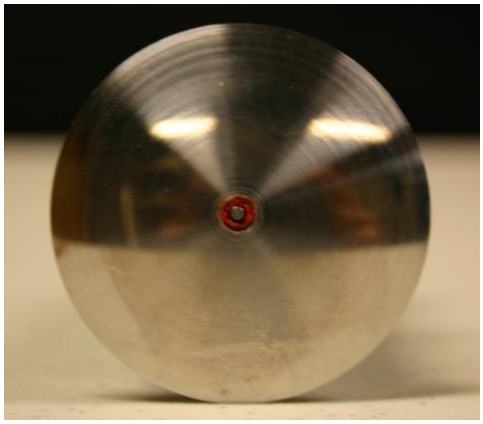

Figure 3.1. Close-up of model nose showing Kulite Pressure transducer

Custom electronics process the raw signal from the transducers. The signal from the transducer is amplified with a gain of 100 using an INA103 chip. The output is then used as the DC trace from the sensor. The sensors are calibrated using a Paroscientific, Inc. Model 740 Digiquartz Portable Standard pressure gauge. Note that the electronics are also designed to further amplify and high-pass filter the AC signal from the transducer to calculate the noise level in the pressure trace. This capability is primarily used to determine high-quality noise level measurements in quiet flow. However, the main objective of the present experiments was only to determine the starting performance of the tunnel, so precise quiet-flow measurements were not needed. Thus, any noise measurements were calculated directly from the less-precise DC trace. Further description of noise-level-calculation techniques will be given on section 3.4.

3.2 Hot Films

In order to determine the behavior of the nozzle-wall boundary layers, Dr. Craig Skoch installed a Senflex hot-film array on the bottom portion of the farthest downstream section of the nozzle [9]. Figure 3.2 shows this array in its test section location. The overheat ratio of the hot films is set by a custom-built Bruhn 6 Constant Temperature Anemometer. Although the hot films were not calibrated, differences in the flow when quiet, noisy, or separated can be qualitatively

determined. Figure 3.3 shows a schematic of the 9 inch long by 3 inch wide hot-film array. Depending on the conditions of each tunnel entry, one or two hot-film signals were recorded.

Figure 3.2. Hot-film array at downstream end of nozzle (Fig. 2.14 from Ref. [10])

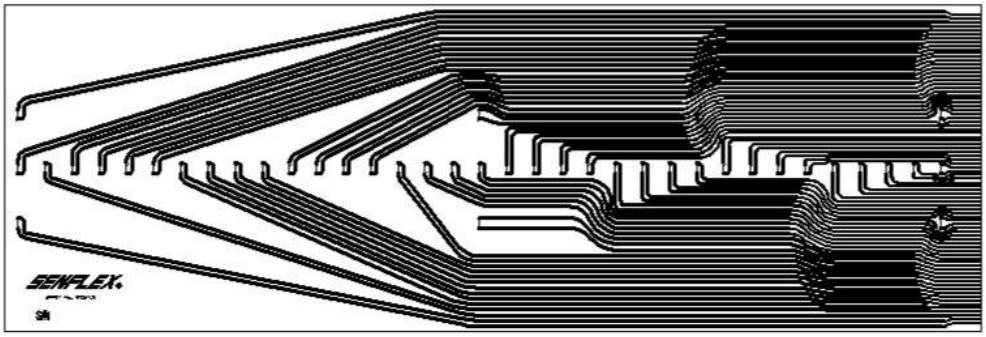

Figure 3.3. Schematic of hot-film array (Fig. 2.13 from Ref. [10])

3.3 Tektronix Oscilloscopes

Data were acquired using Tektronix DPO 7054 and Tektronix TDS 7104 oscilloscopes, each recording data on four separate channels. Since the Tektronix DPO 7054 has a longer record length than the TDS 7104 (approximately 50 megabytes per channel vs. 4 megabytes per channel), data from the hot films and model-nose pressure sensor were recorded on the DPO

7054. All other traces (i.e. the contraction pressure or other pressure readings) were recorded on the TDS 7104. Both scopes were run in High-Res mode, which acquires data at a higher frequency (10 gigahertz from the DPO 7054 and 1 gigahertz from the TDS 7104) and averages on the fly to save at the given sampling frequency with higher resolution.

The scopes were adjusted to capture an entire run, which historically has lasted around 7-9 seconds. Thus, unless otherwise noted, all traces obtained 10 seconds of data per run with a sampling frequency of 20 million samples per second on the DPO 7054 and 2 million samples per second on the TDS 7104. The first tenth of the data traces were recorded before the start of the run to determine pre-run electronics noise levels. Note that the DPO 7054 acquired more data points than necessary for this analysis. Thus, though entire 50-megabyte traces were saved from the oscilloscopes, only every tenth data point was plotted to reduce computational time when processing any data obtained from these experiments.

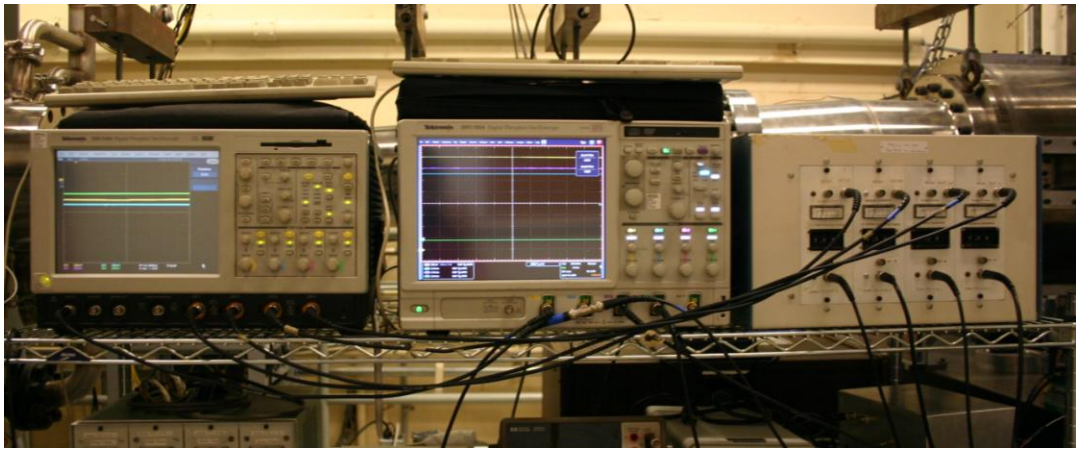

Figure 3.4. Tektronix oscilloscopes and Bruhn 6 constant-temperature anemometer (left to right: Tektronix TDS 7104, Tektronix DPO 7054, Bruhn 6 CTA)

3.4 Noise-Level-Calculation Technique

The noise in the model-nose pressure was assessed using the RMS divided by the mean. In order to determine the RMS fluctuations, a set of *n* pressure value data points are

averaged to acquire a mean. This mean value is then subtracted from each point to determine the fluctuations, x_i. The following function is used to determine the RMS ($R(x)$) [11].

$$R(x) = \sqrt{\frac{\sum_{i=1}^{n} x_i}{n}} \tag{3.1}$$

In all measurements taken from the nose-pressure data, the RMS level and mean value of the pressure trace is taken over 5000 points at a time. This equates to a period of 12.5 for a 5-second trace or 25 ms for a 10-second trace. Source code for this formula is given in Appendix E.1.

3.5 Mach-Number-Calculation Technique

To calculate the Mach number near the nose of the model, a normal shock is assumed to lie ahead of the model at the centerline where the pressure sensor is located. Figure 3.5 shows a schematic of a bow shock created from the blunt sphere-cone model. Under these conditions, the ratio of the upstream stagnation pressure ($p_{0,1}$) to the downstream stagnation pressure ($p_{0,2}$) is shown in equation 3.2. Note that this equation is a modified form of the Rayleigh Pitot formula given in Ref. [6]. Since $p_{0,1}$ is measured using the pressure sensor at the entrance of the contraction, and $p_{0,2}$ is measured with the sensor at the nose of the model, the Mach number can be calculated using this equation. However, since equation 3.2 cannot be solved for M analytically, a bisector root-finding method [12] is used to determine the freestream Mach number upstream of the bow shock from the model. For the source code used to calculate Mach number in this fashion, see Appendix E.2.

$$\frac{p_{0,1}}{p_{0,2}} = \left[1 + \frac{2\gamma}{\gamma+1}\left(M^2 - 1\right)\right]^{1/\gamma-1} \left[\frac{2 + (\gamma-1)M^2}{(\gamma+1)M^2}\right]^{\gamma/\gamma-1} \tag{3.2}$$

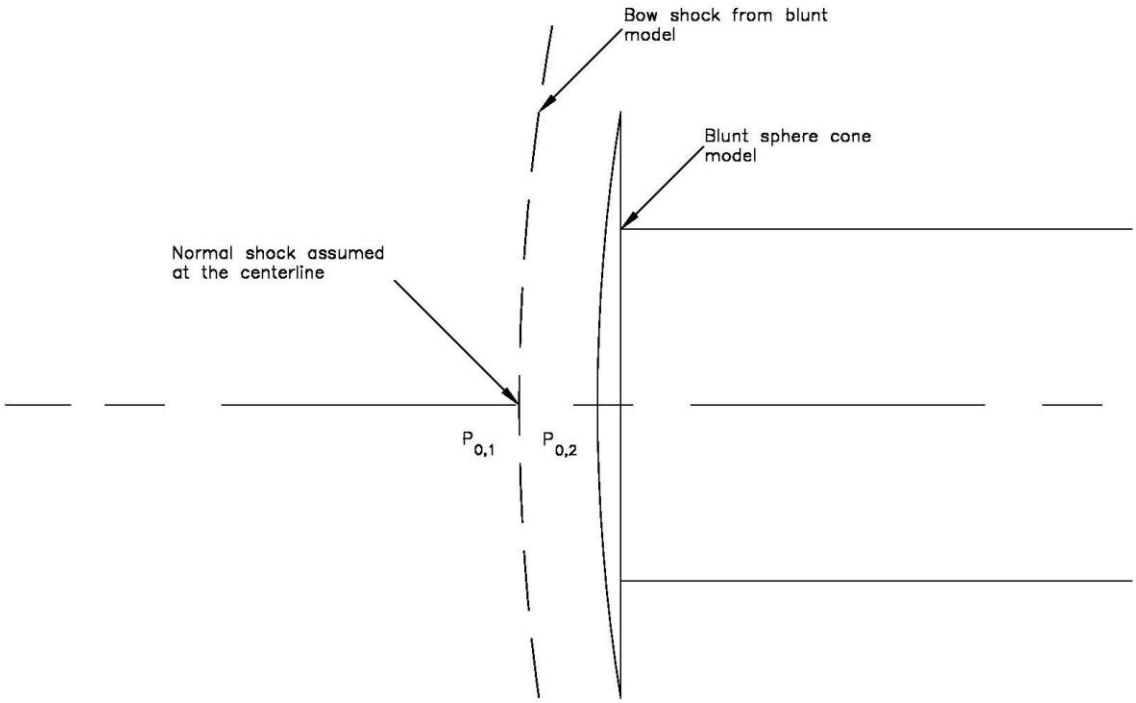

Figure 3.5. Close-up schematic of bow shock created from a blunt sphere-cone model

3.6 Calculating Technique for Fast Fourier Transform

In order to better detect periodic oscillations in the flow, a Fourier analysis is performed using a Hamming window and the Matlab *pwelch* command [13]. The window size for this analysis is set to ensure capturing multiple periodic oscillations, resulting in a clearer peak in the FFT plot. Typically, the 524288 (2^{19}) points are calculated over a one second window of the run. Source code for this application is given on Appendix E.3.

4 EXPERIMENTAL ANALYSIS

4.1 Original Tunnel Configuration

The sphere cone was placed 11 inches upstream of the nozzle exit plane and was held at this streamwise location throughout all experiments performed with the original tunnel configuration. At this location, the bow shock from the model interacts with the tunnel wall boundary layer inside the nozzle. When this interaction is weak enough, the model-nose pressure remains well-behaved, and the flow in the tunnel starts. However, this interaction can often generate unsteady boundary-layer separation. When these disturbances are strong enough, they will feed upstream and cause the boundary layer to oscillate erratically, leaving a fluctuating effective flow area. This causes the model-nose pressure to oscillate, rendering any experimental data useless. Figure 4.1 shows a schematic of this phenomena taking place in the original tunnel configuration. The shock or boundary-layer shapes are not meant to be conceived as accurate, but are to just give an idea of the basic flow characteristics under these conditions.

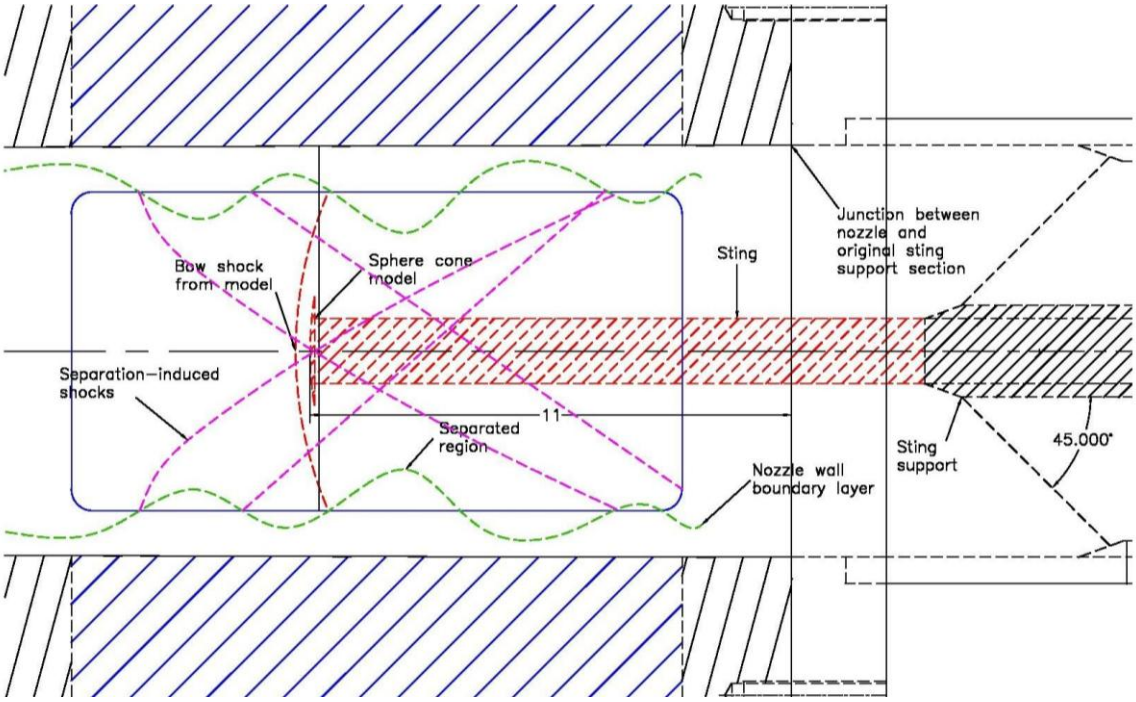

Figure 4.1. Schematic of original tunnel configuration with sphere-cone model showing concept for oscillating flow. Dimensions in inches.

4.1.1 2-Inch Model under Quiet Conditions

Figure 4.2 shows the pressure at the nose of the model along with the contraction pressure from a run with bleeds open. The nose pressure initially oscillates but the oscillations decrease midway through the run when the stagnation pressure drops to 150 psia. After this, there is about 0.25 seconds of noisy flow until another noticeable drop in oscillations occurs at a stagnation pressure around 147 psia. A period of reduced fluctuations then begins, with many turbulent spikes in the nose pressure that correspond to turbulent bursts on the boundary layers on the walls of the tunnel. This is shown in the hot-film traces of the same run plotted on Figure 4.3. Note that the “upstream hot film” (as labeled on Figure 4.3) is located 25.25 inches upstream of the exit of the nozzle, and the “downstream hot film” is located 7.5 inches downstream at 17.75 inches ahead of the nozzle exit.

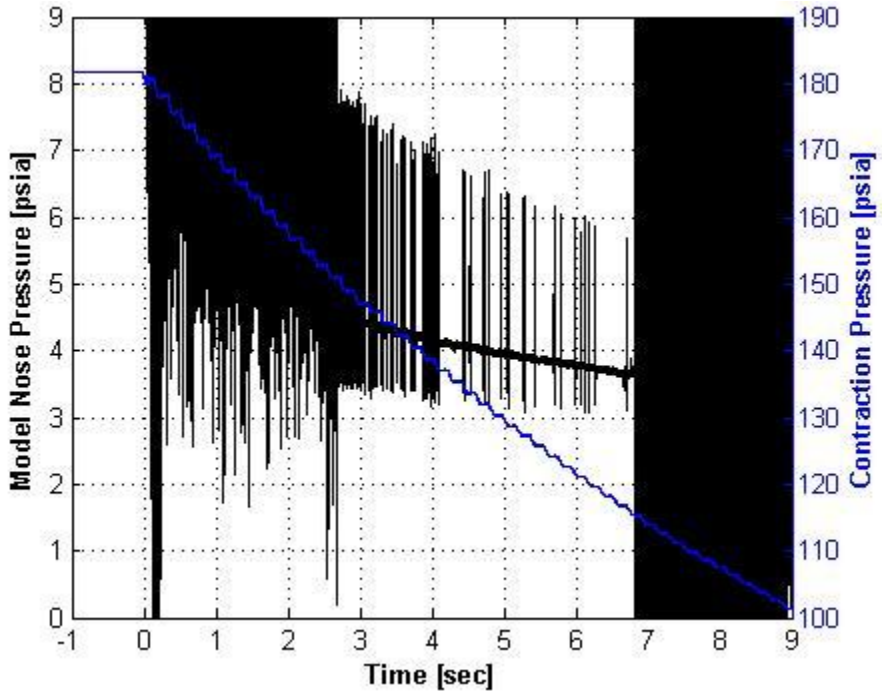

Figure 4.2. Contraction and nose pressure for 2-inch model under quiet conditions (p_d = 181.8 psia, p_v = 3.2 torr, Date: 29 March 2007, $p_{max,quiet}$ = 150 psia)

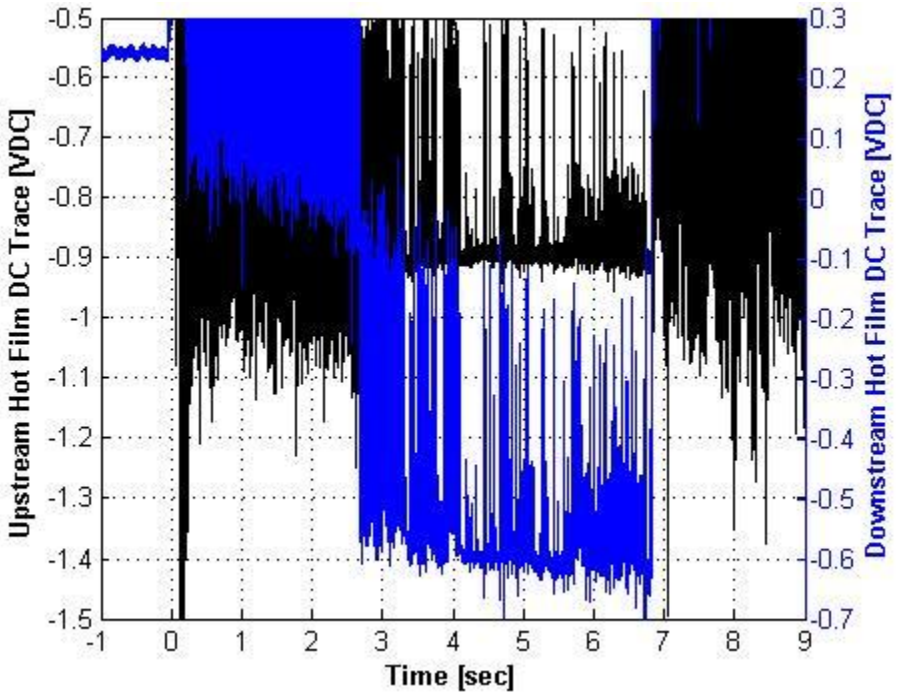

Figure 4.3. Uncalibrated hot-films located 7.5 inches apart on nozzle wall for 2-inch model under quiet conditions (p_d = 181.7 psia, p_v = 3.2 torr, Date: 29 March 2007, $p_{max,quiet}$ = 150 psia)

Figure 4.4 shows the noise level of the model-nose pressure as well as the mean Mach number. During the attached, non-oscillatory portion of the run, the RMS of the pressure trace drops to about 0.5 – 0.6% of the mean value. Per Ref. [10], the noise level of the tunnel thus far has been around 0.05% when running quiet and measuring with a thin pitot probe. By the date this run was made (29 March 2007), the quiet flow in the tunnel already showed evidence of many turbulent spikes like those seen on Figure 4.3, according to BAM6QT research colleagues. Although the noise level of 0.5% is not quiet, it is still significantly less than the 1 – 3% level typically seen during noisy runs [10]. Note also that the Mach number approaches 6 at the onset of the attached portion of the run and decreases slightly as stagnation pressure continues to drop. This trend was noticed by Juliano [10] and is probably due to the boundary layer thickening with decreasing Reynolds number. Taking all this into account, this run appeared to start successfully.

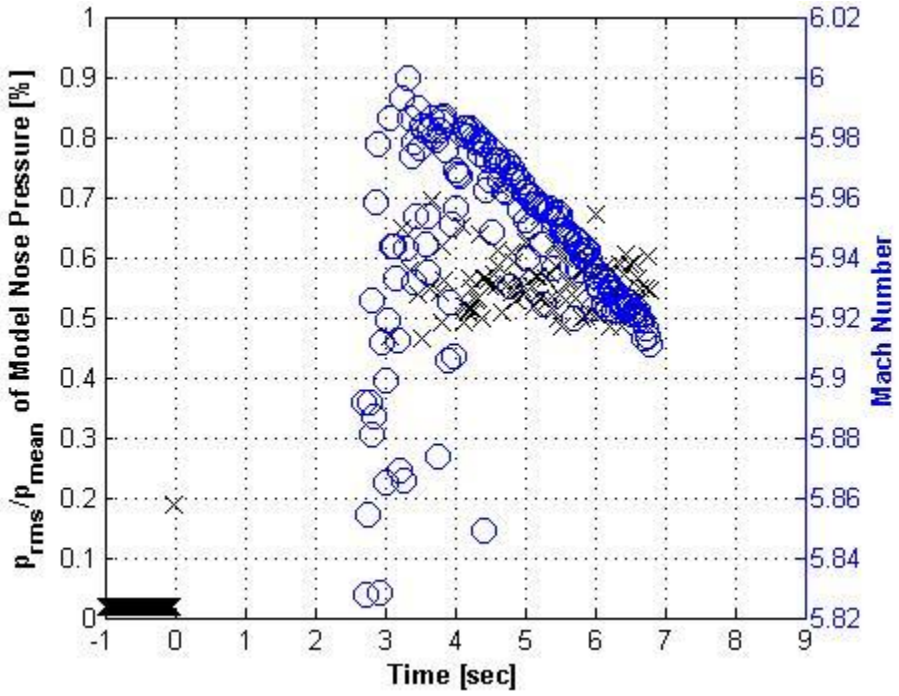

Figure 4.4. Noise level and Mach number for 2-inch model under quiet conditions (p_d = 181.8 psia, p_v = 3.2 torr, Date: 29 March 2007, $p_{max,quiet}$ = 150 psia)

For tunnel runs with an initial stagnation pressure at or under the maximum quiet pressure, there is a period of intermittent oscillations at some point in the run. Figure 4.5 shows the nose and contraction pressure traces from a run with an initial stagnation pressure of 85.6 psia on a date where the maximum quiet pressure was around 80 psia. Following the tunnel startup and a small period of noisy flow from t = 0.2 sec. to t = 0.85 sec., the fluctuations in the model-nose pressure diminish for a small amount of time until t $\cong$ 1 sec. After this, however, the nose trace has intermittent high-level oscillations for about 1.5 seconds until t $\cong$ 2.5 sec. The oscillations then fall to a low level and remain at this level for the remainder of the run, with the exception of a few turbulent spikes.

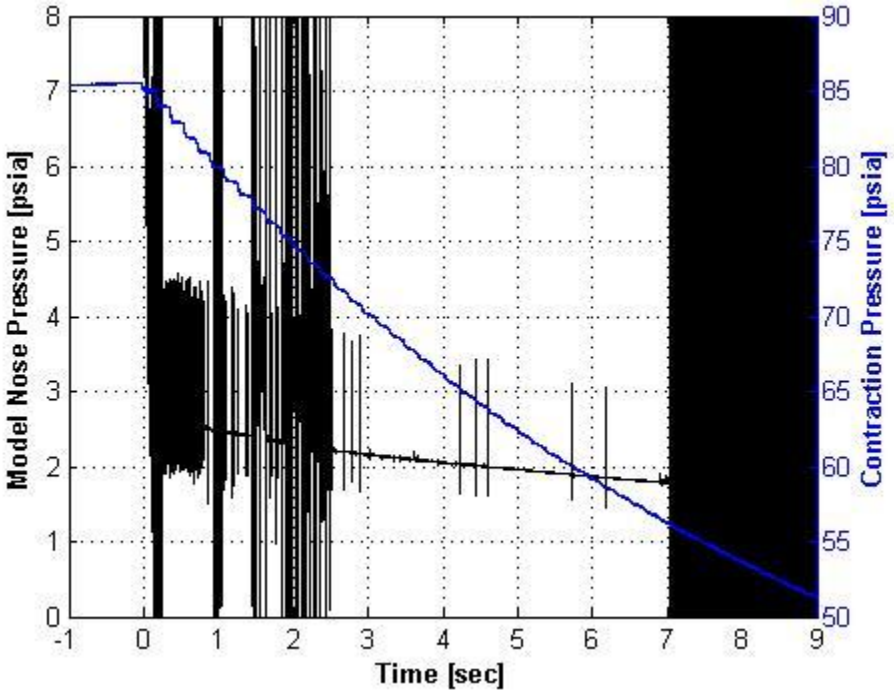

Figure 4.5. Contraction and nose pressure for 2-inch model under quiet conditions (p_d = 85.6 psia, p_v = 3 torr, Date: 23 August, $p_{max,quiet}$ = 80 psia)

Figure 4.6 shows the RMS nose pressure as well as the Mach number for this run. When the high-level oscillations die out, the noise level drops to around 0.07%. This is a significant improvement in noise level from the 0.5% that was seen in Figure 4.4. At this date, the quiet

pressure of the tunnel had already dropped and the quiet performance of the tunnel was more stable. However, the noise in the model-nose pressure remains slightly greater than the 0.05% noise level thus far seen in the tunnel. Yet since noise-level measurements made using a pressure transducer on the nose of a blunt model differ from those taken from a pressure sensor at the end of the slender pitot probe, slightly higher noise levels may occur. The ranges of both plots are limited in order to better capture the noise level and Mach number of the well-behaved portion of the run. Although it is not shown in these ranges, the noise level increases to 5 – 7% and the mean Mach number drops from 5.9 to about 5.4 during the period of high level oscillations between t = 0.9 sec. and t = 2.5 sec. Since the Mach number of the flow is set by the area of the inviscid core, this decrease in Mach number equates to a 31% blockage of the flow. This blockage could be attributed to separation of the boundary layer along the wall of the nozzle.

Periods of intermittent separation of the nozzle-wall boundary layers are common in the BAM6QT. Juliano [10] noticed periods of separation in the flow using a thin pitot probe. During those periods of separation, the pitot pressure would increase in mean value but the fluctuation levels did not increase significantly. For the periods of separation seen in Figure 4.5, however, there is an increase in the mean value but also a significant increase in the fluctuation levels of the model-nose pressure. This is most likely due to disturbances created by the interaction of the bow shock and the separated boundary layer on the tunnel wall. Note also that after the flow re-attaches the Mach number increases to around 5.95 and drops to 5.9 by the end of the run. This is lower than the Mach number of 6 seen on Figure 4.4, perhaps due to increased blockage of the thicker boundary layer at lower Reynolds number.

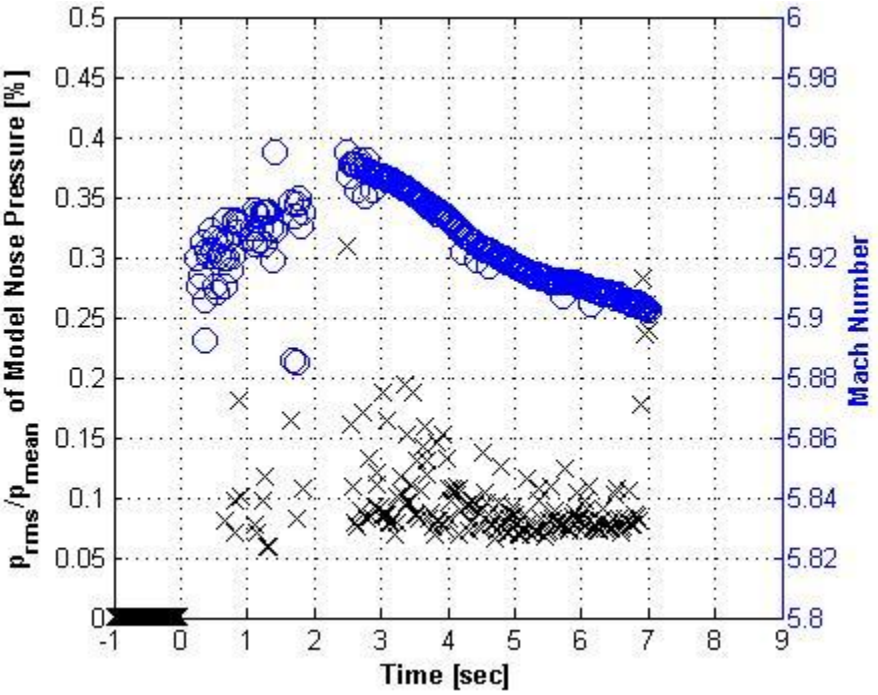

Figure 4.6. Noise level and Mach number for 2-inch model under quiet conditions (p_d = 85.6 psia, p_v = 3 torr, Date: 23 August 2007, $p_{max,quiet}$ = 80 psia)

There is a noticeable change of behavior in the nose pressure when the initial stagnation pressure drops beyond a certain point. This perhaps occurs due to the increasing thickness of the boundary layer at lower Reynolds number. If the boundary layer on the nozzle wall thickens sufficiently, the blockage that is created by the boundary layer as well as the blunt model becomes too great to result in attached flow. This remains true regardless of how much the back pressure is lowered. At this point, the nozzle wall-boundary layer appears to separate throughout the entire run. When employing the 2-inch model in the original tunnel setup, this driver-tube pressure threshold lies somewhere between 60 and 75 psia. To demonstrate this effect, Figure 4.7 shows the contraction and model-nose pressure for a run with an initial driver-tube pressure of 40.6 psia.

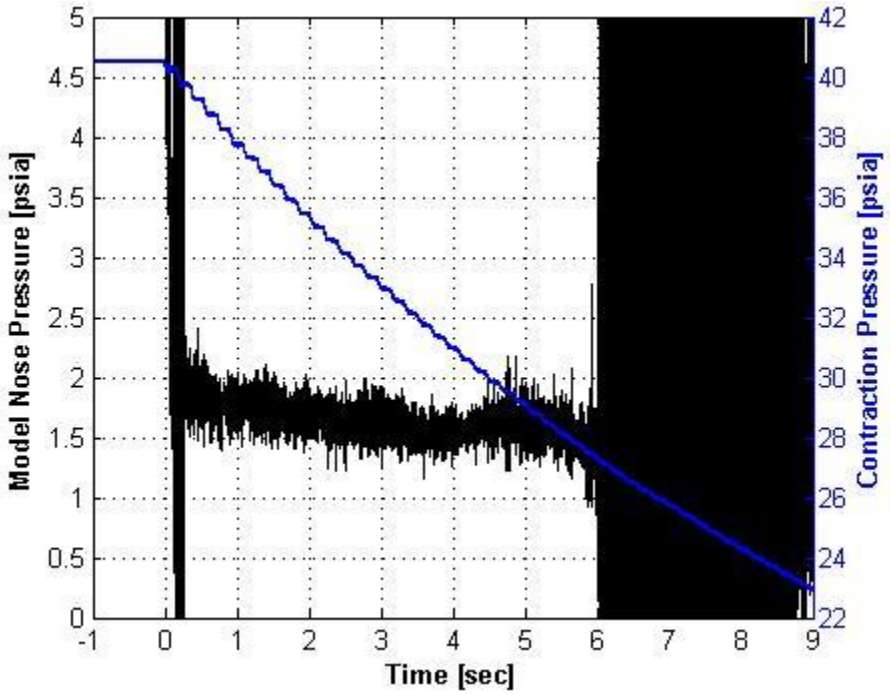

Figure 4.7. Contraction and nose pressure for 2-inch model under quiet conditions (p_d = 40.6 psia, p_v = 6.5 torr, Date: 30 March 2007, $p_{max,quiet}$ = 150 psia)

Figure 4.8 shows the noise level of the model-nose pressure as well as the Mach number. After the startup of the tunnel the noise level of the nose pressure only decreases to between 3 and 9%. This is an obvious increase in fluctuations compared to the 0.07 – 0.5% seen in previous cases. Also, the Mach number decreases to 5.4, remains there through most of the run and drops to around 5.2 toward the end of the run. Recall that the mean Mach number of the portions of intermittent boundary-layer separation in previous runs was around 5.4. Also, upon further inspection of the nose pressure, the model-nose pressure appears to periodically oscillate at 78 Hz (Appendix A.1). These oscillations account for the increase in RMS of the model-nose pressure.

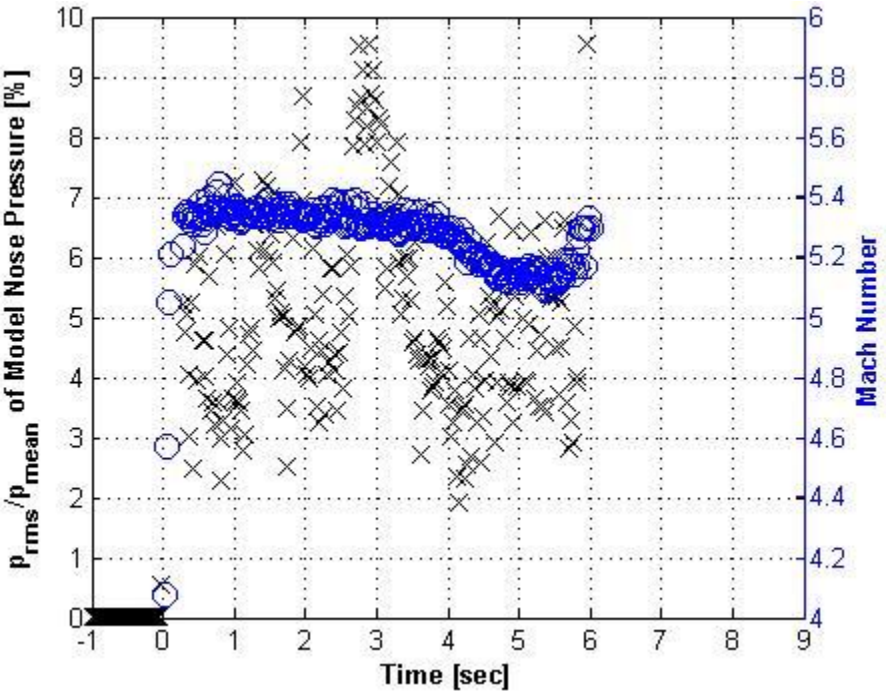

Figure 4.8. Noise level and Mach number for 2-inch model under quiet conditions (p_d = 40.4 psia, p_v = 6.5 torr, Date: 29 March 2007, $p_{max,quiet}$ = 150 psia)

When starting a run at an initial stagnation pressure slightly above the maximum quiet pressure, the nose pressure heavily oscillates until the stagnation pressure drops into the quiet pressure regime and then remains well-behaved and attached for the remainder of the run. At initial driver-tube pressures between 75 psia and the maximum quiet pressure, the flow remains well-behaved but has a period of separation at some point in the run. When running at a driver pressure of 60 psia and below, the nose pressure shows the flow separating and periodically oscillating at a frequency around 70 – 75 Hz throughout the entire run. For more information regarding the flow behavior with the 2-inch model under quiet conditions, see Table B.1.

4.1.2 2.25-Inch Model under Quiet Conditions

After re-polishing the nozzle throat, the maximum quiet pressure increased to around 140 psia. At this point, the bulk of the experiments using the 2.25-inch model were made. When starting the tunnel at an initial driver pressure above the maximum quiet pressure, the

performance of the tunnel running the 2.25-inch model was similar to earlier measurements with the 2-inch model. Figure 4.9 shows the contraction and nose pressures from a run starting at a driver-tube pressure about 40 psia above the maximum quiet pressure. As a result, the stagnation pressure drops into the quiet regime midway through the run. Thus, when the stagnation pressure in the tunnel drops to around 143 psia, the high level oscillations in the model-nose pressure subside. The flow then attaches and remains well-behaved for the remainder of the run.

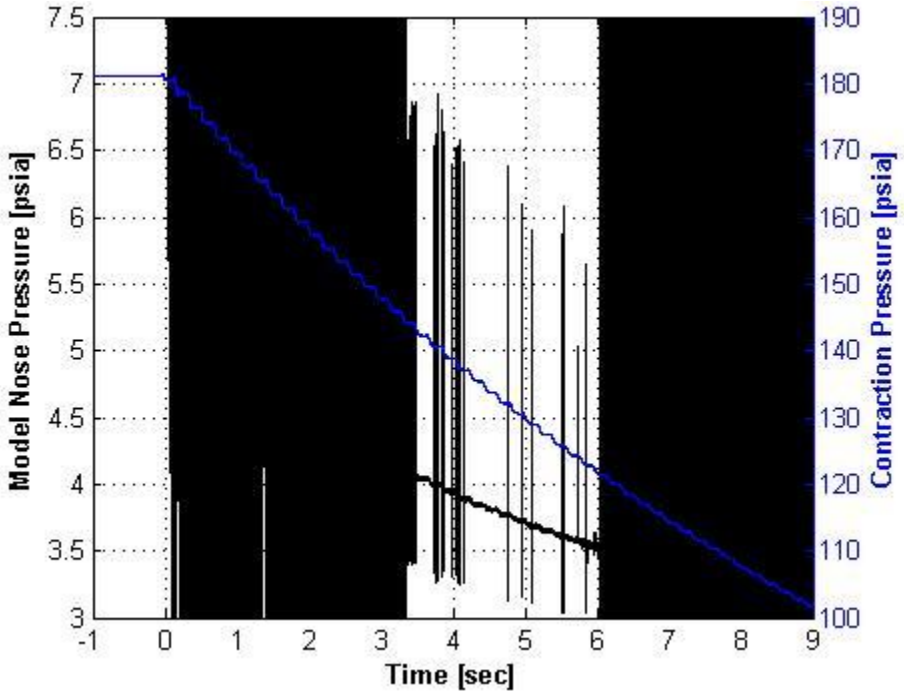

Figure 4.9. Contraction and nose pressure for 2.25-inch model under quiet conditions (p_d = 181.3 psia, p_v = 3.8 torr, Date: 16 October 2007, $p_{max,quiet}$ = 140 psia)

A subtle yet important difference between the performance of the tunnel using the 2-inch and 2.25-inch models is noticed in the noise level of the model-nose pressure. Figure 4.10 shows the noise level and Mach number for this run. Under these conditions, the RMS drops to between 0.08 and 0.25% of the mean value, mostly hovering around 0.1%. This is a small increase from the 0.07% noise level seen when using the 2-inch model at a lower pressure range.

Unfortunately, no runs were made at the same pressure range using the 2-inch model after the nozzle throat had been re-polished, so it is unknown what the noise level or Mach number of the flow might have been. However, one would expect results similar to those seen on Figure 4.10 but perhaps with a slightly lower noise level and higher Mach number due to the smaller model size. Nonetheless, a slight increase in tunnel noise was noticed when using the 2-inch blunt model compared to the thin pitot probe, and there is similarly another minor increase in noise level by increasing the size of the model to 2.25 inches. As a result of the improved quiet flow, the boundary layer decreases in thickness, leaving a larger effective flow area. Due to this effect, the Mach number increases from a maximum of 5.99 with a noise level of 0.5% with the 2-inch-model case (Figure 4.4) to a maximum of 6.06 with a noise level of 0.1% when running the 2.25-inch model.

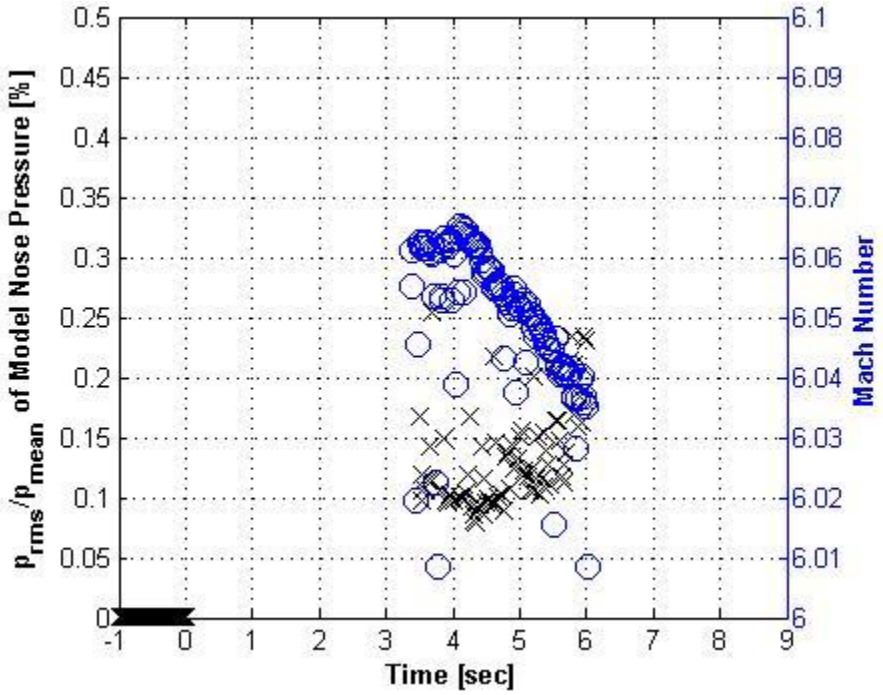

Figure 4.10. Noise level and Mach number for 2.25-inch model under quiet conditions (p_d = 181.3 psia, p_v = 3.8 torr, Date: 16 October 2007, $p_{max,quiet}$ = 140 psia)

Another distinction between the starting performance of the 2-inch model and 2.25-inch model is observed when running the tunnel within the quiet pressure regime. As before, there is a period of intermittent separation in the nose pressure and hot-film traces. Figure 4.11 shows the nose and contraction pressure traces from a run with an initial stagnation pressure of 142.1 psia with a maximum quiet pressure around 140 psia. After the tunnel startup, the fluctuations in the nose pressure decrease for a very small amount of time around t = 0.56 sec. After this, however, the period of separation in the pressure trace lasts from t = 0.66 sec. to t = 2.53 sec. The flow then re-attaches and remains well-behaved for the remainder of the run.

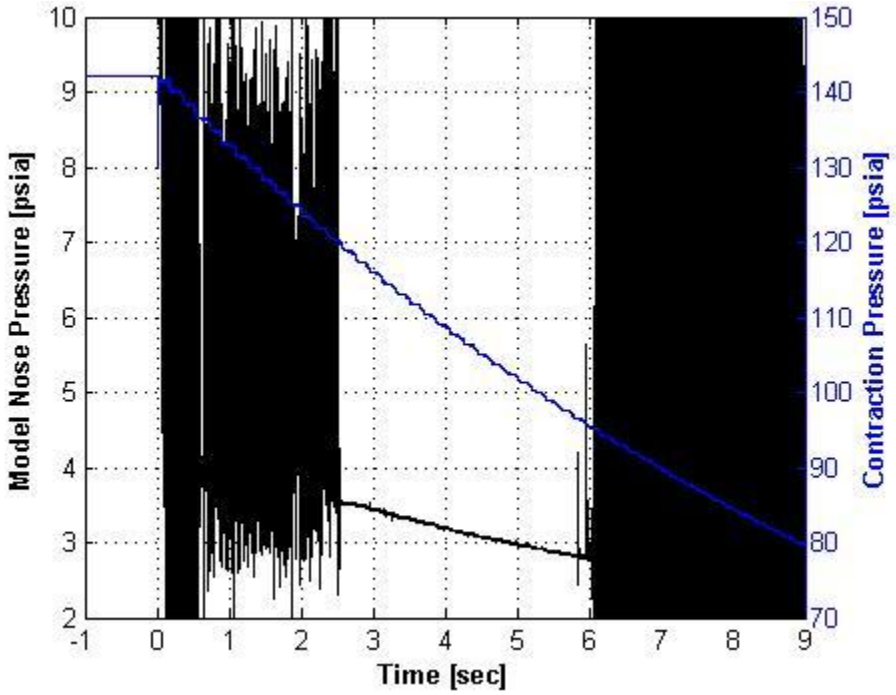

Figure 4.11. Contraction and nose pressure for 2.25-inch model under quiet conditions (p_d = 142.1 psia, p_v = 2.5 torr, Date: 16 October 2007, $p_{max,quiet}$ = 140 psia)

Figure 4.12 shows both the noise level and the mean Mach number for this run. As in Figure 4.10, the RMS drops to around 0.1 – 0.25% of the mean. Correspondingly, the Mach number decreases slightly to 6.02, from around 6.07 when starting a run at a somewhat higher driver-tube pressure. Although this is not shown on the plot, during the period of separation from

this run, the RMS nose pressure increases to 15 – 25%. This is a significant increase from the 5 – 7% seen thus far in separation periods using the 2-inch model. This increase is most likely due to the larger blockage created by the larger model and the stronger disturbances created by the interaction of the bow shock and the separated nozzle-wall boundary layer. With increasing model size, it is expected that the bow shock impinges the boundary layer more perpendicularly. This increases the strength of the shock and resultant adverse pressure gradient. Lastly, the mean Mach number decreases to around 5.4 during the separated portion of the run (from t = 0.66 sec. to t = 2.53 sec.), which is similar to what has been seen with the 2-inch model. Thus, the mean Mach number remains about the same with increasing model size. This decrease in Mach number from 6.01 seen initially to 5.4 during separation is a 36% blockage in flow area. Although the fluctuations in the pressure increase in magnitude, the mean value of the nose pressure does not change much. There was also a noticeable periodic trend in the oscillations of the nose pressure during the separated portion of runs using the 2.25-inch model. In this run, the pressure oscillated at a frequency of 88 Hz (Appendix A.2). These oscillations were not seen in the separation periods of any runs with the 2-inch model in this stagnation pressure range.

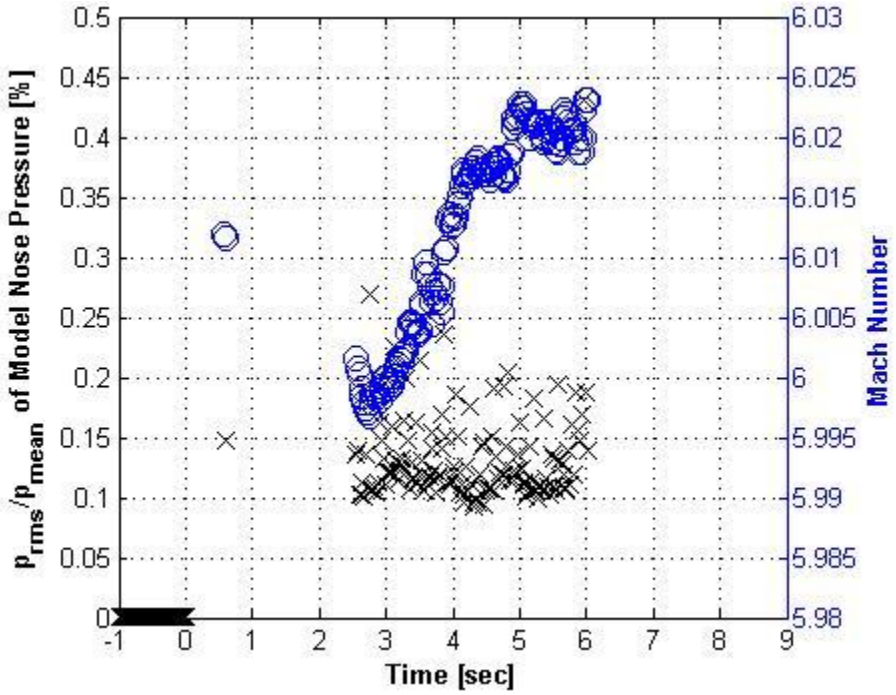

Figure 4.12. Noise level and Mach number for 2.25-inch model under quiet conditions (p_d = 142.1 psia, p_v = 2.5 torr, Date: 16 October 2007, $p_{max,quiet}$ = 140 psia)

When the driver-tube pressure is decreased below 60 – 80 psia, the flow remained separated throughout the entire run. This is similar to the performance using the 2-inch model. However, at an initial stagnation pressure near 40 psia, the RMS nose pressure is higher while running the 2.25-inch model. Figure 4.13 shows the model-nose and contraction pressures for of a run starting at 41.9 psia. From the beginning of the run to around 4.5 seconds into the run, the nose pressure fluctuations increase then drop to levels seen when running the 2-inch model at this stagnation pressure range (see Figure 4.8).

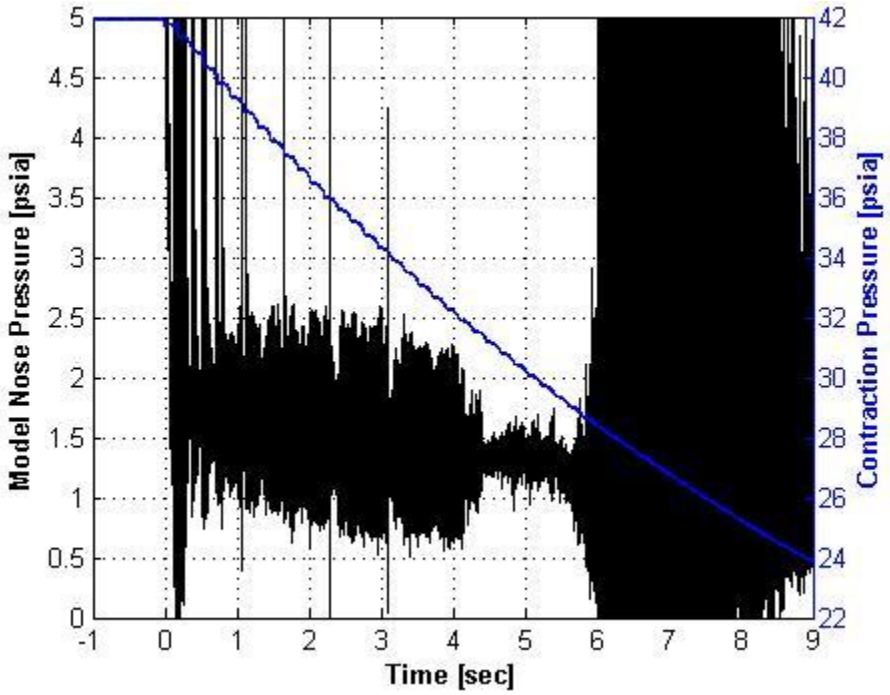

Figure 4.13. Contraction and nose pressure for 2.25-inch model under quiet conditions (p_d = 41.9 psia, p_v = 2.8 torr, Date: 17 October 2007, $p_{max,quiet}$ = 140 psia)

Figure 4.14 shows that the noise level increases from 20 – 40% before dropping to around 5% and remaining at this level until the end of the run. This increase in noise level may be attributed to the larger model and stronger bow shock creating more blockage in the flow and having a greater effect. Periodic oscillations in the nose pressure were seen occurring at a constant frequency around 78 Hz. This frequency is comparable to the peak frequency of oscillation in the flow when running the 2-inch model at driver-tube pressures around 40 psia.

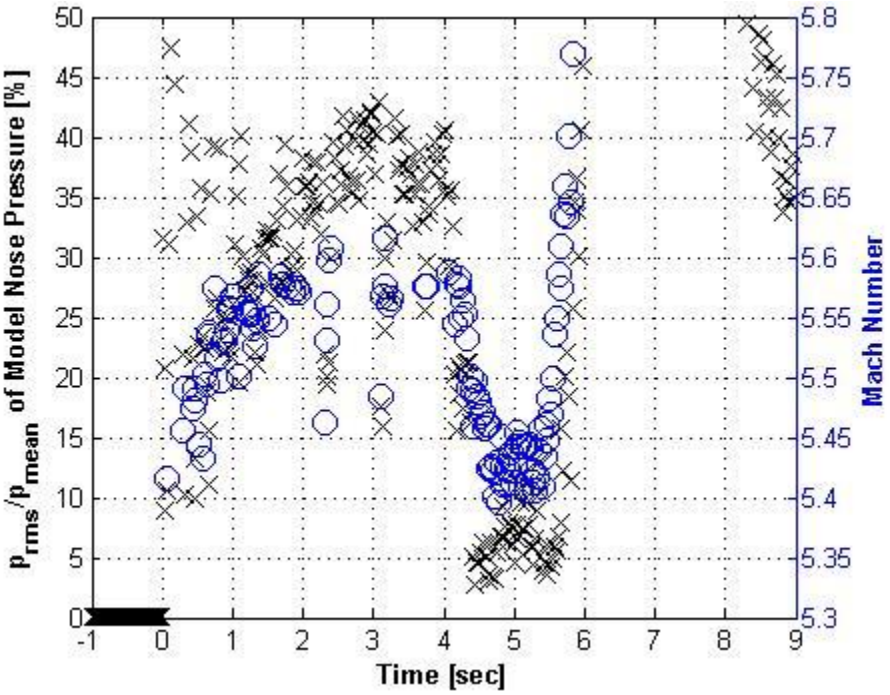

Figure 4.14. Noise level and Mach number for 2.25-inch model with open bleed (p_d = 41.9 psia, p_v = 2.8 torr, Date: 17 October 2007, $p_{max,quiet}$ = 140 psia)

The performance of the 2.25-inch model under quiet conditions in the original tunnel setup is similar to that of the 2-inch model, with subtle differences. At driver-tube pressures slightly above the maximum quiet pressure, the nose pressure shows the flow fluctuating until dropping into the quiet regime. At initial pressures between 75 and the maximum quiet pressure, the flow remained well-behaved and attached with a period of separation occurring at some point in the run. However, during the separation periods, the RMS nose pressure increased from the 5 – 7% seen with the 2-inch model to 15 – 25%. This separation also contained periodic oscillations at 85 – 90 Hz, which were not seen at all when running the 2-inch model. At initial driver pressures of 60 psia and lower, the flow remained separated throughout the entire run with periodic oscillations at 75 – 80 Hz. With a lower initial stagnation pressure of 40 psia, the RMS nose pressure increased to 20 – 40% of the mean. This is much higher than the 2 – 10% noise level seen when running the 2-inch model at driver-tube pressures around 40 psia. For more

information regarding the flow behavior when running the 2.25-inch model under quiet conditions in the original tunnel configuration, see Table B.2.

4.1.3 2.5-Inch Model under Quiet Conditions

The starting performance of the 2.5-inch model depended heavily on the stagnation-to-back-pressure ratio, λ. Assuming a minimum boundary-layer thickness at highest possible Reynolds number, runs were made using the 2.5-inch model at a driver-tube pressure near the maximum quiet pressure of 140 psia. When the vacuum pressure is sufficiently low, the model-nose pressure behaves similarly to runs using the 2-inch and 2.25-inch models at this driver-tube pressure. Figure 4.15 shows the model-nose pressures along with the contraction pressure for a run at an initial stagnation pressure of 140.8 psia and initial vacuum pressure of 1.15 torr. After the startup of the tunnel, the flow is well-behaved from around t = 0.4 sec. to t = 0.55 sec. The nose pressure then begins to oscillate from t = 0.55 to t = 2.3 sec., after which it re-attaches and remains well-behaved for the remainder of the run. Another experiment at a similar driver-tube pressure but with the vacuum pressure decreased further to 0.7 torr produced similar results.

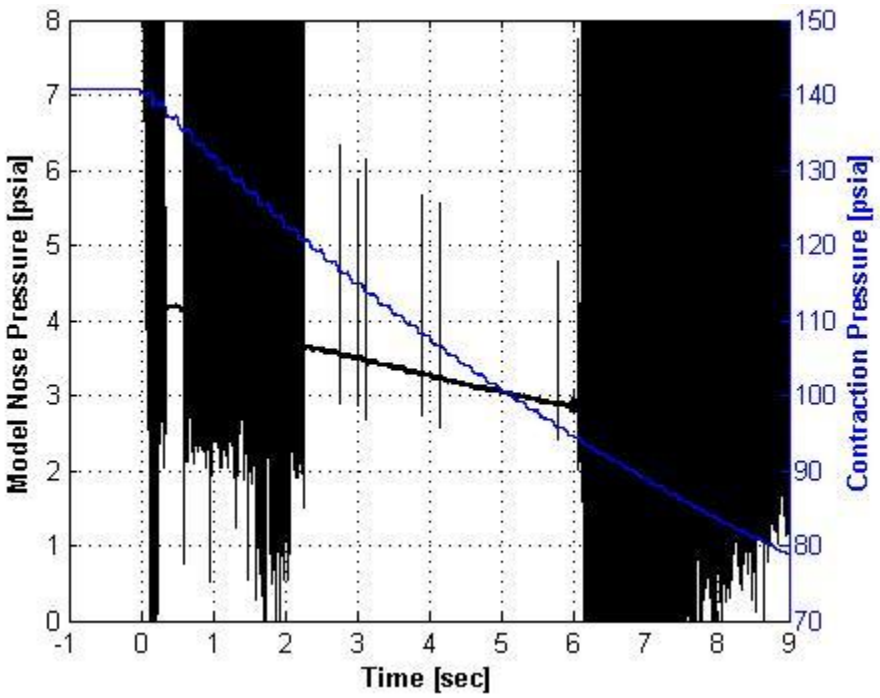

Figure 4.15. Contraction and nose pressure for 2.5-inch model under quiet conditions (p_d = 140.8 psia, p_v = 1.15 torr, Date: 19 October 2007, $p_{max,quiet}$ = 140 psia)

The noise level increases further when the size of the model increases to 2.5 inches in diameter. Figure 4.16 shows the RMS nose pressure and mean Mach number from this run. Under these conditions the RMS nose pressure is near 0.2% of the mean. This is an increase from the 0.1% noise level seen with the 2.25-inch model. Correspondingly, there is a decrease in the Mach number to between 5.96 and 5.98. Also, although it is not shown on this figure, the fluctuation level of the nose pressure during the separation period increases to 30 – 40% of the mean value. This is a very large increase in noise level from the 15 – 25% level that was measured using the 2.25 model. Finally, as with the results seen using the smaller models, the mean Mach number during the separated portion of the run decreased to around 5.4. This separation period also contains a clear trend of periodic oscillations near 69 Hz.

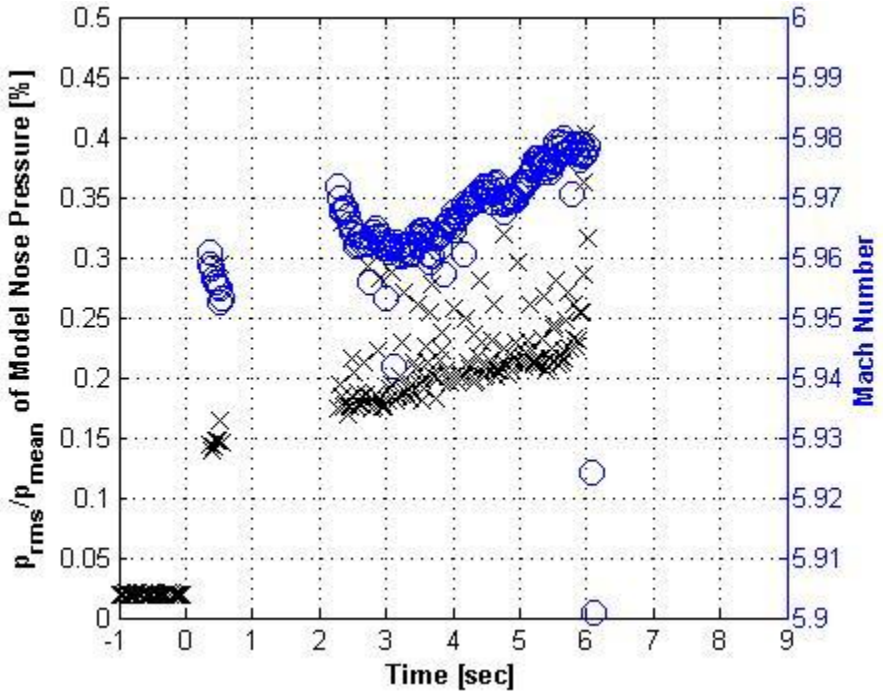

Figure 4.16. Noise level and Mach number for 2.5-inch model under quiet conditions (p_d = 140.8 psia, p_v = 1.15 torr, Date: 19 October 2007, $p_{max,quiet}$ = 140 psia)

When the initial back pressure is increased slightly to 1.5 torr, there is a stark difference in the behavior of the nose pressure. Figure 4.17 shows the nose pressure along with the contraction pressure for this run. The nose pressure fluctuates over the entire range of the pressure transducer throughout the duration of the run. Thus, the flow from this run is unstarted. An attempt to run a 2.75-inch model at a driver-tube pressure near the maximum quiet pressure and initial back pressure of 0.7 torr resulted in an unstarted run as well. It was then assumed that the tunnel would not start when using a model with a base diameter greater than or equal to 2.75 inches.

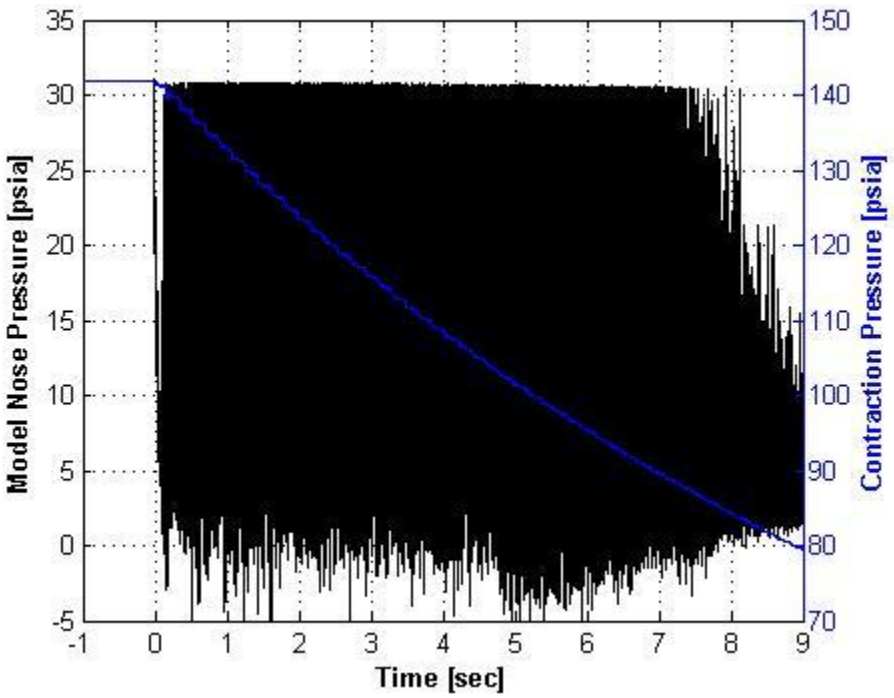

Figure 4.17. Contraction and nose pressure for 2.5-inch model under quiet conditions (p_d = 141.9 psia, p_v = 1.5 torr, Date: 16 October 2007, $p_{max,quiet}$ = 140 psia)

The 2.5-inch model was only able to start under quiet conditions when running at a driver-tube pressure near 140 psia and initial vacuum pressure less than or equal to 1.15 torr. Under these conditions, the flow remained well-behaved and attached with a period of separation in the middle of the run. The RMS nose pressure of the separated portion of this run was 30 – 40% of the mean. This was almost double the RMS of the separated portion of runs using the 2.25-inch model at a driver-tube pressure near 140 psia. When separated, the flow had periodic oscillations around 70 Hz, less than the 85 Hz oscillations seen using the 2.25-inch model. For more information of the flow behavior when running the 2.5-inch model under quiet conditions in the original tunnel setup, see Table B.3.

4.1.4 2-Inch Model under Noisy Conditions

Although turbulent boundary layers are less prone to separate, the starting performance of the tunnel under noisy conditions was much less repeatable than under quiet conditions. When using the 2-inch model in the tunnel with the bleed system closed, the flow would start or unstart depending on the initial stagnation and back pressures, and the results were not repeatable. An example of a flow that was both well-behaved and noisy is given on Figure 4.18. Under the given conditions, the nose pressure appears nominal after the tunnel startup and remains well-behaved throughout the entire run.

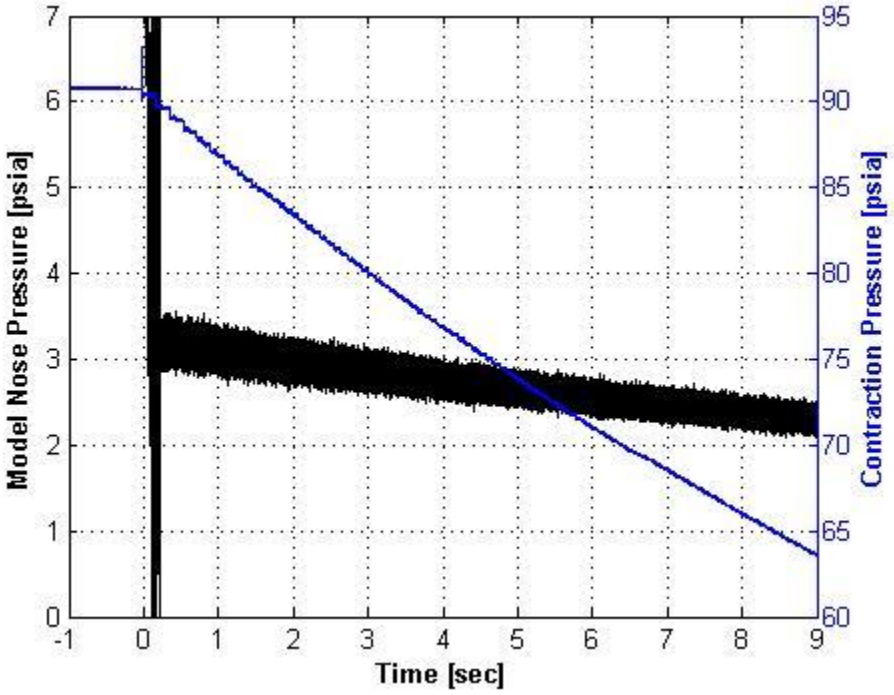

Figure 4.18. Contraction and nose pressure for 2-inch model under noisy conditions (p_d = 90.8 psia, p_v = 4.5 torr, Date: 21 July 2007, $p_{max,quiet}$ = 75 psia)

The noise level and mean Mach number from this run are shown on Figure 4.19. After the startup, the RMS nose pressure drops and remains between 2.1 and 2.9% of the mean. The Mach number holds steady around 5.72 – 5.74 throughout the duration of the run. This decrease in the Mach number from the levels seen under quiet conditions is probably due to the thicker

turbulent boundary layer reducing the effective flow area. The values for noise level and mean Mach number for this run are near those measured by a thin pitot [10]. In runs with the bleeds closed, the run time increased to at least 9 seconds due to lower decreased mass flow.

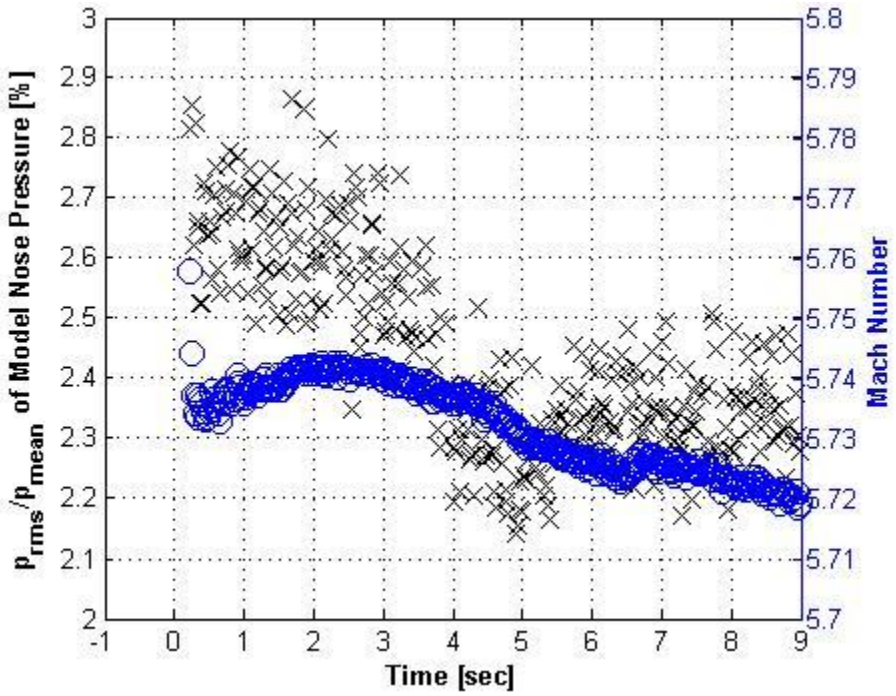

Figure 4.19. Noise level and Mach number for 2.25-inch model under noisy conditions (p_d = 90.8 psia, p_v = 4.5 torr, Date: 21 July 2007, $p_{max,quiet}$ = 75 psia)

Although trends in the starting performance of the 2-inch model in the tunnel with bleeds closed were difficult to detect, Figure 4.20 shows one predictable tendency. This run was performed immediately after the one shown on Figure 4.18. It started at a similar driver-tube pressure, but the vacuum pressure was increased by almost a factor of 4 from 4.5 torr to 16 torr. The large increase in the back pressure causes the flow to unstart. Note that the noise level of this run is between 26 – 34%, a significant increase from the 2 – 3% level seen on Figure 4.19.

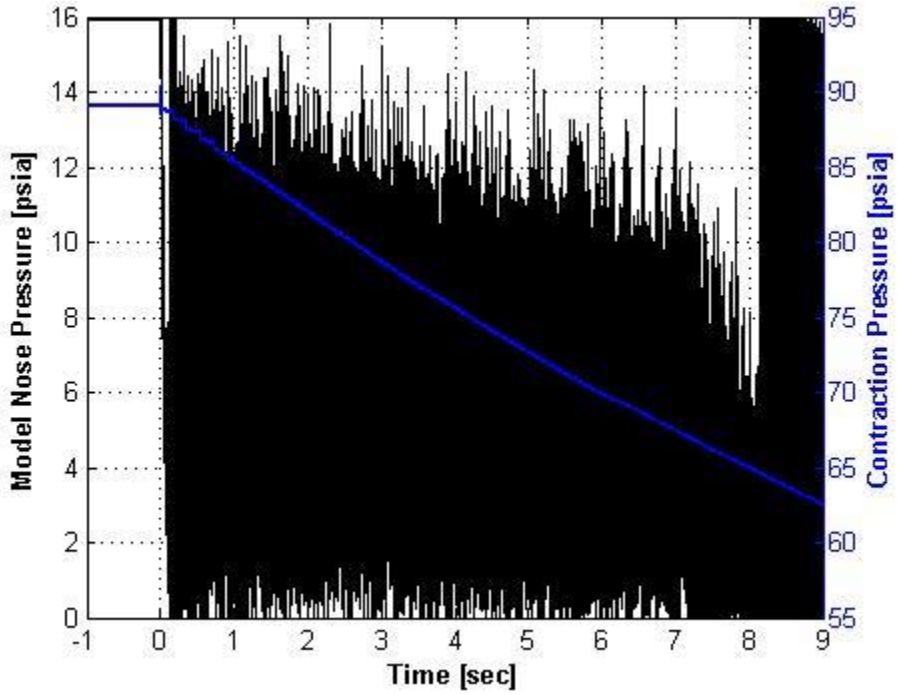

Figure 4.20. Contraction and nose pressure for 2-inch model under noisy conditions (p_d = 89.2 psia, p_v = 16 torr, Date: 21 July 2007, $p_{max,quiet}$ = 75 psia)

However, the starting performance of the noisy flow with the 2-inch model also changed with the date at which the experiments were undertaken. Figure 4.21 shows the model-nose pressure and contraction pressure for a run under similar conditions as Figure 4.18, but performed about two months later on 13 September 2007. This run clearly resulted in unstarted flow. The noise level increased an order of magnitude, from an average of 2.5% to an average of about 30%. In general, noisy tunnel runs using the 2-inch model rarely resulted in started flow. It appears that the size of this model lies near a boundary between starting and unstarting. Thus, as expected, all runs using larger models in the tunnel with bleeds closed result in unstarted flow.

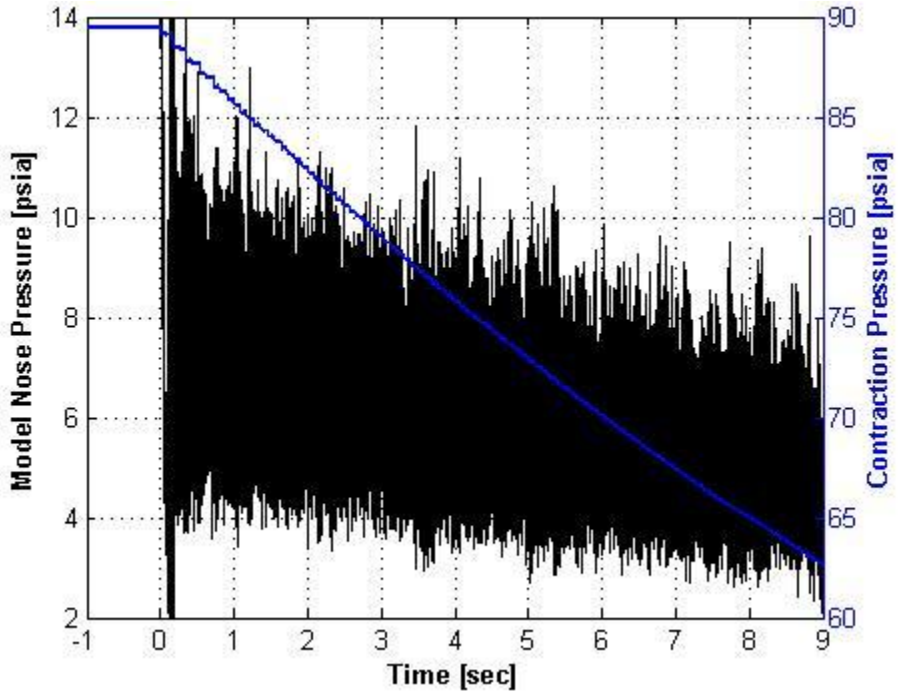

Figure 4.21. Contraction and nose pressure for 2-inch model under noisy conditions (p_d = 89.5 psia, p_v = 4.5 torr, Date: 13 September 2007, $p_{max,quiet}$ = 60 psia)

The starting performance of the 2-inch model under noisy conditions was difficult to detect. While some runs resulted in started flow, these runs were not repeatable. Most unstarted runs resulted in nose pressures that oscillated at a periodic frequency around 150 Hz (Appendix A.3). For more information on the starting performance of the original tunnel configuration under noisy conditions, see Table B.4 and Table B.5.

4.1.5 Summary of Performance of Original Tunnel Configuration

Figure 4.22 summarizes the starting performance of the original tunnel configuration with respect to the driver-tube and vacuum pressure. Runs are labeled as “started” based on whether there was any section of the run with well-behaved pressure data (with tunnel noise levels at or below 3 – 5%) and nominal mean Mach number (at or above 5.7). Runs labeled as “separated” are those that remained separated throughout the entire run. These runs had noise levels anywhere from 2 – 40% and a mean Mach number near 5.4 and typically occurred at lower

Reynolds number. All remaining runs are labeled “unstarted.” Also, runs that are denoted as “quiet” do not necessarily mean that the noise levels of the nose pressures are less than 0.1%, the standard metric for quiet flow. Rather it is an indication of the run being performed under quiet conditions, meaning that the bleeds were open and at some point during the run the stagnation pressure dropped into the quiet pressure regime of the tunnel. Conversely, runs labeled as “noisy” are those that were made with bleeds open and a driver-tube pressure above the maximum quiet pressure, or with bleeds closed.

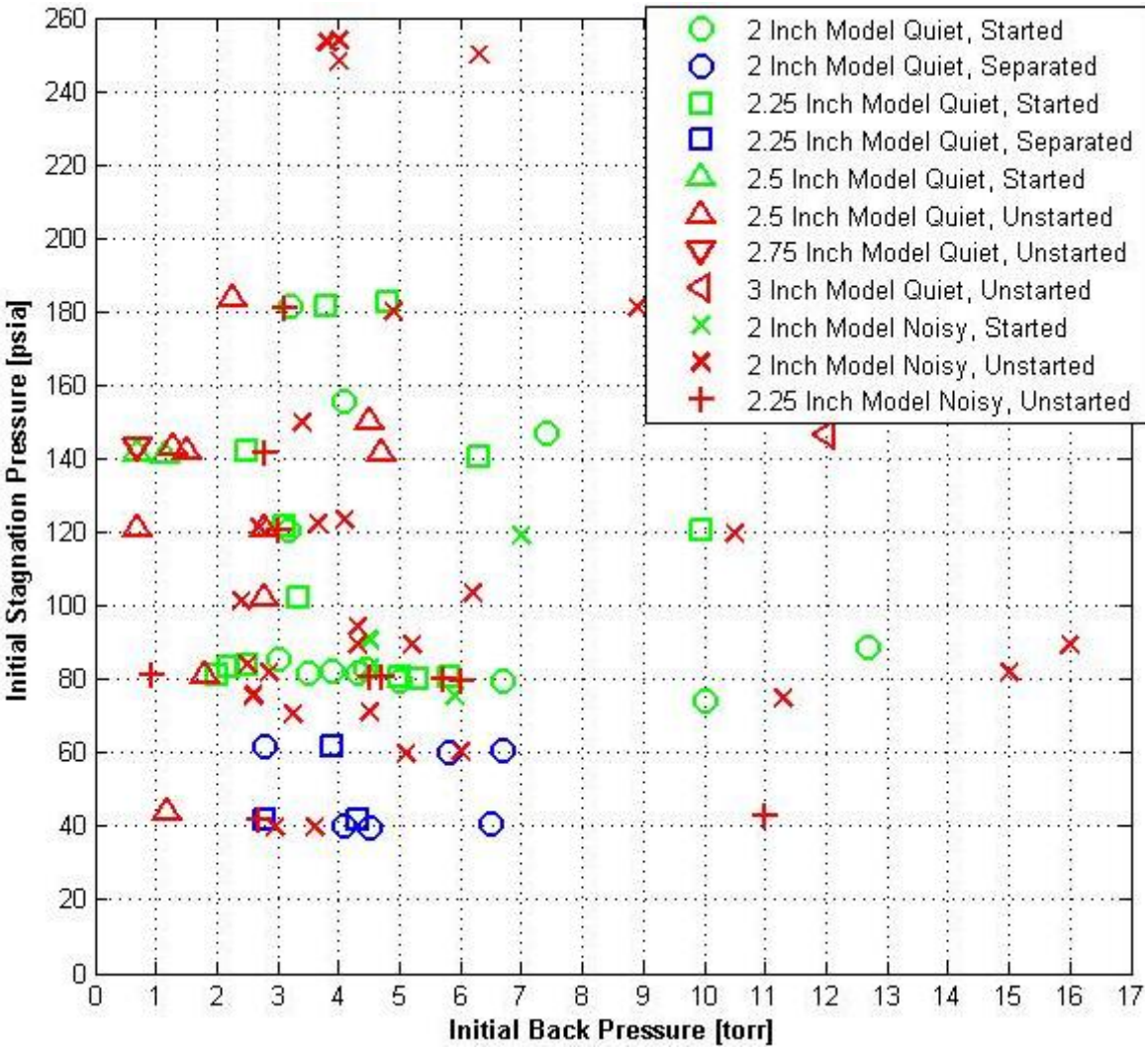

Figure 4.22. Starting performance of the original tunnel configuration

This figure does not reveal many clear trends in the starting performance of the tunnel. Nonetheless, it does show that all runs made under quiet conditions above a driver-tube pressure of 70 psia result in started flow for both the 2-inch and 2.25-inch models. However, runs attempted below 70 psia under quiet conditions with the 2 and 2.25-inch models result in separated flow throughout the duration of the run. Figure 4.23 shows the performance behavior of these models under quiet conditions.

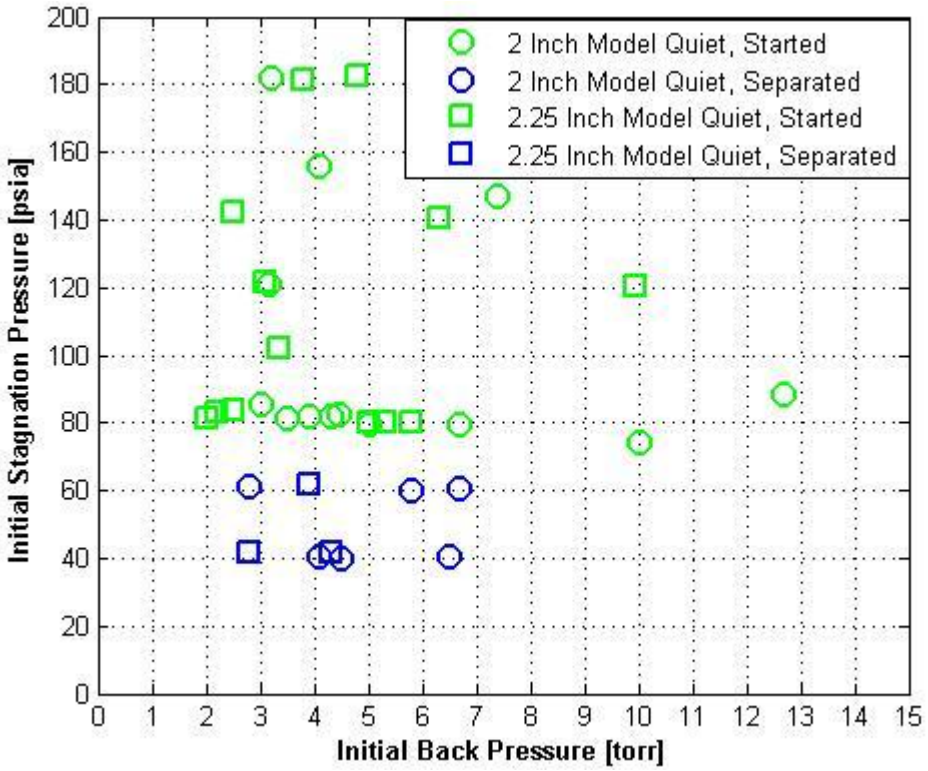

Figure 4.23. Summary of the starting performance of the 2-inch and 2.25-inch models under quiet conditions in the original tunnel configuration

There is significant influence of the initial pressure conditions on the starting performance of the 2.5-inch model under quiet conditions. Although the flow starts at an initial stagnation pressure around 140 psia and vacuum pressures of 0.7 and 1.15 torr, it unstarts when increasing the vacuum pressure to 1.5 torr. In fact, the flow does not even start at an initial vacuum pressure of 0.7 torr when the driver-tube pressure is dropped to 120 psia. The flow unstarts

when using the 2.75-inch model under quiet conditions. Figure 4.24 gives the performance of the 2.5-inch and 2.75-inch models under quiet conditions in the original tunnel configuration.

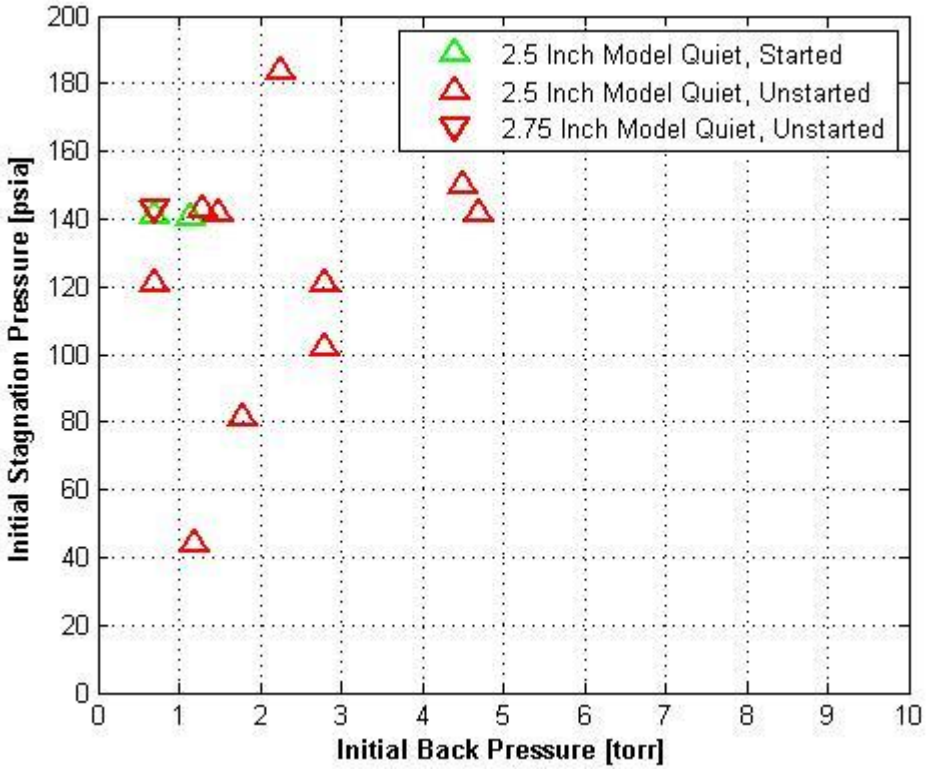

Figure 4.24. Summary of the starting performance of the 2.5-inch and 2.75-inch models under quiet conditions in the original tunnel configuration

Under noisy conditions, the flow rarely starts when running the 2-inch model, and these started runs are not repeatable. Nor could correlations be made between the conditions of each run and their resulting starting performance. This could be an indication that the 2-inch-model size lies near a boundary of the performance of the original tunnel configuration under noisy conditions. Figure 4.25 shows the performance of the 2-inch model under noisy conditions. Note that runs were made with larger models under noisy conditions, all of which resulted in flow unstarting. Overall, the largest sphere-cone model that can be started in the original tunnel setup appears to lie near 2 inches in base diameter under noisy conditions and between 2.5 and 2.75 inches under quiet conditions.

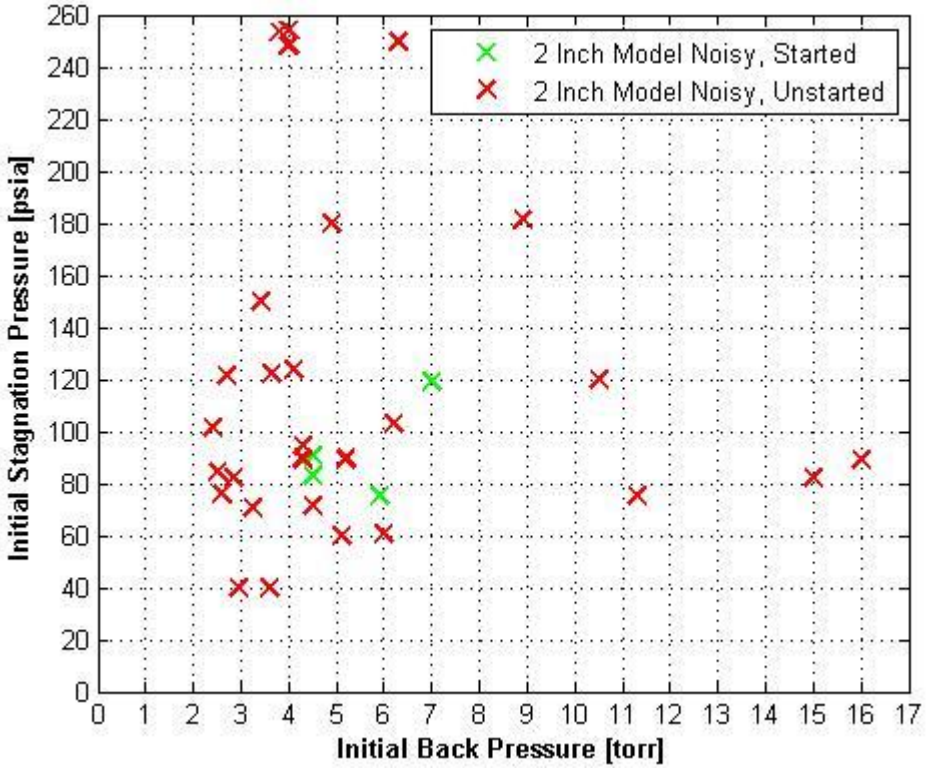

Figure 4.25. Summary of the starting performance of the 2-inch model under noisy conditions in the original tunnel configuration

4.2 Modified Tunnel Configuration

Using the modified tunnel setup, the sphere cone was originally placed at the downstream end of the 45° expansion to the new sting-support section. The intent of this placement was to allow the bow shock from the model to impinge on the free shear layer downstream of the nozzle. The boundary layer would then experience a highly favorable pressure gradient created by the expansion at the upstream end of the larger sting-support section. This gradient would hopefully prevent any disturbances from feeding upstream in the subsonic portion of the boundary layer. Under these conditions, the tunnel might start when running larger models. Figure 4.26 shows a conceptual drawing of this theoretical flow in the new tunnel configuration. The shock or boundary-layer shapes are not meant to be conceived as accurate, but are to just give an idea of the basic flow phenomena under these conditions.

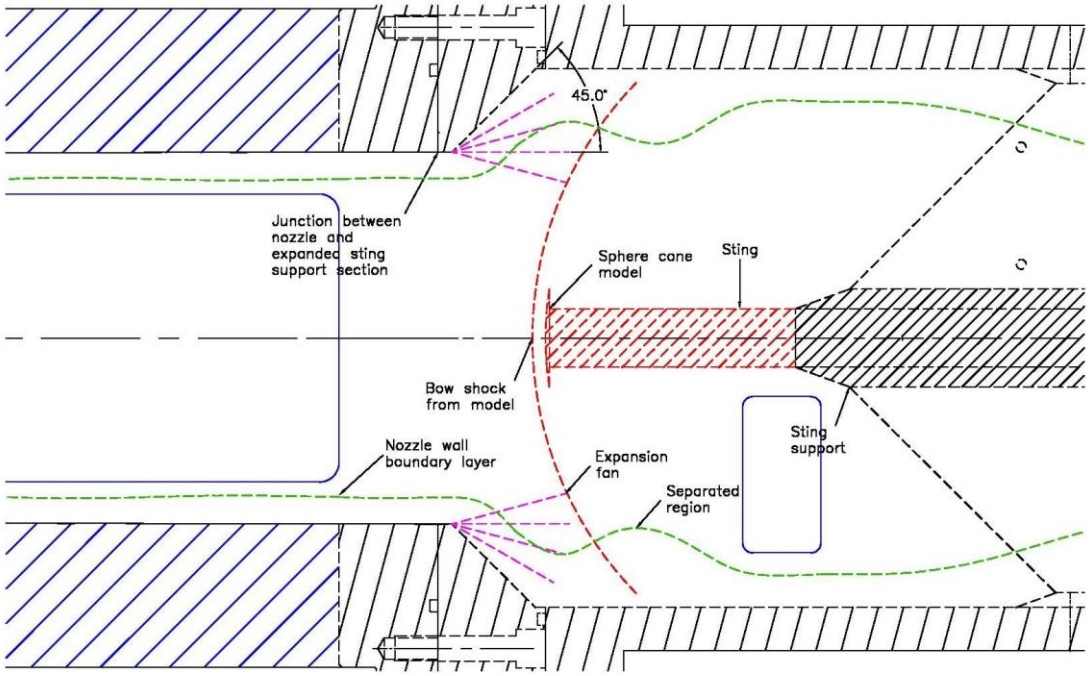

Figure 4.26. Schematic of modified tunnel configuration with sphere-cone model

4.2.1 Streamwise Variation of Starting Performance

Unfortunately, when placing the 2-inch model at this streamwise location, the performance of the new tunnel was inferior to that of the old setup. Figure 4.27 shows the model-nose and contraction pressure from a run at this streamwise location under quiet conditions. The driver-tube pressure is near the maximum quiet pressure, and the initial back pressure is the lowest possible vacuum pressure. Recall that these conditions were the optimal starting conditions for the original tunnel configuration. However, the nose pressure fluctuates over the entire range of the pressure sensor, meaning the tunnel has unstarted during this run. Instead of diminishing the shock interaction, the large separation zone aft of the ramp has apparently amplified it. Upon closer inspection, there are noticeable 200 Hz oscillations in the nose pressure as well as hot-film traces in all runs performed with the model at this streamwise location (Appendix A.4).

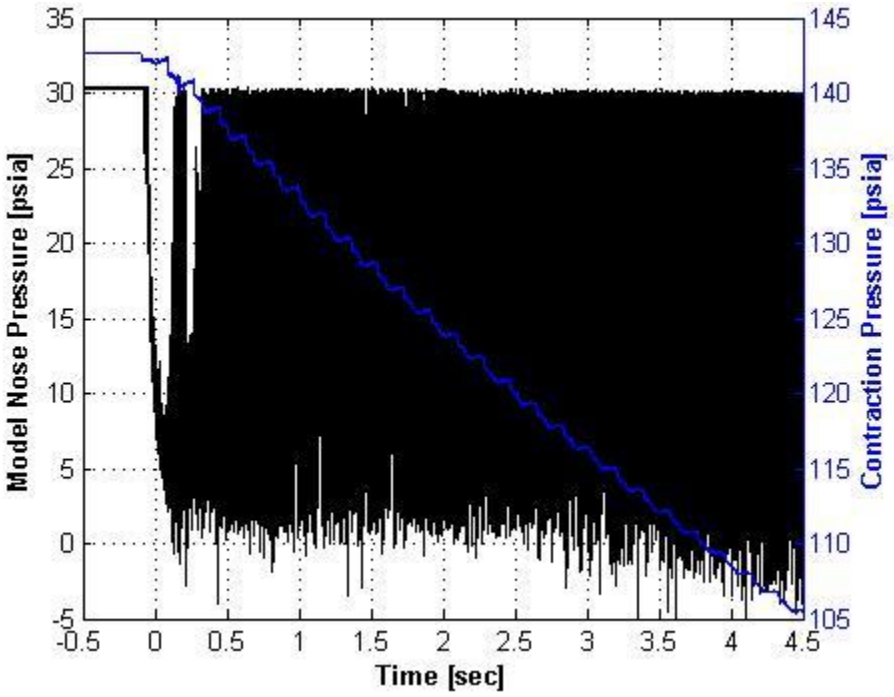

Figure 4.27. Contraction and nose pressure for 2-inch model under quiet conditions and model nose located at the downstream end of the expansion ramp (p_d = 142.6 psia, p_v = 0.58 torr, Date: 1 February 2008, $p_{max,quiet}$ = 140 psia)

Similar tests were performed after moving the model 6 and 8 inches upstream, showing no difference in the behavior of the flow. The flow behavior did not improve until the model was placed 11.125 inches upstream. At this location—about 8.375 inches upstream of the nozzle exit plane—there is a small amount of quiet, attached flow. Figure 4.28 shows the nose pressure along with the contraction pressure from a run at this streamwise location under quiet conditions. The initial stagnation pressure is near the maximum quiet pressure, and the initial back pressure is comparable to that of the run shown on Figure 4.27. Under these conditions, the flow attaches around t = 0.35 sec. and remains well-behaved for the next 0.35 seconds. After this, the flow appears to separate until around t = 2.08 sec., at which point it unstarts.

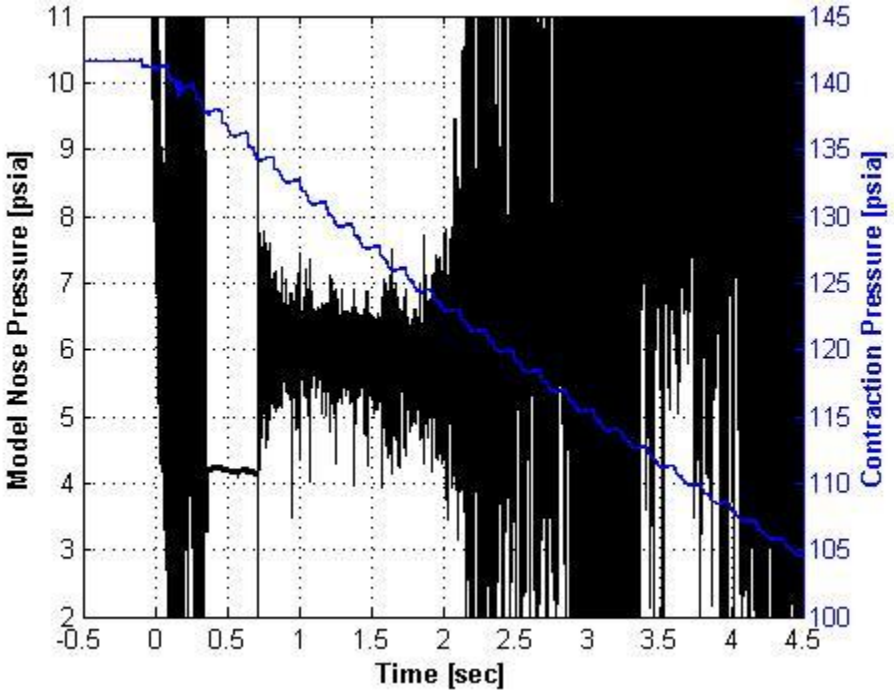

Figure 4.28. Contraction and nose pressure for 2-inch model under quiet conditions and model nose located 8.375 inches upstream of nozzle exit (p_d = 141.7 psia, p_v = 0.85 torr, Date: 31 January 2008, $p_{max,quiet}$ = 140 psia)

Figure 4.29 shows the RMS nose pressure and Mach number for this run. On the small period of attached flow, the noise level drops to about 0.2%, and the Mach number reaches 5.94 – 5.96. These levels are similar to those seen when using the 2.5-inch model in the original tunnel setup. During the separated portion of the run, the noise level increases to 2 – 7%, and the Mach number drops to around 5.4, similar to the flow behavior seen during the separated portions of runs using the 2-inch model in the old setup.

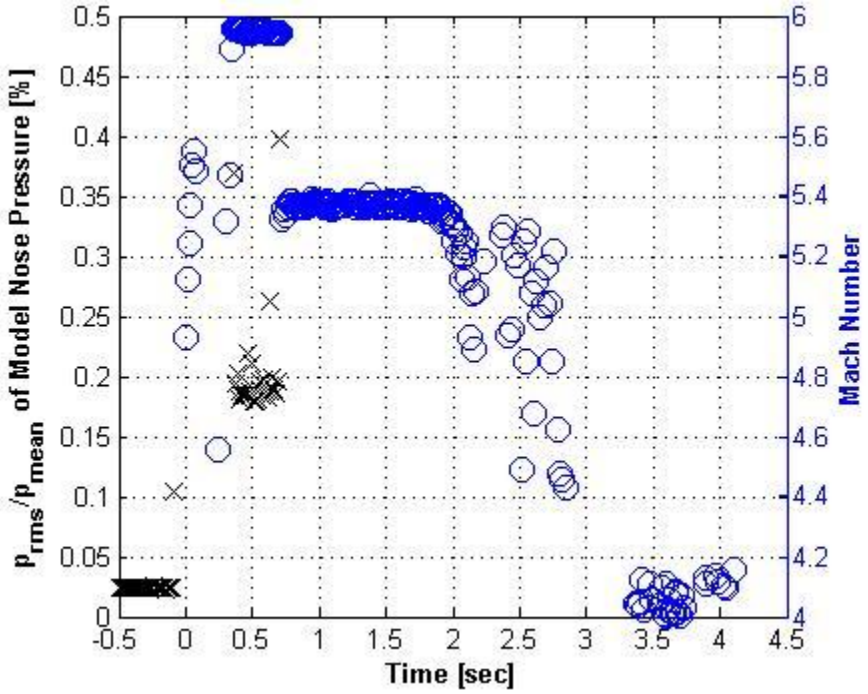

Figure 4.29. Noise level and Mach number for 2-inch model located 8.375 inches upstream of nozzle exit under quiet conditions (p_d = 141.7 psia, p_v = 0.85 torr, Date: 31 January 2008, $p_{max,quiet}$ = 140 psia)

4.2.2 Starting Performance at Farthest Upstream Location

At the farthest possible upstream location, which was set by the length of the sting, the run time was increased to about 3 seconds, less than half of the run times seen using the original tunnel setup. Figure 4.30 shows the nose pressure and contraction pressure from with the model approximately 10.25 inches upstream of the nozzle exit. Although the initial back pressure is somewhat higher than in previous runs shown, the model-nose pressure still shows the flow

attaching and remaining well-behaved until reaching a period of separation from t = 0.75 sec. to t = 2.1 sec. After this section of the run, the flow re-attaches until t = 3 sec., at which point the flow unstarts. This is an approximately 50% decrease in run time, which is most likely due to a reduction in the pressure recovery in the diffuser caused by the massive separation at the expansion ramp. As a result of the shorter run time, the data-recording time period was cut in half. Thus, data from runs using the modified tunnel configuration were recorded at twice the acquisition rate of runs in the old setup.

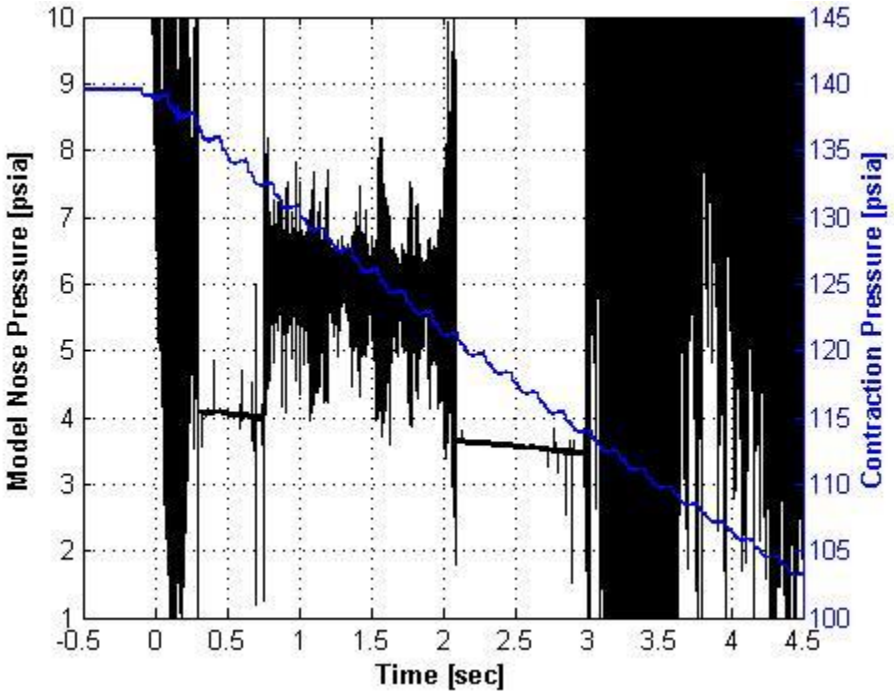

Figure 4.30. Contraction and nose pressure for 2-inch model under quiet conditions and model nose located 10.125 inches upstream of nozzle exit (p_d = 139.7 psia, p_v = 3.35 torr, Date: 31 January 2008, $p_{max,quiet}$ = 140 psia)

During the initial period of attached flow and during the separation period, the noise level and Mach number are similar to the previous run. However, when the flow reattaches the noise level steadily increases from 0.2% to 0.25% until the flow unstarts, as shown on Figure 4.31. Recall that under similar conditions in the original tunnel setup, the noise levels were around 0.07 – 0.1% when using the 2-inch model. Thus, the noise level effectively doubles with the modified

tunnel setup, even though the tunnel is only changed well downstream of the model. Correspondingly, the Mach number steadily decreases from 6 to 5.97 during this same period of the run. This is a decrease of 0.1 from what was seen under similar initial pressure conditions with the 2.25-inch model in the original tunnel configuration (Figure 4.10). Due to changes in the quiet performance in the original tunnel configuration, this is the closest possible comparison to the old setup.

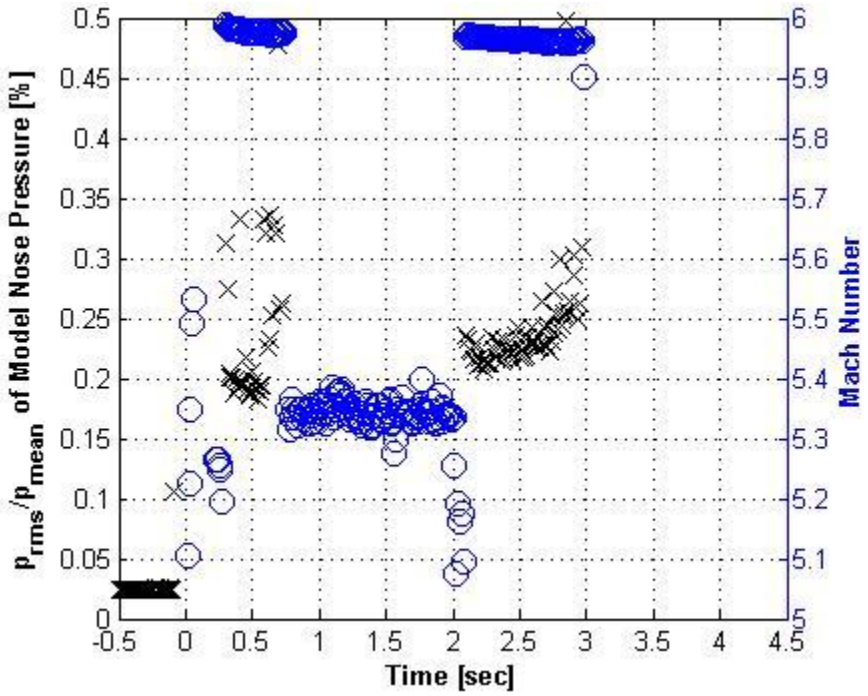

Figure 4.31. Noise level and Mach number for model located 10.125 inches upstream of nozzle exit under quiet conditions (p_d = 139.7 psia, p_v = 3.35 torr, Date: 31 January 2008, $p_{max,quiet}$ = 140 psia)

4.3 Summary of Performance of Modified Tunnel Configuration

Figure 4.32 shows the starting performance of the tunnel at the farthest upstream location, 10.125 inches upstream of the nozzle exit. At this streamwise location a 2.5-inch model still starts in this setup at the maximum quiet pressure of 140 psia and low back pressure. Thus, the starting performance of the modified tunnel configuration is similar to that of the original tunnel setup. However, the flow separated throughout the run when starting the tunnel at 110 psia or

lower in the modified configuration. This 110 psia is a significant increase from the 60 – 80 psia threshold for separated flow that was seen with the original tunnel setup. Lastly, although there are no figures shown from runs made under noisy conditions, all such runs resulted in unstarted flow regardless of streamwise location. Overall, the starting performance in terms of model size of the modified tunnel with the model at this streamwise location is comparable to that of the old setup. However, the noise level doubles, and the run time is cut in half. Also, note that the flow only starts when placing the model far upstream of the expansion corner. Recall that the purpose of the new section was to improve starting performance by placing the model downstream of the expansion.

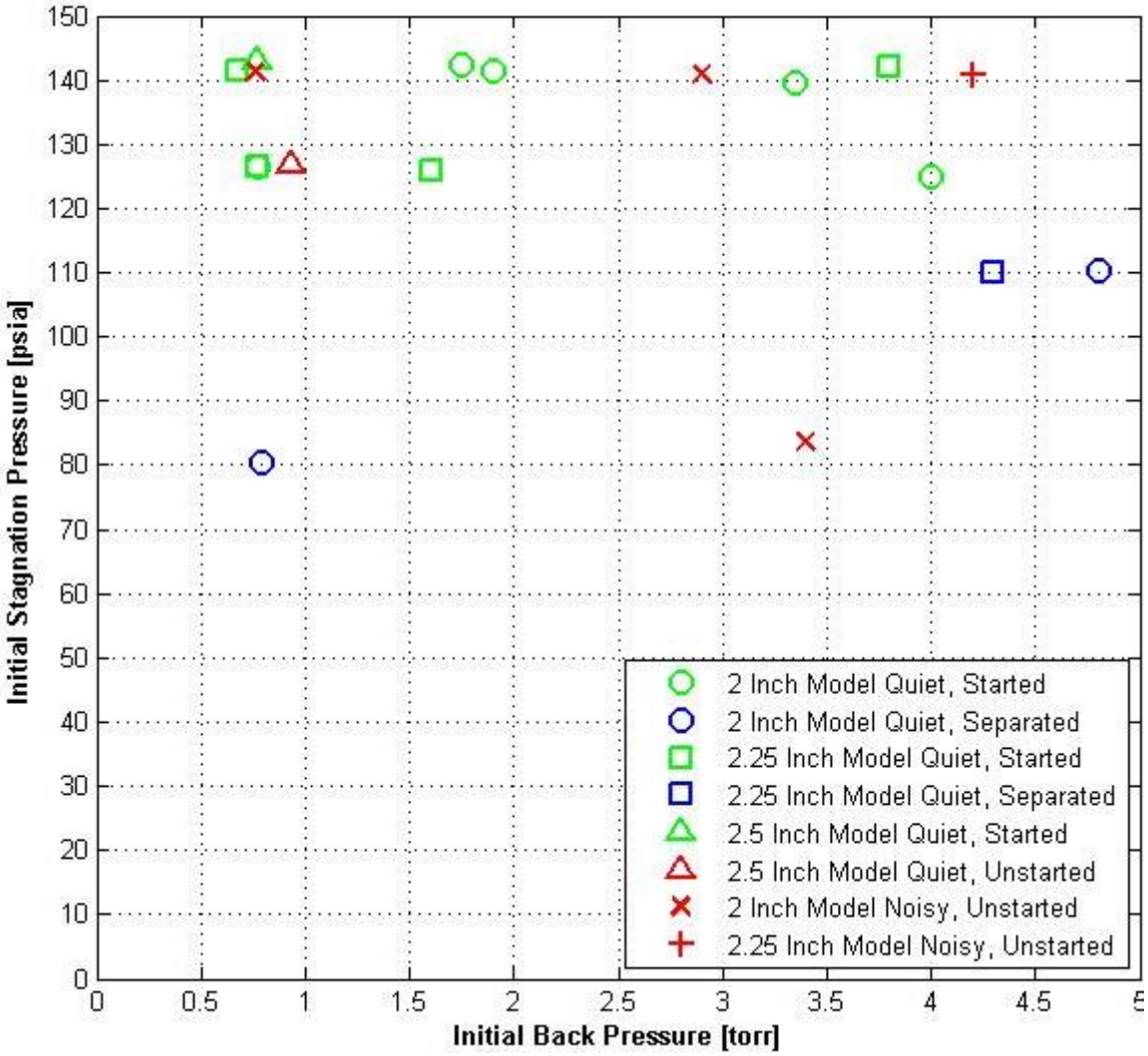

Figure 4.32. Starting performance of the modified tunnel configuration with the model placed 10.25 inches upstream of nozzle exit

5 CONCLUSIONS AND FUTURE WORK

The diffuser of the BAM6QT was modified in an attempt to improve the starting performance. However, to date the performance has not even matched the performance of the original tunnel configuration. The rapid expansion at the downstream end of the nozzle may have caused a large separation region at the corner of the ramp. This separation caused more problems than expected. This is also evident in the streamwise dependence of the starting performance of the new tunnel configuration. The starting performance is best when the bow shock impinges well upstream of the expansion corner and deteriorates as the model is moved downstream.

While this is not currently possible in the BAM6QT, visual experimental techniques would be useful in determining causes of the flow unstarting. Computation methods would also be helpful in approximating the entire flowfield around the sphere-cone model in the tunnel. The original plan for the new diffuser required the installation of inserts to provide a more gradual expansion and recompression downstream of the nozzle. However, the new sting-support and diffuser sections took much longer to build than was initially expected, so the tests shown here were carried out without inserts. Ongoing work is being carried out to test two types of inserts. Figure 5.1 shows a schematic of a 9-degree nylon insert that is placed on top of the expansion ramp. By decreasing the turning angle the flow is less prone to separate. However, preliminary tests to date show no improvements.

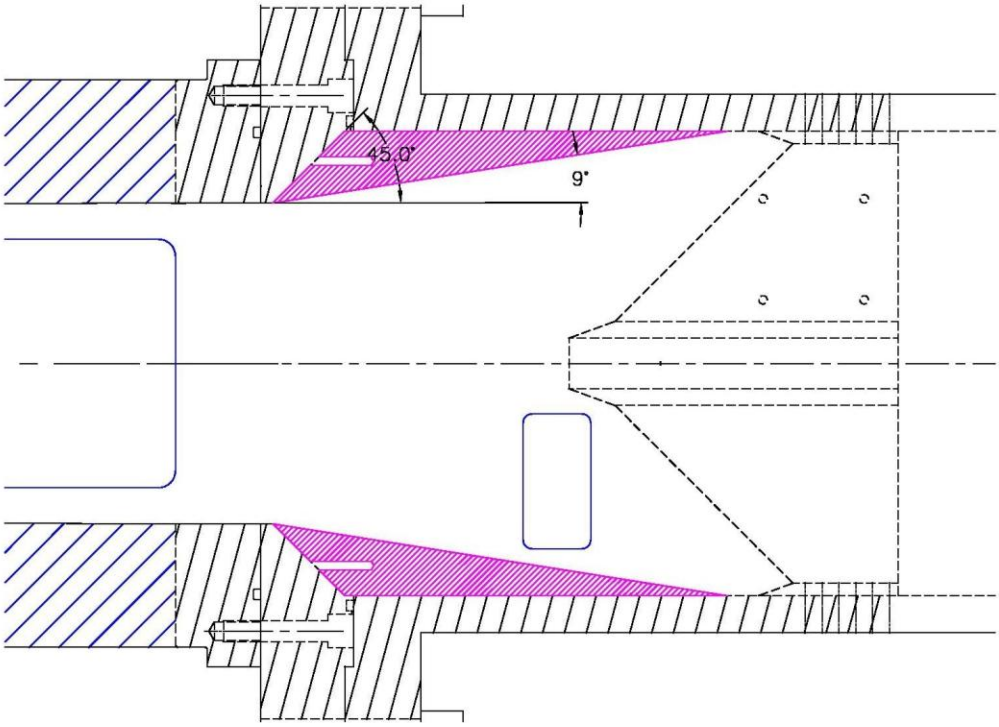

Figure 5.1. Schematic of 9-degree nylon insert in modified tunnel section

Figure 5.2 shows a schematic of a straight-pipe insert made of stainless steel. This insert provides a variable slot between the downstream end of the nozzle and the insert. Theoretically, the pressure on the outside of this region would be lower than the centerline freestream pressure. The suction from this pressure difference would then remove much of the upstream boundary layer. Preliminary tests to date again show no noticeable improvements. However, no tests have been made to determine the effect of the slot width (variable from 0 to 1.5 inches). Also, a porous straight-pipe insert might be helpful in improving the starting performance and is also to be built.

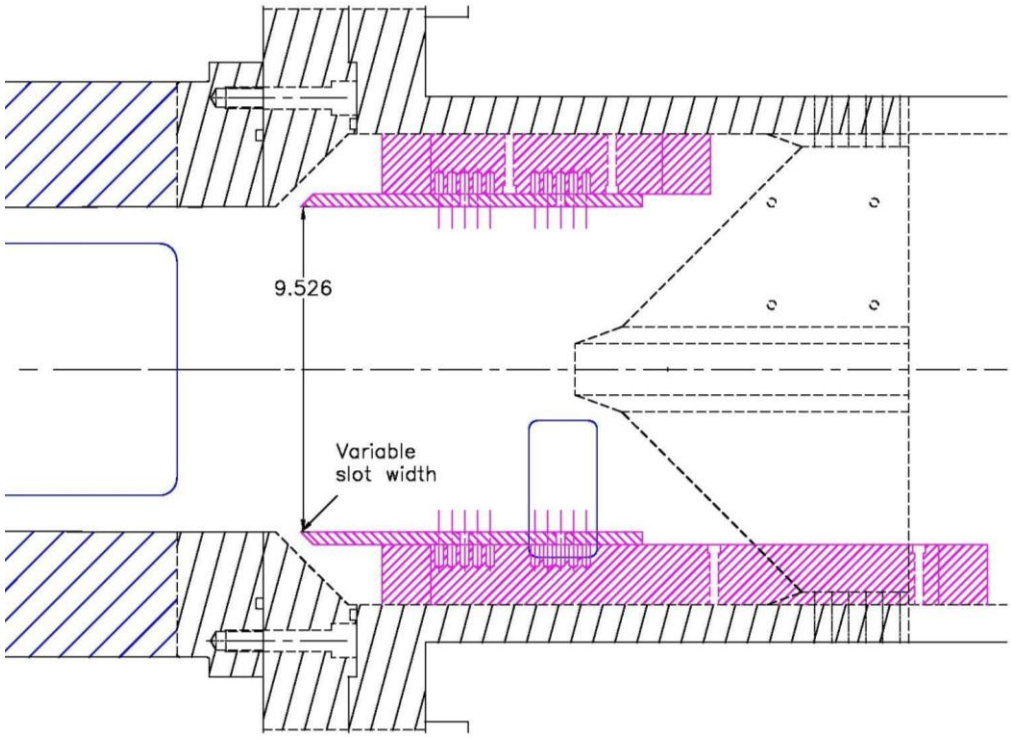

Figure 5.2. Schematic of steel straight-pipe insert in modified tunnel section. Dimensions in inches.

LIST OF REFERENCES

LIST OF REFERENCES

[1] Alan Pope and Kennith L. Goin. *High-Speed Wind Tunnel Testing*, chapter 1, High Speed Wind Tunnel Theory. Robert E. Krieger Publishing Co., Inc., Malabar, FL, 1978.

[2] Steven P. Schneider. The development of hypersonic wind tunnels. AIAA Paper 2007-4486, June 2007.

[3] C.J. Schueler, An Investigation of Model Blockage for Wind Tunnels at Mach Numbers 1.5 to 19.5, AEDC TN 59-165, 1960.

[4] R.H. Sabersky, A.J. Acosta, E.G. Hauptmann, and E.M. Gates. *Fluid Flow: A First Course in Fluid Mechanics*, chapter 8, Flow over External Surfaces. Prentice-Hall, Upper Saddle River, NJ, 1999.

[5] Frank M. White. *Viscous Fluid Flow*, chapter 4, Laminar Boundary Layers. McGraw-Hill, New York, NY, 3rd edition, 2006.

[6] John D. Anderson Jr. *Fundamentals of Aerodynamics*, chapter 15.2, Qualitative Aspects of Viscous Flow. McGraw-Hill, New York, NY, 3rd edition, 2001.

[7] John D. Anderson Jr. *Hypersonic and High Temperature Gas Dynamics*, chapter 7.5, Hypersonic Shock-Wave/Boundary Layer Interactions. American Institute of Aeronautics and Astronautics, Inc., Reston, VA, 1989.

[8] Steven P. Schneider. Initial shakedown of the Purdue Mach-6 quiet-flow Ludwieg tube. AIAA Paper 2000-2592, June 2000.

[9] Craig R. Skoch. *Disturbances from Shock/Boundary-Layer Interactions Affecting Upstream Hypersonic Flow*. Ph.D. thesis, Purdue University School of Aeronautics and Astronautics, December 2005.

[10] Thomas J. Juliano. *Nozzle Modifications for High-Reynolds-Number Quiet Flow in the Boeing/AFOSR Mach-6 Quiet Tunnel*. Master's thesis, Purdue University School of Aeronautics and Astronautics, December 2006.

[11] Eric W. Weisstein. "Root-Mean-Square." From *Mathworld*—A Wolfram Web Resource. http://mathworld.wolfram.com/Root-Mean-Square.html

[12] Curtis F. Gerald and Patrick O. Wheatley. *Applied Numerical Analysis*. Chapter 0.4, Implementing Bisection. Addison Wesley Longman, Inc., Reading, MA, 1999.

[13] *MATLAB User's Manual*, Mathworks Inc., MA, USA, 1999.

[14] Steven P. Schneider, Craig Skoch, Shann Rufer, Erick Swanson, and Matthew Borg. Bypass transition on the nozzle wall of the Boeing/AFOSR Mach-6 quiet tunnel. AIAA Paper 2004-0250, January 2004.

[15] *Type 1035/El-O-Matic Rack-and-Pinion Rotary Actuator Instruction Manual*, p. 6, Emerson Process Management, Marshalltown, IA, 2007.

[16] *Series V & T Valves Versa Bulletin VT-2003*, p. 35, Versa Products Company, Inc., Paramus, NJ, 2003.

[17] Ray E. Boltz and George L. Tuve. *CRC Handbook of tables for Applied Engineering Science*, Table 1-57, Mechanical Properties of Metals and Alloys. CRC Press, Inc. Boca Raton, FL, 1976.

[18] Scot Finney. Drawings of Boeing Mach-6 Ludwieg tube sting-support section – rev. P, sheet 5. Anderson Tool & Engineering Co., Anderson, IN, 2007.

APPENDICES

A. Detailed Analysis of Experiments

A.1 Periodic Oscillations at Lower Reynolds Number in Original Tunnel Configuration under Quiet Conditions

There is a noticeable change of behavior in the nose pressure traces when the initial stagnation pressure drops beyond a certain point. At this point, the nozzle-wall boundary layer appears to separate throughout the entire run. From Figure 4.22, it appears that this threshold for initial stagnation pressure lies somewhere between 60 and 75 psia for tunnel runs employing the 2-inch model in the original tunnel setup. Recall from Figure 4.7 and Figure 4.8 that at such low initial stagnation pressures this separation increases the RMS fluctuations as well as the mean of the nose pressure. An expanded view of a portion of Figure 4.7 is shown on Figure A.1. Periodic oscillations are evident. These dominate the RMS. The FFT for the period between 1 – 2 seconds after the start of the run is given on Figure A.2, which shows the oscillations peak at a frequency of 78 Hz. These oscillations are evidently a periodic resonance caused by the shock-boundary layer interactions.

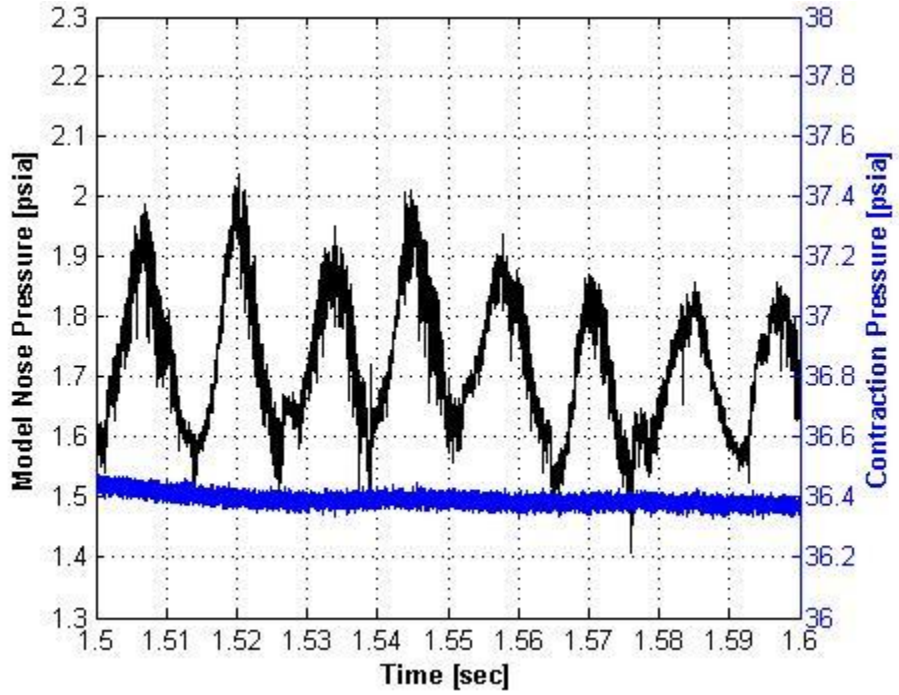

Figure A.1. Close-up view of contraction and nose pressure traces for 2-inch model under quiet conditions (p_d = 40.6 psia, p_v = 6.5 torr, Date: 30 March 2007, $p_{max,quiet}$ = 150 psia)

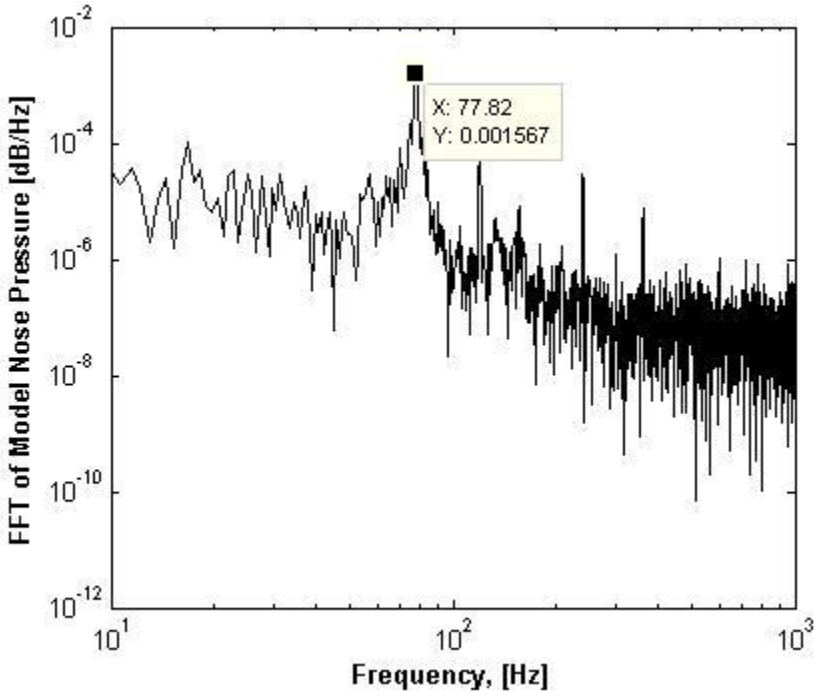

Figure A.2. Fast Fourier transform of nose pressure trace for 2-inch model under quiet conditions (p_d = 40.6 psia, p_v = 6.5 torr, Date: 30 March 2007, $p_{max,quiet}$ = 150 psia)

A.2 Periodic Oscillations with Larger Models under Quiet Conditions in Original Tunnel Configuration

Figure A.3 shows a close-up view of the separation period from Figure 4.11. There are very noticeable periodic oscillations in the model-nose pressure when using the 2.25-inch model. These oscillations were not observed when using the 2-inch model. This appearance of periodic oscillations when running the 2.25-inch model may be attributed to the stronger interactions of the bow shock and nozzle-wall boundary layers. These interactions may have higher amplitude when running with the 2.25-inch model than with the 2-inch model. Figure A.4 gives an FFT from the separated portion of the run taken from t = 1 sec. to t = 2 sec., showing a peak frequency of 88 Hz.

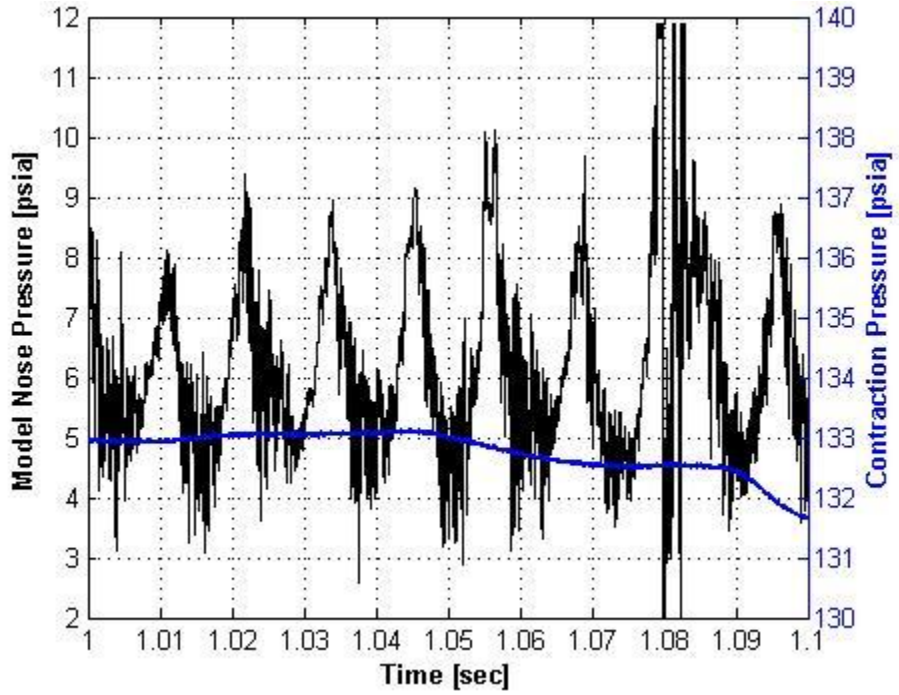

Figure A.3. Close-up view of contraction and nose pressure traces for 2.25-inch model under quiet conditions (p_d = 142.1 psia, p_v = 2.5 torr, Date: 16 October 2007, $p_{max,quiet}$ = 140 psia)

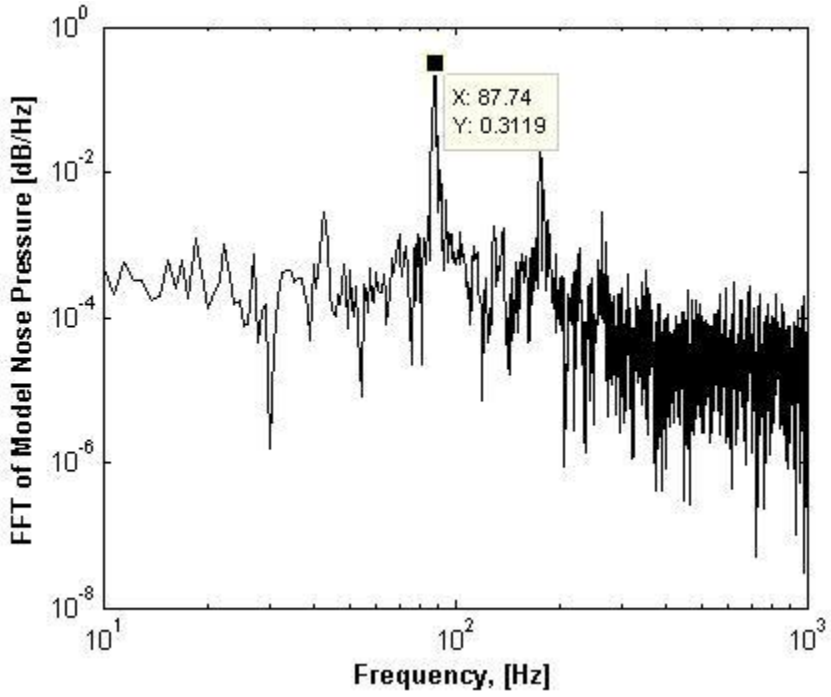

Figure A.4. Fast Fourier transform of nose pressure trace for 2.25-inch model under quiet conditions (p_d = 142.1 psia, p_v = 2.5 torr, Date: 16 October 2007, $p_{max,quiet}$ = 140 psia)

A.3 Periodic Oscillations with Unstarted Runs in Original Tunnel Configuration

Periodic oscillations are also seen in runs that unstarted. Figure A.5 gives a close-up view of the nose pressure trace from a run using the 2-inch model under noisy conditions. Throughout the duration of this run, the pressure fluctuated across almost the entire range of the model-nose pressure transducer. However, when viewed more closely, there is a very evident trend of periodic behavior in the pressure trace. Figure A.6 shows the FFT with a peak frequency of 149 Hz. From this information, it is possible that the cause of the large oscillations is not due to the tunnel unstarting in the conventional sense (with the freestream flow dropping subsonic). Instead, these oscillations may be caused by the shock-boundary layer interaction on the tunnel walls. For more information on the frequency of oscillations in unstarted runs, see Appendix B.

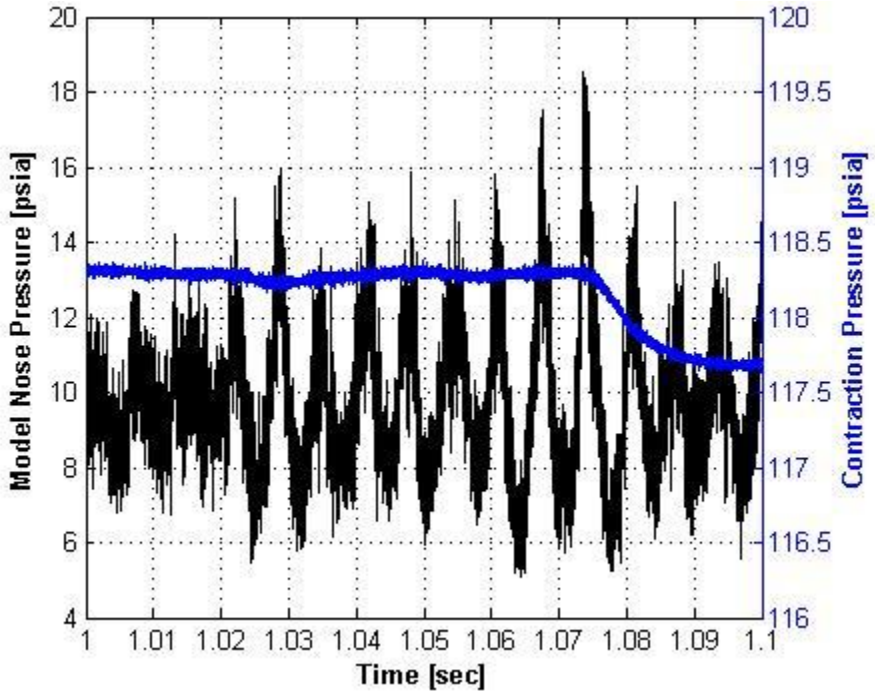

Figure A.5. Close-up view of contraction and nose pressure traces for 2-inch model under noisy conditions (p_d = 123.6 psia, p_v = 4.1 torr, Date: 13 September 2007, $p_{max,quiet}$ = 60 psia)

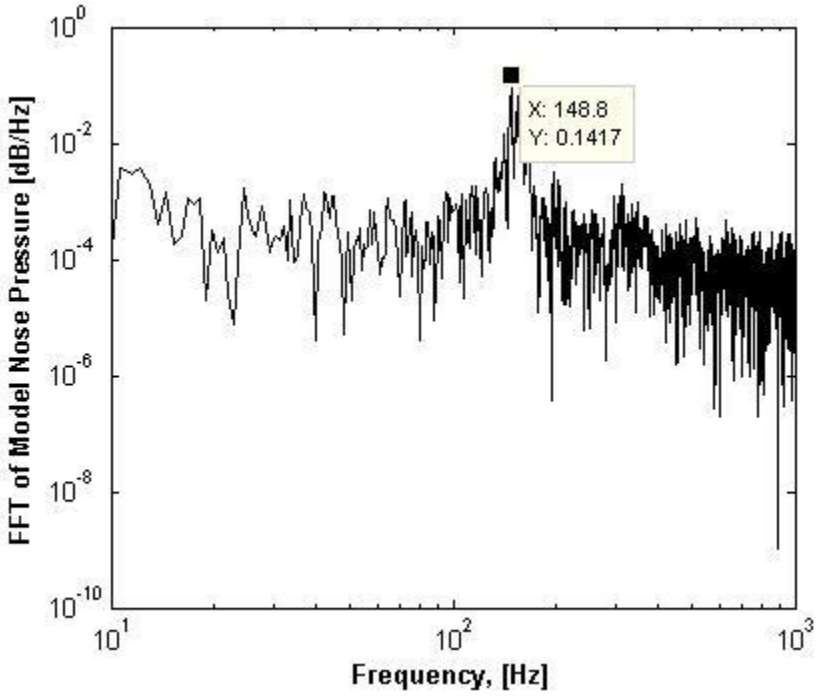

Figure A.6. Fast Fourier transform of nose pressure trace for 2-inch model under noisy conditions (p_d = 123.6 psia, p_v = 4.1 torr, Date: 13 September 2007, $p_{max,quiet}$ = 60 psia)

A.4 Periodic Oscillations with Modified Tunnel Configuration

The 2-inch model was placed in the tunnel such that the nose of the model was located at the exit plane of the expansion downstream of the nozzle. A close-up view of the nose pressure trace from 1 to 1.05 seconds is shown in Figure A.7. The periodic oscillations are noticeable. Figure A.8 shows the oscillations also occurring on the hot films. With close inspection the waves on the downstream hot film appear to be leading those of the hot film located 7.25 inches upstream by approximately 1 ms. Based on these results, it appears that under these conditions, there is a disturbance in the flow traveling upstream at about 600 ft/sec. An FFT shown on Figure A.9 shows a peak frequency of 194 Hz.

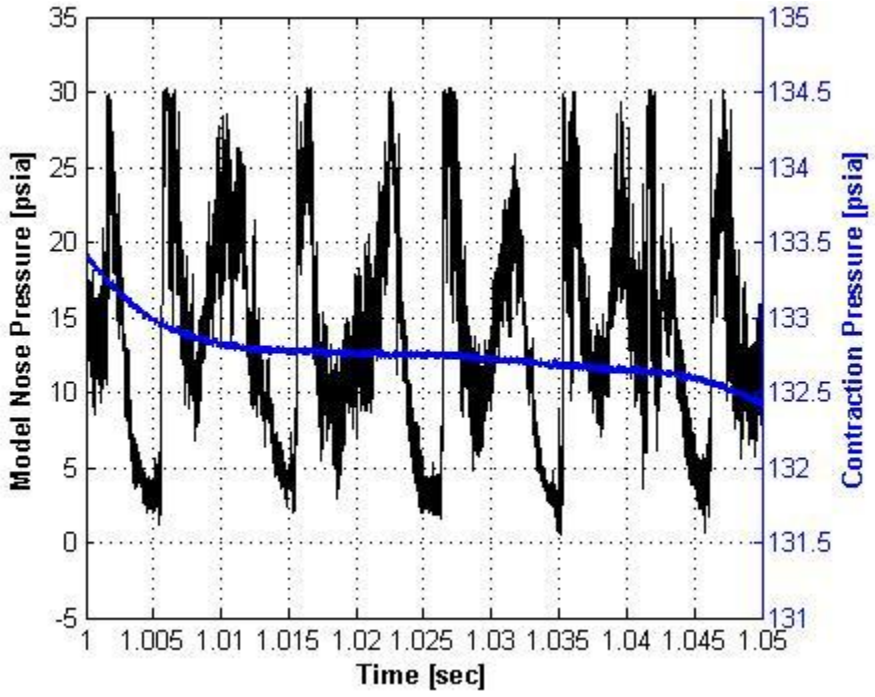

Figure A.7. Close-up view of contraction and nose pressure traces for 2-inch model under quiet conditions at nozzle exit (p_d = 142.6 psia, p_v = 0.58 torr, Date: 1 February 2008, $p_{max,quiet}$ = 140 psia)

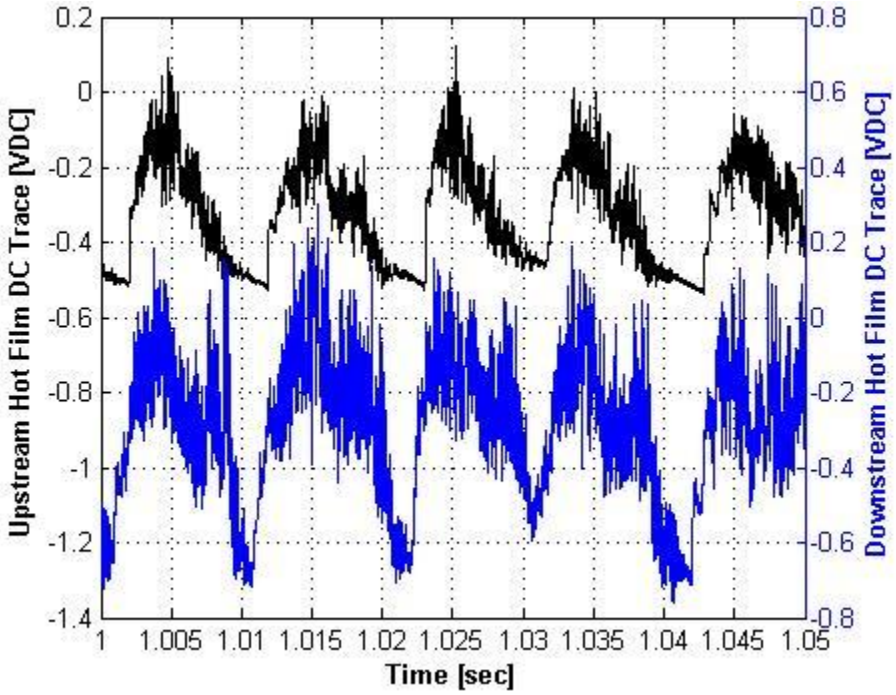

Figure A.8. Close-up of uncalibrated hot-film traces for 2-inch model under quiet conditions at nozzle exit (p_d = 142.6 psia, p_v = 0.58 torr, Date: 1 February 2008, $p_{max,quiet}$ = 140 psia)

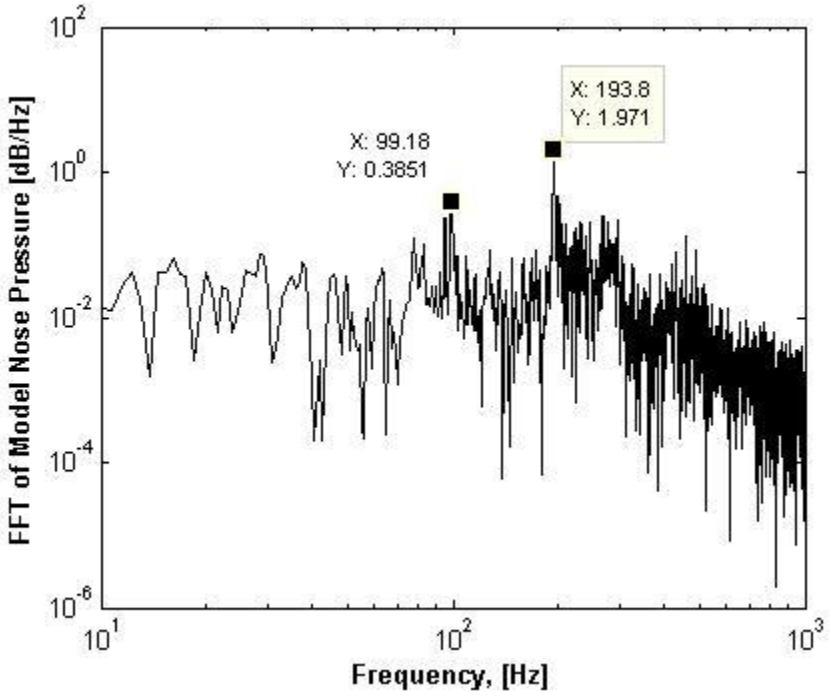

Figure A.9. Fast Fourier transform of nose pressure trace for 2-inch model under quiet conditions at nozzle exit (p_d = 142.6 psia, p_v = 0.58 torr, Date: 1 February 2008, $p_{max,quiet}$ = 140 psia)

B. Run-Data Tables

Table B.1. 2-inch model under quiet conditions in the original tunnel configuration (in decreasing order of p_d, model located at x = 11 inches)

#	Run Date	$p_{max,quiet}$ [psia]	p_d [psia]	p_v [torr]	T_{sep} [sec]	p_{rms}/p_{mean} [%]	M	F_{sep} [Hz]	$F_{unstart}$ [Hz]	Pressure Trace Data Notes
9	3/29/2007	150	181.7	3.2	n/a	0.53 to 0.59	5.91 to 5.99	n/a	152.6	Well-behaved and attached with many spikes after dropping to quiet pressure
12	3/30/2007	150	155.8	4.1	0.75 to 2	0.6 to 1.4	5.94 to 5.99	n/a	n/a	Well-behaved and attached after dropping to quiet pressure with period of separation in the middle of the run
20	3/31/2007	150	148.4	3.25	n/a	1.7 to 3.4	5.6 to 5.7	n/a	n/a	Well-behaved and attached for very short time with the remainder of the run noisy. Later noticed loose model wires.
13	3/30/2007	150	147	7.4	0.68 to 2.1	0.4 to 1.8	5.9 to 5.97	n/a	n/a	Well-behaved and quiet with period of separation in the middle of the run
5	3/28/2007	150	120.8	3.18	0.36 to 2	0.3 to 0.5	5.94 to 5.96	n/a	n/a	Well-behaved and quiet with period of separation in the middle of the run
4	7/20/2007	75	88.6	12.7	1.6 to 4.1	0.1 to 0.25	5.86 to 5.89	89	153.4	Well-behaved and quiet after dropping to quiet pressure at 1.6 sec. and period of separation
3	8/23/2007	80	85.6	3	0.9 to 2.5	0.08 to 0.2	5.9 to 5.95	n/a	n/a	Well-behaved and quiet after dropping to quiet pressure with period of separation in the middle of the run
9	9/13/2007	60	82.8	4.45	n/a	0.14 to 0.2	5.92 to 5.95	n/a	145.7	Well-behaved and quiet after dropping to quiet pressure
2	3/28/2007	150	82	3.9	0.2 to 3	0.6 to 1	5.78 to 5.87	n/a	n/a	Well-behaved and quiet after period of separation from 0.2 to 3 sec.
21	9/15/2007	60	81.7	4.3	n/a	0.16 to 0.22	5.97 to 5.99	n/a	149.5	Well-behaved and quiet after dropping to quiet pressure

#	Run Date	$p_{max,quiet}$ [psia]	p_d [psia]	p_v [torr]	T_{sep} [sec]	p_{rms}/p_{mean} [%]	M	F_{sep} [Hz]	$F_{unstart}$ [Hz]	Pressure Trace Data Notes
4	8/23/2007	80	81.6	3.5	0.4 to 4.2	0.07 to 0.23	5.92 to 5.94	n/a	n/a	Well-behaved and quiet with period of separation in the middle of the run from 0.4 to 4.2 sec.
1	7/20/2007	75	79.8	6.7	0.4 to 3.7	0.08 to 0.19	5.82 to 5.87	151	151	Well-behaved and quiet after period of separation, from 0.4 to 3.7 sec.
10	9/13/2007	60	79.3	5	n/a	0.15 to 0.23	5.9 to 5.96	n/a	142.7	Well-behaved and quiet after dropping to quiet pressure
2	7/20/2007	75	74.2	10	0.25 to 4.2	0.1 to 0.23	5.82 to 5.84	n/a	n/a	Well-behaved and quiet after period of separation, from 0.25 to 4.2 sec.
2	8/22/2007	80	61.5	2.8	n/a	2 to 7	5.3 to 5.5	72	n/a	Separated throughout
20	9/15/2007	60	60.5	6.7	n/a	3 to 7	5.35 to 5.5	87	n/a	Separated throughout
16	9/14/2007	60	60.1	5.8	n/a	2.5 to 6	5.4 to 5.5	69	n/a	Separated throughout
17	3/30/2007	150	40.6	6.5	n/a	3 to 9	5.1 to 5.4	78	n/a	Separated throughout
15	9/14/2007	60	40.3	4.1	n/a	2 to 9.5	5.3 to 5.55	75	n/a	Separated throughout
11	9/13/2007	60	39.7	4.5	n/a	2 to 7	5.3 to 5.57	76	n/a	Separated throughout

Table B.2. 2.25-inch model under quiet conditions in the original tunnel configuration (in decreasing order of p_d, model located at x = 11 inches)

#	Run Date	$p_{max,quiet}$ [psia]	p_d [psia]	p_v [torr]	T_{sep} [sec]	p_{rms}/p_{mean} [%]	M	F_{sep} [Hz]	$F_{unstart}$ [Hz]	Pressure Trace Data Notes
5	10/16/2007	140	182.6	4.8	n/a	0.1 to 0.25	6.01 to 6.06	n/a	145.7	Started after dropping quiet
4	10/16/2007	140	181.3	3.8	n/a	0.08 to 0.2	6.04 to 6.06	n/a	145.7	Started after dropping quiet
1	10/16/2007	140	142.1	2.5	0.66 to 2.53	0.1 to 0.35	6 to 6.02	88	n/a	Started after dropping quiet with period of separation in the middle of run
2	10/16/2007	140	140.6	6.3	0.7 to 2.7	0.1 to 0.32	6.02 to 6.03	88	n/a	Well-behaved after dropping quiet with period of separation in the middle of run
7	10/16/2007	140	121.4	3.1	0.43 to 3.06	0.1 to 0.3	5.98 to 6	85	n/a	Well-behaved after dropping quiet with period of separation in the middle of run
8	10/16/2007	140	120.5	9.95	0.35 to 2.7	0.1 to 0.3	5.985 to 6.005	85	n/a	Well-behaved after dropping quiet with period of separation in the middle of run
9	8/23/2007	80	102.3	3.35	n/a	0.15 to 0.31	5.98 to 6.005	n/a	143.4	Well-behaved and quiet after dropping to quiet pressure
7	8/23/2007	80	83.9	2.5	0.5 to 4.6	0.17 to 0.31	5.89 to 5.93	68	n/a	Well-behaved and quiet after dropping quiet at 0.5 sec. and period of separation from 0.5 to 4.6 sec.
8	8/23/2007	80	83.1	2.2	0.5 to 4.6	0.18 to 0.32	5.91 to 5.92	66	n/a	Well-behaved and quiet after dropping quiet at 0.5 sec. and period of separation
25	9/17/2007	60	81.4	2	n/a	0.19 to 0.25	5.92 to 5.95	n/a	141.1	Well-behaved and quiet after dropping to quiet pressure
26	9/17/2007	60	80.4	5	n/a	0.2 to 0.26	5.89 to 5.92	n/a	140.4	Well-behaved and quiet after dropping to quiet pressure
11	10/17/2007	140	80.4	5.8	0 to 3.9	0.1 to 0.2	5.915 to 5.94	82	n/a	Well-behaved and quiet after dropping to quiet pressure and period of separation

#	Run Date	$p_{max,quiet}$ [psia]	p_d [psia]	p_v [torr]	T_{sep} [sec]	p_{rms}/p_{mean} [%]	M	F_{sep} [Hz]	$F_{unstart}$ [Hz]	Pressure Trace Data Notes
12	10/17/2007	140	80.3	5.3	0 to 2.5	0.1 to 0.24	5.905 to 5.94	76	n/a	Well-behaved and quiet after dropping to quiet pressure and period of separation
10	10/17/2007	140	61.6	3.9	n/a	1.75 to 4.5	5.35 to 5.53	77	n/a	Separated throughout
16	10/17/2007	140	41.9	2.8	n/a	4 to 42	5.4 to 5.6	78	n/a	Separated throughout
18	10/17/2007	140	41.8	4.3	n/a	10 to 80	5 to 5.4	79	n/a	Separated throughout

Table B.3. 2.5-inch model under quiet conditions in the original tunnel configuration (in decreasing order of p_d, model located at x = 11 inches)

#	Run Date	$p_{max,quiet}$ [psia]	p_d [psia]	p_v [torr]	T_{sep} [sec]	p_{rms}/p_{mean} [%]	M	F_{sep} [Hz]	$F_{unstart}$ [Hz]	Pressure Trace Data Notes
23	10/18/2007	140	183.8	2.25	n/a	n/a	n/a	n/a	141.1	Not useful
19	3/31/2007	150	150	4.5	n/a	n/a	n/a	n/a	141.9	Not useful
20	10/17/2007	140	143.1	1.3	n/a	0.15 to 0.2	5.86 to 6	n/a	n/a	Not useful
22	10/18/2007	140	141.9	1.5	n/a	n/a	n/a	n/a	134.3	Not useful
21	10/17/2007	140	141.7	4.7	n/a	n/a	n/a	n/a	130.5	Not useful
24	10/18/2007	140	141.4	0.7	0.55 to 2.3	0.17 to 0.4	5.95 to 5.97	68	n/a	Started with period of separation in the middle of the run
30	10/19/2007	140	140.8	1.15	0.55 to 2.3	0.15 to 0.13	5.95 to 5.98	69/135	n/a	Started with period of separation in the middle of the run
25	10/18/2007	140	121.1	2.8	n/a	n/a	n/a	n/a	107	Not useful
26	10/18/2007	140	120.9	0.7	n/a	n/a	n/a	n/a	135	Not useful
10	8/23/2007	80	102.2	2.8	n/a	n/a	n/a	n/a	138.9	Not useful
27	10/18/2007	140	81.4	1.8	n/a	n/a	n/a	n/a	102	Not useful
28	10/19/2007	140	44.1	1.2	n/a	25 to 50	n/a	n/a	128.4	Not useful

Table B.4. 2-inch model under noisy conditions in the original tunnel configuration (in decreasing order of p_d, model located at x = 11 inches)

#	Run Date	$p_{max,quiet}$ [psia]	p_d [psia]	p_v [torr]	Bleeds Status	p_{rms}/p_{mean} [%]	M	$F_{unstart}$ [Hz]	Pressure Trace Data Notes
7	7/26/2007	75	254	4	Closed	n/a	n/a	149.3	Not useful
1	8/22/2007	80	253.3	3.8	Open	n/a	n/a	n/a	Not useful
8	3/29/2007	150	249.9	6.3	Open	n/a	n/a	150.3	Not useful
7	3/29/2007	150	248.3	4	Open	n/a	n/a	148.6	Not useful
10	3/29/2007	150	181.1	8.9	Closed	20 to 30	4.6	152.8	Not useful
3	9/13/2007	60	180	4.9	Closed	10 to 25	4.6	149.2	Not useful
11	3/30/2007	150	149.9	3.4	Closed	21 to 29	4.6	147.5	Not useful
5	9/13/2007	60	123.6	4.1	Closed	10 to 25	4.6 to 4.7	149	Not useful
4	9/13/2007	60	122.2	3.65	Closed	10 to 30	4.6 to 4.7	147.4	Not useful
6	9/13/2007	60	121.4	2.7	Open	10 to 25	4.6	144.8	Not useful
14	3/30/2007	150	119.8	10.5	Closed	23 to 30	4.6	147.6	Not useful
6	3/28/2007	150	119.3	7	Closed	2 to 2.75	5.67 to 5.71	n/a	Well-behaved and noisy throughout entire run
15	3/30/2007	150	103.3	6.2	Closed	23 to 32	4.6	148	Not useful
7	9/13/2007	60	101.2	2.4	Closed	10 to 25	4.6 to 4.7	150.5	Not useful
24	9/15/2007	60	94.4	4.3	Closed	10 to 22	4.6 to 4.72	149.2	Not useful
5	7/21/2007	75	90.8	4.5	Closed	2.2 to 2.8	5.72 to 5.74	n/a	Well-behaved and noisy throughout entire run
23	9/15/2007	60	89.5	5.2	Closed	10 to 24	4.6 to 4.71	146.7	Not useful
8	9/13/2007	60	89.5	4.3	Closed	11 to 23	4.6 to 4.71	147.6	Not useful
6	7/21/2007	75	89.2	16	Closed	26 to 34	4.66 to 4.74	149.5	Not useful
6	8/23/2007	80	84.2	2.5	Closed	24 to 34	4.66 to 4.74	149.5	Not useful
3	3/28/2007	150	83	4.5	Closed	2 to 2.5	5.6 to 5.66	n/a	Well-behaved and noisy throughout entire run
5	8/23/2007	80	82.1	2.85	Closed	23 to 34	4.68 to 4.75	151.8	Not useful
16	3/30/2007	150	82	15	Closed	24 to 34	4.59 to 4.66	149.5	Not useful
17	9/14/2007	60	75.7	2.6	Closed	10 to 20	4.6 to 4.72	151.1	Not useful
19	9/15/2007	60	75.4	5.9	Closed	1.75 to 2.1	5.67 to 5.69	n/a	Well-behaved and noisy throughout entire run
3	7/20/2007	75	75.1	11.3	Closed	27 to 33	4.64 to 4.72	146.5	Not useful
4	3/28/2007	150	71.3	4.5	Closed	26 to 35	4.63 to 4.69	148	Not useful
1	3/27/2007	150	70.8	3.25	Closed	26 to 35	4.64 to 4.71	148	Not useful
22	9/15/2007	60	60.5	6	Closed	11 to 19	4.64 to 4.74	147.2	Not useful
18	9/14/2007	60	59.9	5.1	Closed	10 to 22	4.64 to 4.72	144.2	Not useful
13	9/14/2007	60	39.9	3.6	Closed	11 to 19	4.64 to 4.72	148.8	Not useful
14	9/14/2007	60	39.9	2.95	Closed	11 to 18	4.64 to 4.71	147.6	Not useful

Table B.5. 2.25-inch model under noisy conditions in the original tunnel configuration (in decreasing order of p_d, model located at x = 11 inches)

#	Run Date	$p_{max,quiet}$ [psia]	p_d [psia]	p_v [torr]	Bleeds Status	p_{rms}/p_{mean} [%]	M	$F_{unstart}$ [Hz]	Pressure Trace Data Notes
6	10/16/2007	140	181	3.1	Closed	63 to 74	n/a	149.5	Not useful
3	10/16/2007	140	141.6	2.8	Closed	61 to 77	n/a	149.5	Not useful
9	10/16/2007	140	120.6	3	Closed	66 to 78	n/a	146.5	Not useful
14	10/17/2007	140	81.4	0.94	Closed	60 to 75	n/a	150.3	Not useful
13	10/17/2007	140	80.8	4.7	Closed	64 to 74	n/a	149.5	Not useful
28	9/17/2007	60	80.6	4.5	Closed	n/a	n/a	145.7	Not useful
15	10/17/2007	140	80.3	5.7	Closed	62 to 74	n/a	150.3	Not useful
27	9/17/2007	60	79.6	6	Closed	13 to 60	n/a	n/a	Not useful
17	10/17/2007	140	43	11	Closed	15 to 53	4.33 to 4.46	132	Not useful
19	10/17/2007	140	41.8	2.7	Closed	23 to 35	4.24 to 4.34	131.2	Not useful

Table B.6. 2-inch model under quiet conditions in the modified tunnel configuration (in increasing order of x_{nose} then decreasing order of p_d)

#	Run Date	$p_{max,quiet}$ [psia]	p_d [psia]	p_v [torr]	x_{nose} [in.]	T_{sep} [sec]	p_{rms}/p_{mean} [%]	M	F_{sep} [Hz]	$F_{unstart}$ [Hz]	Pressure Trace Data Notes
20	2/1/2008	140	142.6	0.58	-2.75	n/a	30 to 66	n/a	n/a	193.8	Not useful
5	12/17/2007	140	139.6	7.6	-2.75	n/a	n/a	n/a	n/a	93.84	Not useful
21	2/1/2008	140	111.2	2.7	-2.75	n/a	20 to 70	n/a	n/a	90.79/273.1	Not useful
22	2/1/2008	140	82.1	3.3	-2.75	n/a	25 to 70	n/a	n/a	93.08/280	Not useful
25	12/21/2007	140	141.7	1.9	2.25	n/a	15 to 75	n/a	n/a	105.3/211.3	Not useful
26	12/21/2007	140	141	1.8	5.25	n/a	10 to 55	n/a	n/a	97.66/196.1	Not useful
24	12/20/2007	140	151.1	2.9	8.375	n/a	2 to 9	5.2 to 5.5	n/a	150	Not useful
19	1/31/2008	140	141.6	0.85	8.375	n/a	0.17 to 0.2	5.95 to 5.98	n/a	n/a	Not useful
22	12/20/2007	140	140.8	3.5	8.375	n/a	0.14 to 0.17	5.95 to 5.96	n/a	n/a	Not useful
18	1/31/2008	140	137.8	11	8.375	n/a	0.22 to 0.25	5.96 to 5.97	n/a	n/a	Not useful
23	12/20/2007	140	101.7	2.5	8.375	n/a	1 to 3.5	5.4 to 5.45	n/a	n/a	Separated throughout
2	1/26/2008	140	142.4	1.75	10.25	0.69 to 2.03	n/a	n/a	n/a	n/a	Started with period of separation in the middle of the run
27	12/21/2007	140	141.5	1.9	10.25	0.65 to 2.18	0.14 to 0.18	5.93 to 5.95	n/a	n/a	Started with period of separation in the middle of the run
1	1/26/2008	140	139.6	3.35	10.25	0.75 to 2.1	0.17 to 0.3	5.97 to 6	n/a	n/a	Started with period of separation in the middle of the run
8	1/28/2008	140	126.5	0.77	10.25	0.66 to 2.22	0.2 to 0.35	5.96 to 5.99	n/a	n/a	Started with period of separation in the middle of the run
7	1/28/2008	140	124.9	4	10.25	0.63 to 2.3	0.16 to 0.24	5.95 to 5.98	n/a	n/a	Started with period of separation in the middle of the run
6	1/28/2008	140	110.3	4.8	10.25	n/a	2 to 9.5	5.3 to 5.4	n/a	n/a	Separated throughout
5	1/28/2008	140	80.4	0.79	10.25	n/a	1.3 to 8	5.25 to 5.43	n/a	n/a	Separated throughout

Table B.7. 2.25-inch model under quiet conditions in the modified tunnel configuration (in increasing order of x_{nose} then decreasing order of p_d)

#	Run Date	$p_{max,quiet}$ [psia]	p_d [psia]	p_v [torr]	x_{nose} [in.]	T_{sep} [sec]	p_{rms}/p_{mean} [%]	M	F_{sep} [Hz]	$F_{unstart}$ [Hz]	Pressure Trace Data Notes
11	1/30/2008	140	142.1	3.8	10.25	0.7 to 2.28	0.17 to 0.27	5.97 to 6	86.21	n/a	Started with period of separation in the middle of the run
10	1/28/2008	140	141.5	0.68	10.25	0.64 to 2.33	0.17 to 0.3	5.97 to 7	85.45	n/a	Started with period of separation in the middle of the run
14	1/30/2008	140	126.6	0.77	10.25	0.58 to 2.55	0.19 to 0.32	5.95 to 6	81.63	n/a	Started with period of separation in the middle of the run
13	1/30/2008	140	126	1.6	10.25	0.25 to 2.3	0.21 to 0.3	5.95 to 5.97	81.63	n/a	Started after period of separation
15	1/30/2008	140	110.1	4.3	10.25	n/a	2 to 18	4.95 to 5.8	80.87	n/a	Separated throughout

Table B.8. 2.5-inch model under quiet conditions in the modified tunnel configuration (in increasing order of x_{nose} then decreasing order of p_d)

#	Run Date	$p_{max,quiet}$ [psia]	p_d [psia]	p_v [torr]	x_{nose} [in.]	T_{sep} [sec]	p_{rms}/p_{mean} [%]	M	F_{sep} [Hz]	$F_{unstart}$ [Hz]	Pressure Trace Data Notes
16	1/31/2008	140	143	0.77	10.25	0.54 to 2.16	0.17 to 0.3	5.95 to 6	68.66	n/a	Started with period of separation in the middle of the run
17	1/31/2008	140	126.7	0.93	10.25	n/a	20 to 45	n/a	n/a	104.5	Not useful

Table B.9. 2-inch model under noisy conditions in the modified tunnel configuration (in increasing order of x_{nose} then decreasing order of p_d)

#	Run Date	$p_{max,quiet}$ [psia]	p_d [psia]	p_v [torr]	x_{nose} [in.]	p_{rms}/p_{mean} [%]	M	$F_{unstart}$ [Hz]	Pressure Trace Data Notes
3	12/15/2007	140	251	2.6	-2.75	n/a	n/a	n/a	Not useful
4	12/15/2007	140	250	4.7	-2.75	n/a	n/a	n/a	Not useful
24	2/1/2008	140	142.2	2.6	-2.75	13 to 35	n/a	29.75	Not useful
1	12/14/2007	140	141	2.9	-2.75	15 to 30	n/a	33.57	Not useful
2	12/15/2007	140	141	7	-2.75	n/a	n/a	n/a	Not useful
23	2/1/2008	140	85.1	3.9	-2.75	13 to 30	n/a	28.99	Not useful
6	12/17/2007	140	81.6	2	-2.75	n/a	n/a	n/a	Not useful
3	1/28/2008	140	141.2	0.76	10.25	14 to 35	4.5 to 4.8	148	Not useful
4	1/28/2008	140	140.9	2.9	10.25	13 to 35	4.5 to 4.8	150.3	Not useful
9	1/28/2008	140	83.8	3.4	10.25	14 to 35	4.5 to 4.9	146.5	Not useful

C. Schematics of Sphere-Cone Model

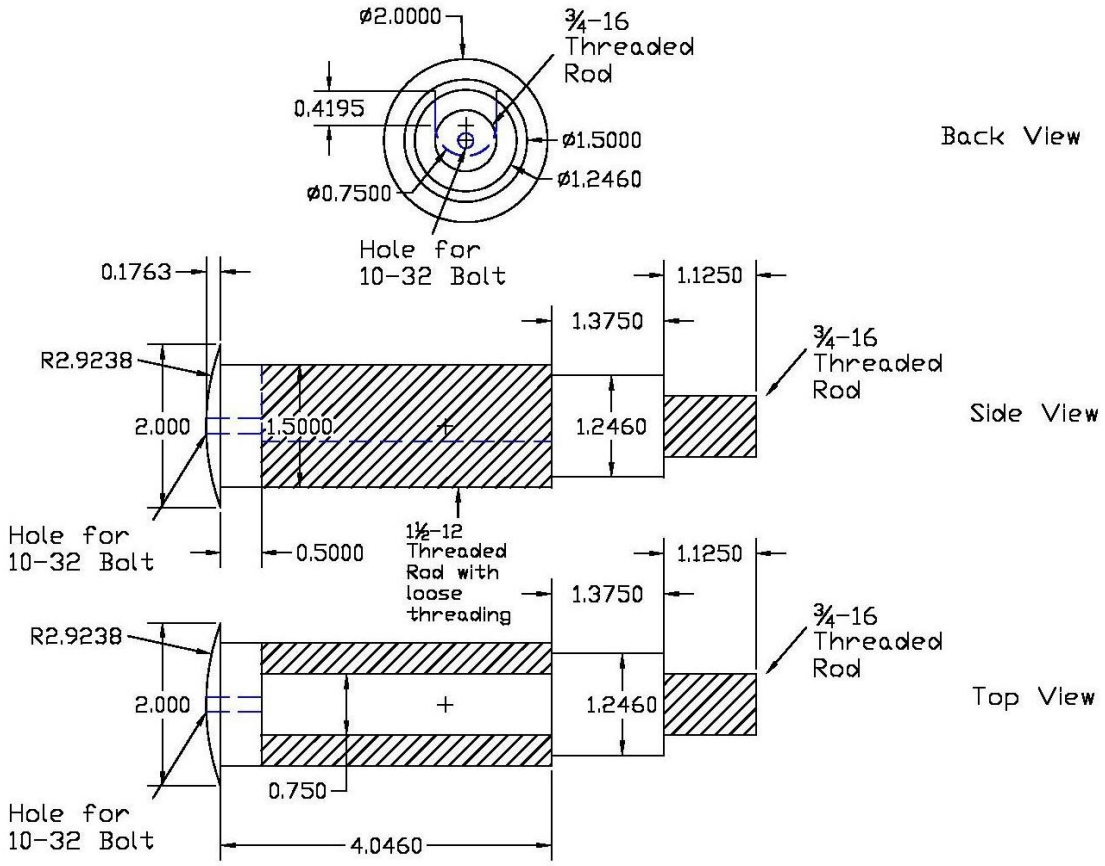

Figure C.1. Schematic of 2-inch-diameter model. Dimensions in inches.

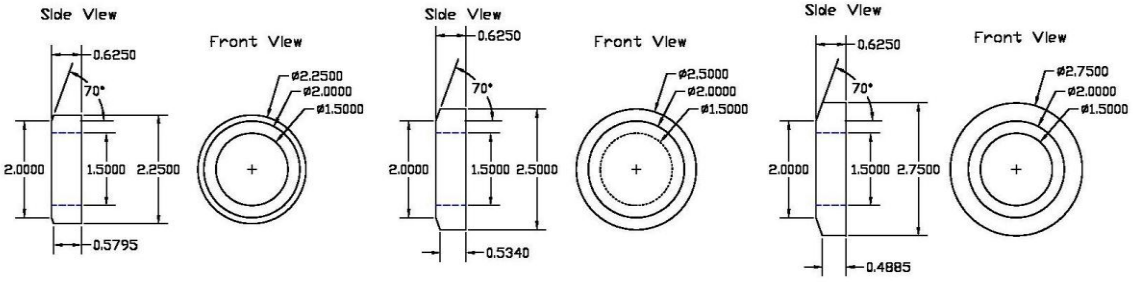

Figure C.2. Schematic of sphere cone base diameter additions (left to right: 2.25 inch, 2.5 inch, 2.75 inch outer diameter). Dimensions in inches.

D. Additional Tunnel Hardware

D.1 Fast-Acting Valve

To aid in improving the starting performance of the wind tunnel, a fast-acting valve was installed. Figure D.1 shows the fast valve mounted in the tunnel bleed line.

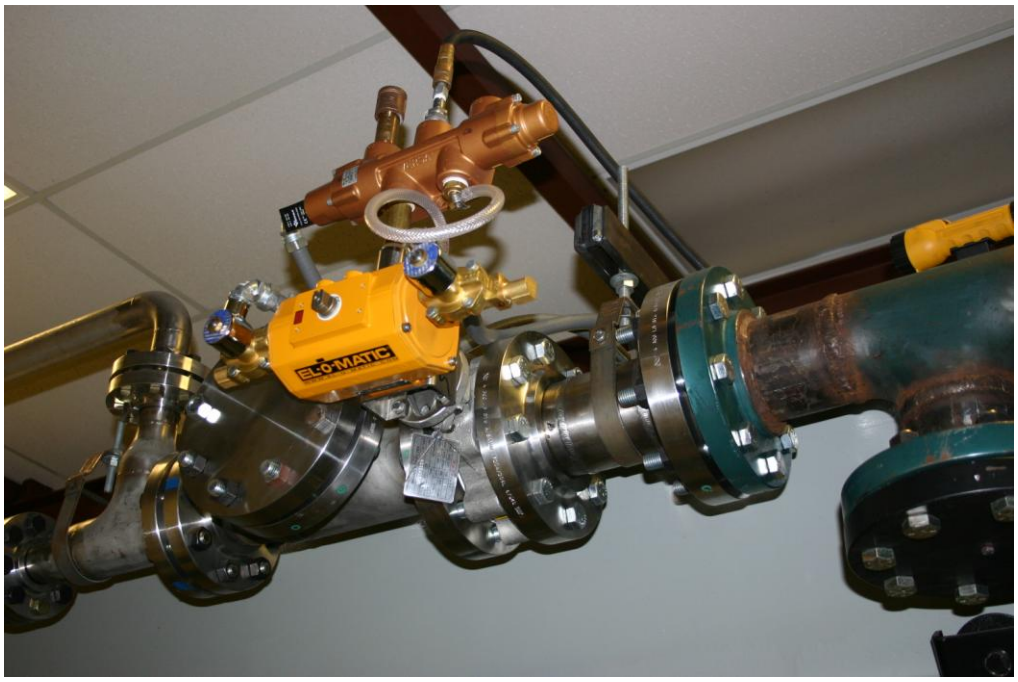

Figure D.1. Fast valve installed in BAM6QT bleed line

Prior to this installation, the air bled from the throat was usually plumbed to the diffuser section when running with the bleeds open. A jet therefore impinged on the flow downstream of the test section, which caused more blockage in the flow. This jet was seen to cause extra disturbances in the flow upstream in the test section by Skoch [9]. The fast valve in the bleed line enabled removal of the plumbing to the original diffuser section. An earlier valve made it possible to pass bleed air directly into the vacuum tank [14]. But the valve reacted too slowly at the start of each run, especially at low driver-tube pressures.

A customized El-O-Matic P&E Series Pneumatic EDA 100 actuator was installed to hasten the opening time of the new valve. The modifications made to the actuator by Ken Auer at Flow Systems, Inc. are listed below. Figure D.2 shows a close-up view of the altered actuator with all additional parts as well as ports labeled.

1. Opening the ¼" inlet to the actuator to ½" without interfering with the 3/32" exhaust bleed port, and reducing the size of the internal piston to prevent any blockage from the larger air intake.
2. Drilling holes on the end caps and installing a 3/8" 2-way 24-VDC GC Solenoid on both ends to allow for faster air evacuation from the closed actuator.
3. Installing a solenoid-activated VSG-4622-HC-3-A 120 Versa valve to the ports of the actuator to automatically redirect the incoming, externally-supplied air.

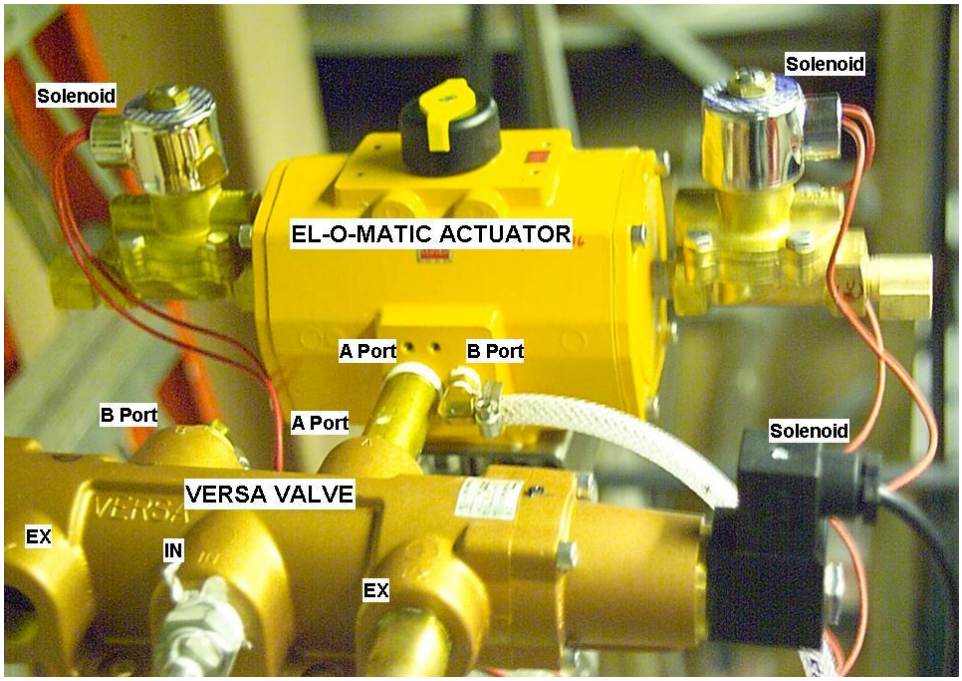

Figure D.2. Close-up view of augmented El-O-Matic actuator

A schematic of the El-O-Matic actuator is shown on Figure D.3. The Versa valve is shown in Figure D.4. While the valve is closed, air passes through the outgoing B port on the Versa valve (as shown on valve-closed position on Figure D.4) and pressurizes the “Port B Chamber” (as shown on Figure D.3). When activated, though, the solenoid at the end of the Versa valve redirects the externally-supplied air through the outgoing A port into the “Port A Chamber” of the actuator. The air originally pressurized in the port B chamber is directed through a 3/32” exhaust bleed port. Furthermore, in order to accelerate this process, the two solenoids at the end caps of the actuator are activated, which then open the 3/8” holes to increase the flow of pressurized air from the Port B chamber. The normal cycle period for the EDA 100 actuator is around 1.2 seconds. With these alterations to the design the opening time improves to 0.1 seconds.

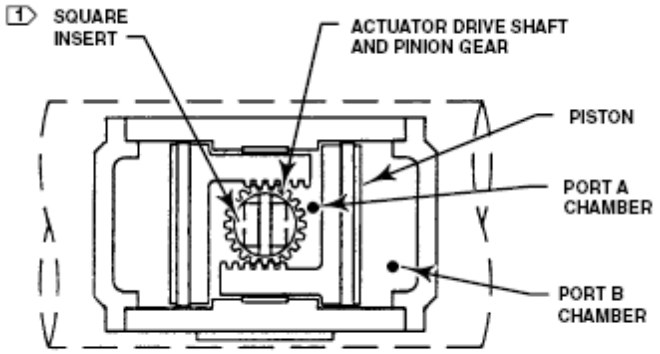

Figure D.3. Schematic of El-O-Matic actuator [15]

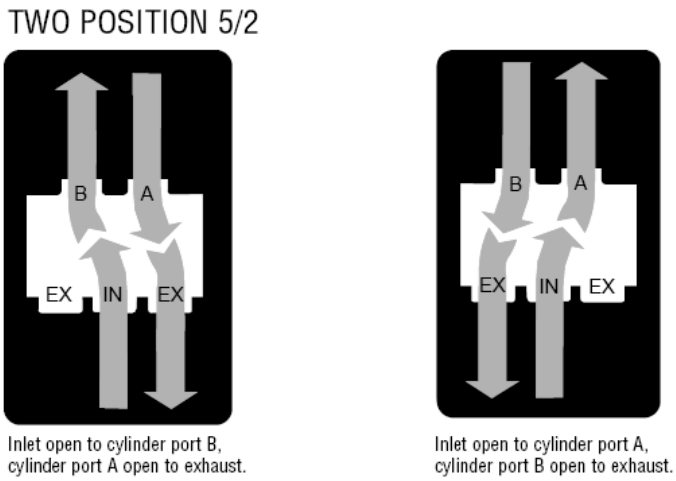

Figure D.4. Schematic of Versa valve (left to right: valve-closed position, valve-open position) [16]

The circuitry of the fast valve is designed to receive a signal from the oscilloscopes and also coordinate with the 12-inch gate valve located downstream of the diffuser section. Figure D.5 shows the fast valve electronics box, which houses this circuitry.

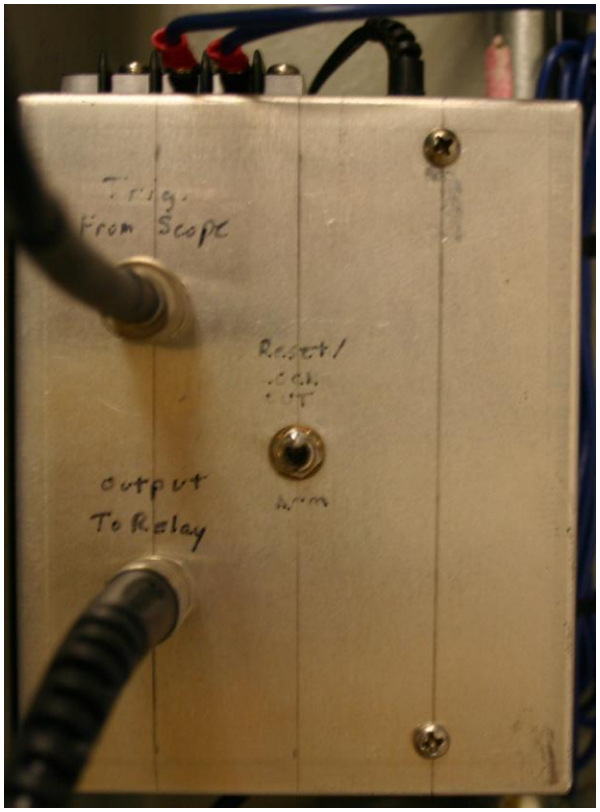

Figure D.5. Exterior of fast valve electronics box

This circuit is connected to the output of the oscilloscopes through a BNC cable to enable opening the fast valve at the beginning of any bleeds-open run. Under normal procedures, a pressure transducer is placed in the diffuser section. When the run starts, the pressure of the air at this region drops drastically. The oscilloscopes trigger after detecting this drop. When programmed to do so, the scopes then send a trigger-out signal to the input of the fast-valve circuit, shown on Figure D.6. The signal from the oscilloscope passes through a gating circuit to determine the status of the gate valve (open or closed) and the manual switch on the front of the electronics box (set to either “reset/lock out” or “arm”). If the gate valve is closed or the manual switch is set to “reset/lock out,” the input signal is grounded, and the valve remains closed. Otherwise, if the gate valve is open and the manual switch is set to “arm,” a +15 VDC signal is transmitted through a BNC cable to a solid state relay, which activates the solenoids and opens the fast valve. If this occurs, the circuit then keeps the valve open until the gate valve closes

again. This reduces the risk of contaminants from the less-filtered air in the vacuum tank traveling upstream through the bleed line and causing damage to the throat. Note that all hardware and circuitry for the fast-acting valve was designed and built by John Phillips of the Purdue University AAE Department Electronics Shop.

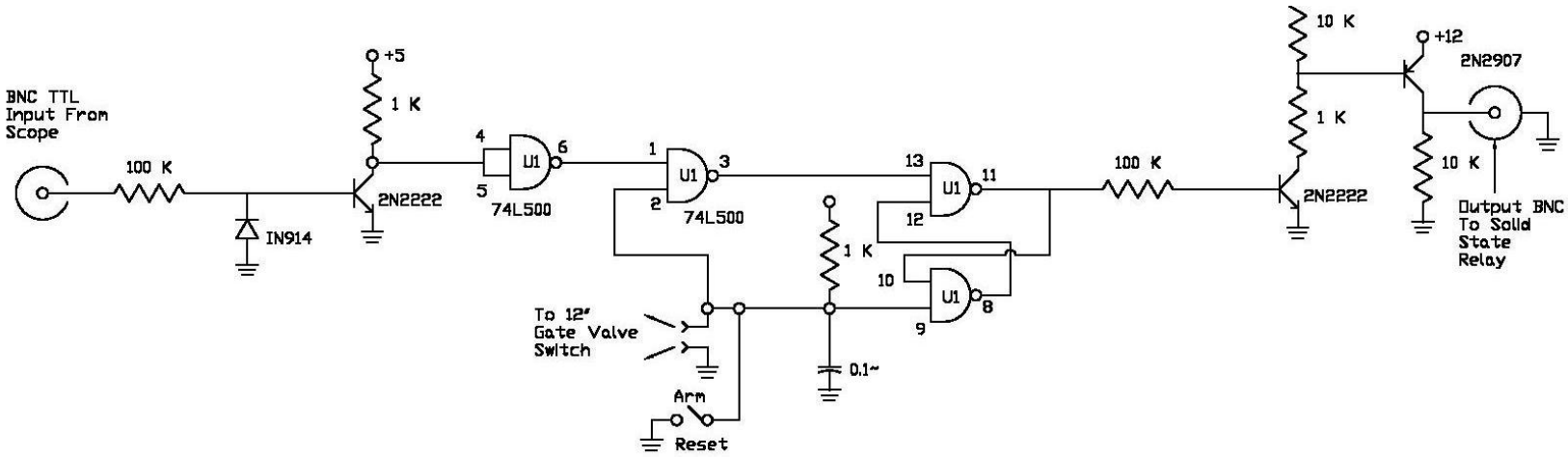

Figure D.6. Schematic of fast-valve circuit

Measurements were taken with a pressure transducer at the plenum of the bleed slot and near the location of the fast valve to determine the response time of the valve. The response time of the old bleed line depended on the pressure difference across the valve [9]. Thus, at low driver-tube pressures, the response time of the valve was unsatisfactory. However, upon close inspection the performance of the new fast-acting valve has very little dependence on the pressure difference. This is expected due to the externally-supplied air that drives the valve to open. Figure D.7 shows the ratio of the bleed-slot plenum pressure to the stagnation pressure during runs with differing driver-tube pressures and similar vacuum pressures. At time t = 0, the diaphragms burst and the oscilloscopes trigger. On all cases, the pressure in the bleed slot drops below the sonic pressure line (p_{pl}/p_0 = 0.528) within 0.2 seconds, the startup time of the tunnel. This is the point at which suction is achieved in the bleed slot. It also appears that as the driver-tube pressure is decreased by a factor of 3, the time to achieve suction in the bleeds in increased by less than 10 ms.

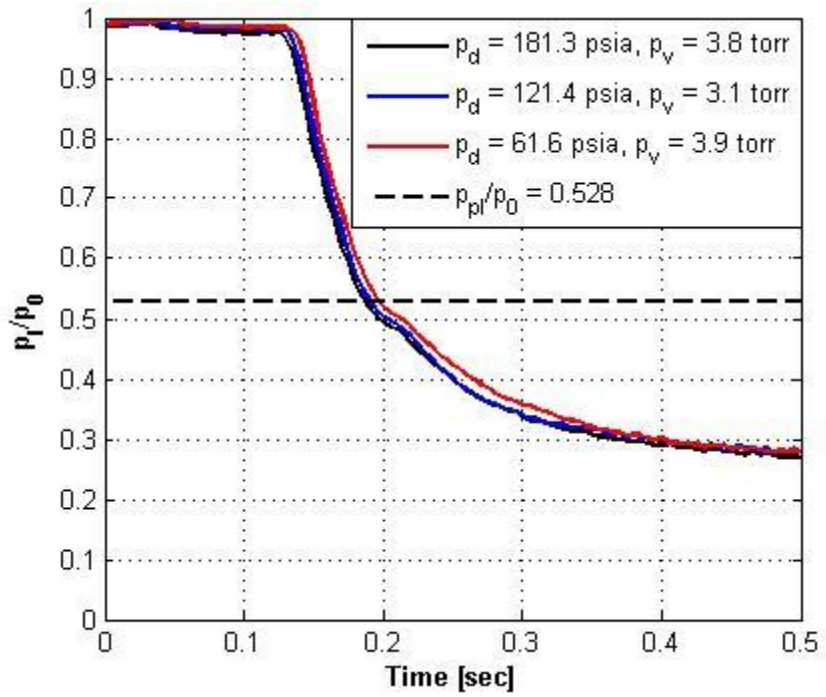

Figure D.7. Summary of fast-valve response at different driver-tube pressures

Figure D.8 demonstrates the response time of the fast valve during a run taken at a low driver-tube pressure of 41.9 psia. It gives the plenum-to-contraction-pressure ratio (p_{pl}/p_0), the pressure of the air near the fast valve normalized by its maximum value ($p_{fv}/p_{max,fv}$) and the trigger-output signal (as a ratio of twice the maximum output signal voltage of the oscilloscope). The oscilloscope triggers at t = 0, and an output signal is sent to the fast-valve electronics 15 microseconds later. From the fast-valve-pressure trace, the valve appears to open about 0.1 seconds later. Video tests of the fast valve performed before its installation in the bleed line showed the valve opening within 0.03 seconds. The cause for the increased 0.07 seconds in the opening time of the valve is unknown. Information that the fast valve has opened reaches the bleed slot after the valve opens at t ≈ 0.13 sec. This time difference of 0.03 second is roughly the time needed for a sound wave to travel the 30-foot distance in the bleed line between the fast valve and the bleed slot. Nearly 0.2 seconds after the start of the run, the plenum pressure drops below the sonic threshold (p_{pl}/p_0 = 0.528), and suction in the bleeds is achieved.

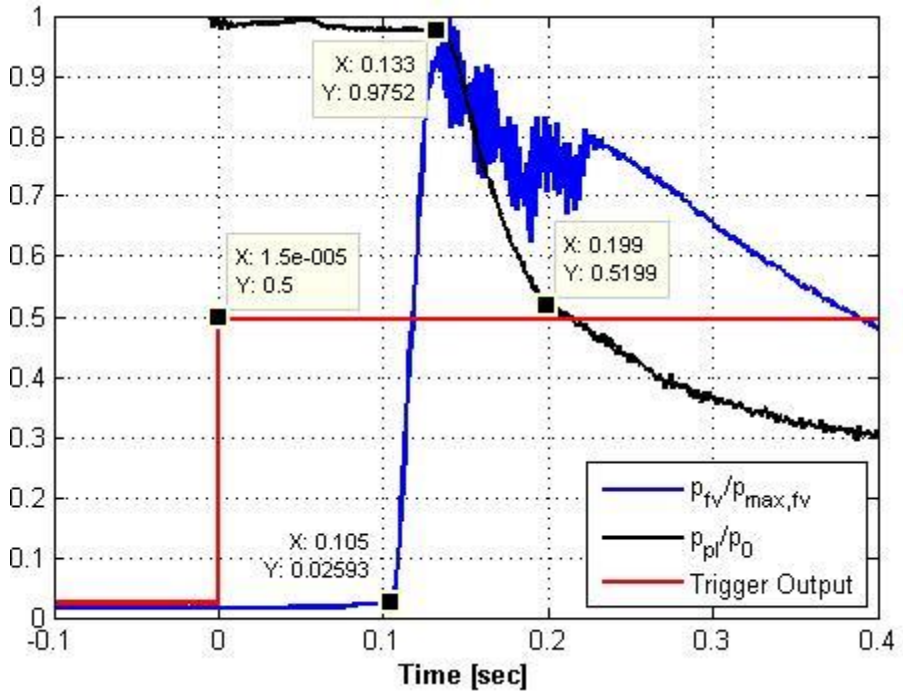

Figure D.8. Measured response of fast valve at low Reynolds number (p_d = 41.9 psia, p_v = 2.8 torr, Date: 17 October 2007, $p_{max,quiet}$ = 140 psia)

D.2 Support System for Modified Configuration

I-beams located above the main components of the BAM6QT support the tunnel through a system of trolleys, turnbuckles and crossbars, which are attached to eyebolts drilled and tapped into the flanges of each section. Due to the increased flange size, the eyebolts of the new sections were at different locations as those from the original sections, so a new support structure was created. This support structure is shown pictorially on Figure D.9 and as a schematic on Figure D.10.

Stress analysis for this support system was performed using a technique prepared by a former BAM6QT research colleague, Dr. Erick Swanson. This method assumes a concentrated load of 1500 pounds (the approximate weight of each new section) at the bottom-center location of the 1018 carbon-steel crossbars. This gives a conservative estimate on the maximum stress on the support system. The analysis determines that the maximum stress occurs on the bottom face of the crossbar due to a combination of axial and bending stress. Based on this method, the maximum stress on the crossbar is calculated at 5.6 ksi with a tensile load of 887 lb. on the turnbuckles. The crossbars have a maximum yield stress of 30 ksi [17], and the turnbuckles have a work load limit of 2200 lbs. each (McMaster-Carr part no. 2999T55). Thus, there is a safety factor of 5.3 on the crossbars beyond the conservative estimates of the calculations and of more than 2.5 on the turnbuckles, beyond the safety factor implemented by the vendor.

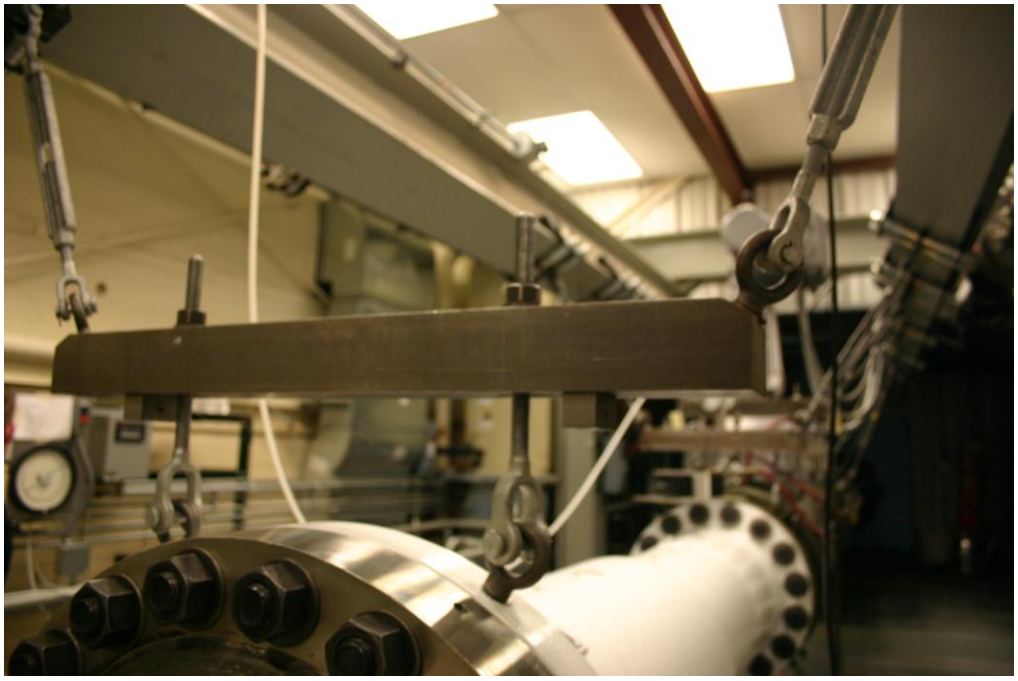

Figure D.9. Crossbar support system connected to larger flanges on modified tunnel configuration

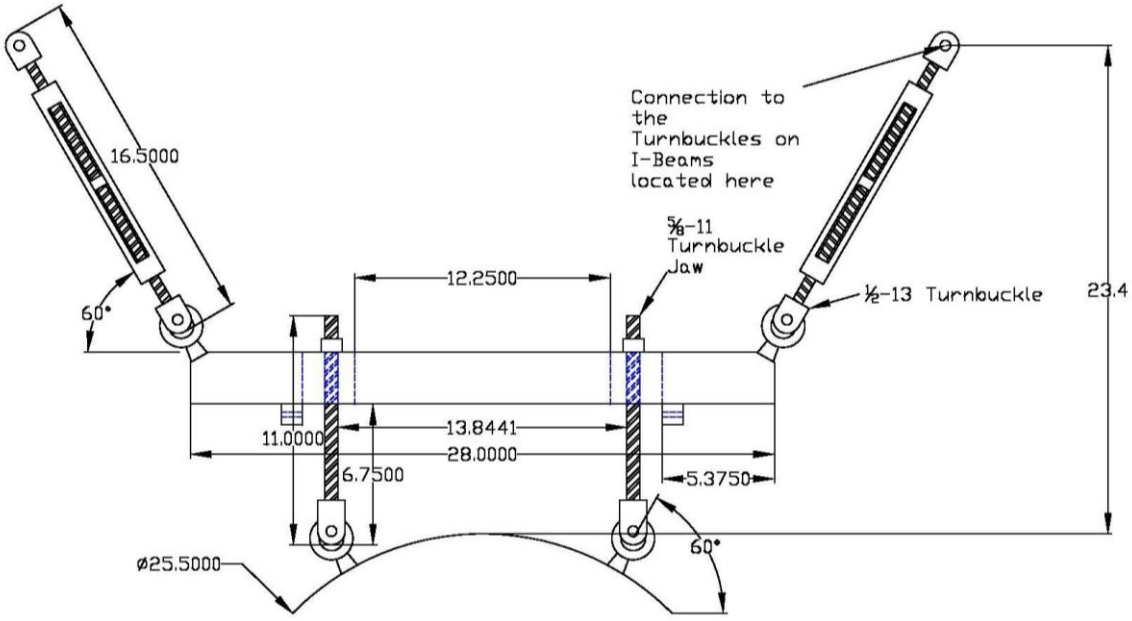

Figure D.10. Schematic of support structure for the 25-½" outer diameter flanges of the new sections. Dimensions in inches.

D.3 Modified Trolleys

Two pairs of 1-ton trolleys attaching the support system to the I-beam were modified to enable closer proximity to one another. The upstream set of trolleys attaches to the adapter flange, located at the downstream end of the nozzle. The downstream set attaches to the upstream flange of the new sting-support section. This junction is often separated in order to place models or other experimental hardware in the tunnel. D ue to the weight of both tunnel sections, support is needed on both ends to prevent cantilevering when the tunnel is open. Since these attachment points are so close to one another, the following modifications were made to enable support on both sides. The modified trolley setup is shown on Figure D.11.

1. The tapped holes for the eyebolts on the upstream flange of the sting-support section were moved 0.3275 inches downstream from center to increase the distance between the attachment points on the trolleys.
2. The bumpers at the downstream end of the face plate on the adapter-flange trolleys and upstream end of the face plate of the sting-support section trolleys were removed to enable the trolleys to travel closer to one another.
3. The support brackets on the sting-support section trolleys were altered to connect to the turnbuckles just inside the upstream wheels.
4. The support brackets on the adapter-flange trolleys were altered to connect to the turnbuckles just outside the downstream wheels. This caused the trolley to tilt, which prevented the upstream wheel from traveling on the I-beam. Instead, the face plate would drag on the underside of the I-beam. To avoid this, ball bearings were installed on the upstream end of the brackets to roll on the bottom face of the I-beam when the trolley tilts. A closer view of these ball bearings is given on Figure D.12.

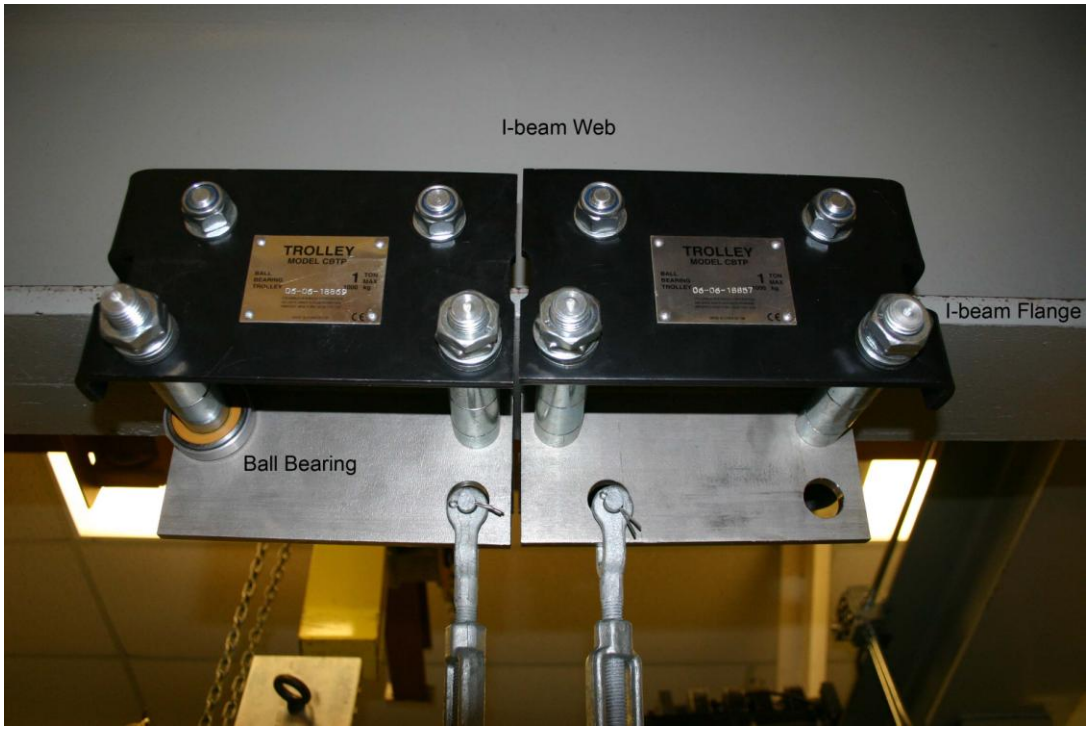

Figure D.11. Modified trolleys at the junction between the adapter flange and sting-support section

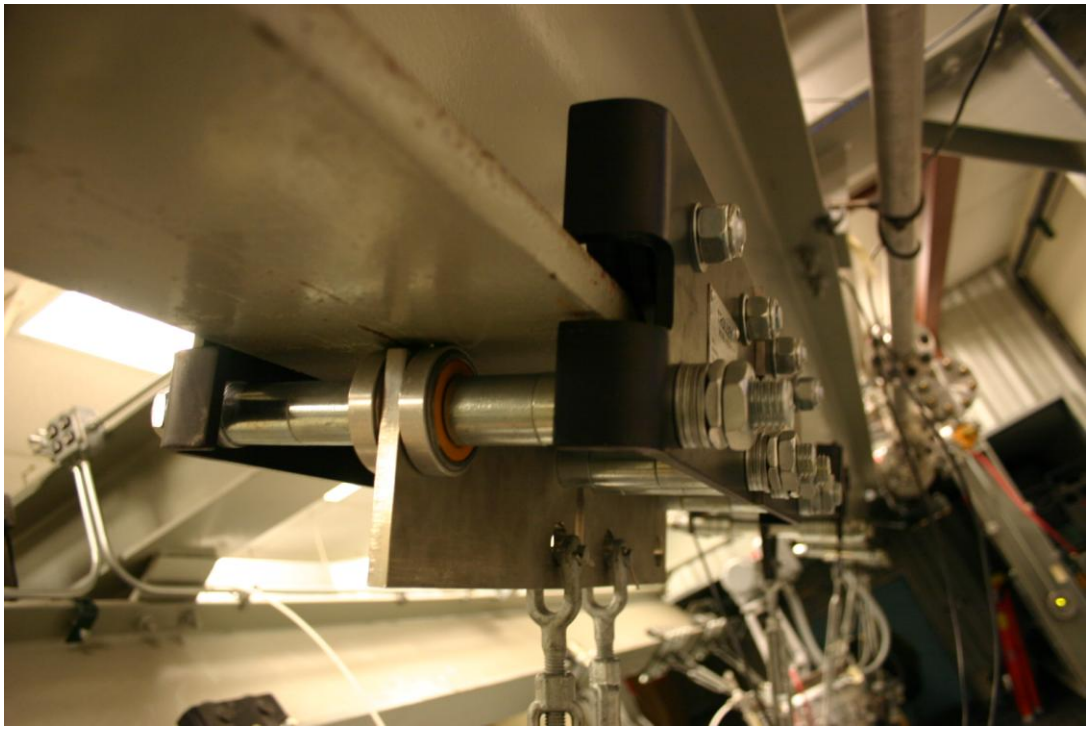

Figure D.12. Modified-trolley ball bearings on bottom face of support I-beam

D.4 Traverse Bar

The outside of the original sting-support section flange was flush with the outside of the test section. The downstream end of the traverse bar—located 10.69 inches above the centerline at the test section—was then free to travel downstream of the junction of the nozzle and sting-support section. However, the flanges located immediately downstream of the nozzle in the modified setup have a much larger outer diameter than that of the test section. These larger flanges would block passage of the traverse bar as it was passed beyond the downstream end of the nozzle. Thus, a slot was installed on both the adapter flange and the upstream sting-support section flange to allow downstream travel of the traverse bar. This slot is shown on Figure D.13. The downstream end of the traverse bar was modified to minimize the size of the slot. However, after welding on the upstream flange to the sting-support section, the flange warped and the slot was no longer straight. The size of the traverse bar then had to be further reduced to travel through the misshapen slot. Figure D.14 shows a schematic of the finalized drawing of the traverse bar.

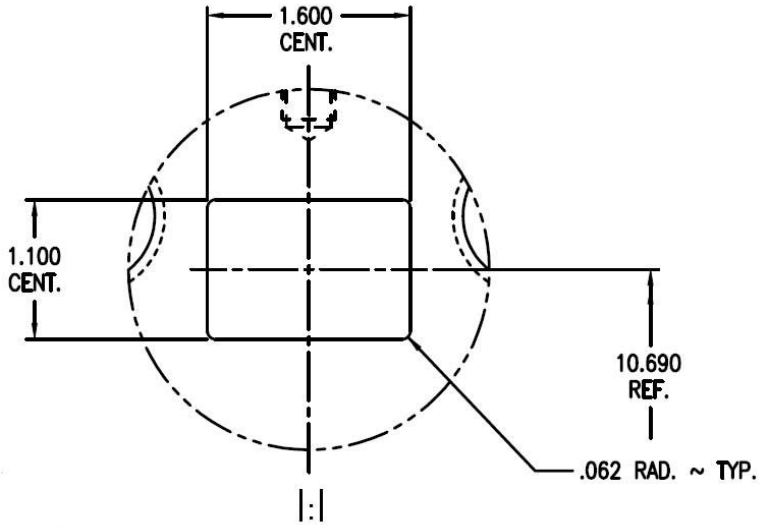

Figure D.13. Slot machined at top center of adapter flange and upstream flange of new sting-support section. Dimensions in inches. [18]

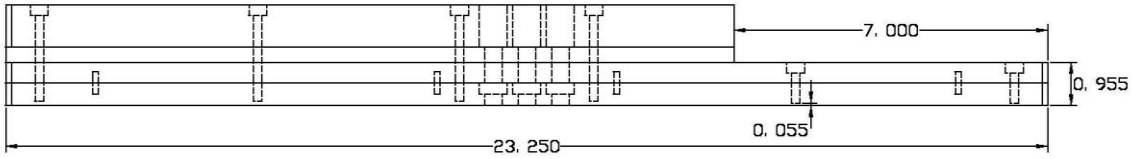

Figure D.14. Schematic of 1.5 inch wide modified traverse bar. Dimensions in inches.

E. Matlab Source Codes

E.1 Noise-Level Calculator

This code was used to determine the noise level (p_{rms}/p_{mean}) of the model-nose pressure traces given the time trace, pressure trace and number of points over which to average.

```
function [t_mean,y_RMS_mean,y_mean,y_RMS] = get_mean_RMS(t_array,y_array,n)

    num_points = length(t_array)/n;

    for i = 1:num_points

        if i == 1

            y_mean(i) = mean(y_array(1:n));
            RMS_sum(i) = 0;
            t_mean(i) = t_array(i);

        else

            y_mean(i) = mean(y_array(n*(i-1) + 1:n*(i)));
            RMS_sum(i) = 0;
            t_mean(i) = t_array(n*(i-1) + 1);

        end

        for j = 1:n

            y_ac = y_array(j + n*(i-1)) - y_mean(i);
            RMS_sum(i) = RMS_sum(i) + y_ac^2;

        end

        y_RMS(i) = sqrt(RMS_sum(i)/n);
        y_RMS_mean(i) = y_RMS(i)/y_mean(i);
```

```
end
```

E.2 Mach-Number Calculator

This code was used to determine the ratio of total pressures across a shock given a freestream Mach number. It is based on Equation 3.2.

```
function p_rat = getp01_p02(M)

    gamma = 1.4;
    p_rat = (1 + 2*gamma/(gamma + 1)*(M^2 - 1))^(1/(gamma - 1))*...
          ((2 + (gamma - 1)*M^2)/((gamma + 1)*M^2))^(gamma/(gamma - 1));

end
```

This code is a bisector subroutine that uses the previous code to determine the outputted pressure ratio based on a guessed value for the freestream Mach number. It inputs the desired pressure ratio and a Mach number range containing the solution.

```
function M = get_M(p01_p02_ex,M_low,M_high)

    gamma = 1.4;
    p01_p02_low = getp01_p02(M_low);
    p01_p02_high = getp01_p02(M_high);
    diff_mid = 1;
    tol = 1e-6;
    diff_low = p01_p02_ex - p01_p02_low;
    diff_high = p01_p02_ex - p01_p02_high;

    if p01_p02_ex < 1

        M = 0;

    else

    while abs(diff_mid) > tol

        if abs(diff_low) < tol
            M_mid = M_low;
            break
        elseif abs(diff_high) < tol
```

```
            M_mid = M_high;
            break
        else
            M_mid = 0.5*(M_low + M_high);
            p01_p02_mid = getp01_p02(M_mid);
            diff_mid = p01_p02_ex - p01_p02_mid;

            if abs(diff_mid) < tol
                break
            else
                if (diff_mid*diff_low < 0) && (diff_mid*diff_high > 0)
                    M_high = M_mid;
                    diff_high = diff_mid;
                elseif (diff_mid*diff_high < 0) && (diff_mid*diff_low > 0)
                    M_low = M_mid;
                    diff_low = diff_mid;
                else
                    error('There are multiple roots for Mach number.')
                end
            end

        end

    end

    M = M_mid;

    end

end
```

E.3 Fast-Fourier-Transform Calculator

This code gives a fast Fourier transform analysis over a selected section of a data trace. It inputs the time trace and data trace as well a start and end time of the selected portion to analyze using the Matlab *pwelch* command.

```
function [A_fft,f_fft,t_fft,y_fft] = get_fft(t_array,y_array,t_start,t_end)

   for i = 2:length(t_array)

      if t_array(i) == t_start | ...
        (t_array(i) > t_start && t_array(i-1) < t_start)

        i_begin = i;

      elseif t_array(i) == t_end | ...
            (t_array(i) > t_end && t_array(i-1) < t_end)

         i_end = i;
         break

      end

   end

   Fs = 1/(t_array(2) - t_array(1));
   t_fft = t_array(i_begin:i_end);
   y_fft = y_array(i_begin:i_end);
   [A_fft,f_fft] = pwelch(y_fft,length(t_fft),length(t_fft) - 1,[],Fs);

end
```